

# **Electroactive Conjugated Polymers as Charge-Transport Materials for Optoelectronic Thin-Film Devices**

Dissertation zur Erlangung des  
naturwissenschaftlichen Doktorgrades  
der Bayerischen Julius-Maximilians-Universität Würzburg

vorgelegt von

**Rainer Stahl**

aus Haßfurt

Würzburg 2005

Eingereicht am: \_\_\_\_\_

bei der Fakultät für Chemie und Pharmazie

1. Gutachter: \_\_\_\_\_

2. Gutachter: \_\_\_\_\_

der Dissertation

1. Prüfer: \_\_\_\_\_

2. Prüfer: \_\_\_\_\_

3. Prüfer: \_\_\_\_\_

des Öffentlichen Promotionskolloquiums

Tag des Öffentlichen Promotionskolloquiums: \_\_\_\_\_

Doktorurkunde ausgehändigt am: \_\_\_\_\_

Die vorliegende Arbeit wurde in der Zeit von Januar 2002 bis Dezember 2005 am  
Institut für Organische Chemie der Universität Würzburg angefertigt.

Mein besonderer Dank gilt

*Herrn Prof. Dr. Christoph Lambert*

Für die Überlassung dieses interessanten Themas und die mit vielen hilfreichen  
Anregungen und Diskussionen verbundene Betreuung der Arbeit.

## Abbreviations

AFM	atomic force microscopy
AM1	Austin model 1
Cbz	carbazole
CV	cyclic voltammogram
DCH	<i>trans</i> -1,2-diaminocyclohexane
EOAM	electrooptical absorption measurements
ETM	electron transport material
HOMO	highest occupied molecular orbital
HTM	hole transport material
IV-CT	inter-valence charge-transfer
ITO	indium tin oxide
LUMO	lowest unoccupied molecular orbital
NIR	near infrared
OCVD	organic chemical vapour deposition
OD	optical density
OLED	organic light emitting diode
PPP	poly( <i>para</i> -phenylene)
PPV	poly( <i>para</i> -phenylenevinylene)
TAB	triarylborane
TBAP	tetrabutylammonium perchlorate
TBAPF <sub>6</sub>	tetrabutylammonium hexafluorophosphate
TBE	two-band electrode
UV	ultraviolet
Vis	visible

# Contents

<b>1</b>	<b>Introduction</b> .....	<b>1</b>
<b>2</b>	<b>Bipolar Polymers with Intrinsic Electron and Hole Transport Properties</b> .....	<b>9</b>
2.1	Introduction.....	9
2.2	Bipolar Polymers Based on Carbazole-Substituted Oxadiazoles .....	12
2.2.1	Synthesis of the Monomers .....	12
2.2.2	Cyclic Voltammetry .....	14
2.2.3	Spectroelectrochemistry .....	19
2.2.4	Absorption and Emission Spectroscopy.....	21
2.2.5	Conclusions .....	24
2.3	Bipolar Polymers Based on Carbazole-Substituted Triarylboranes .....	26
2.3.1	Synthesis of the Monomers .....	26
2.3.2	Cyclic Voltammetry .....	28
2.3.3	Spectroelectrochemistry .....	32
2.3.4	Absorption and Emission Spectroscopy.....	33
2.3.5	Time-resolved Fluorescence Spectroscopy .....	46
2.3.6	Polarised Steady-State Fluorescence Spectroscopy .....	47
2.3.7	Solid-State Fluorescence of <i>poly-4</i> on ITO-coated Glass .....	51
2.3.8	Titration of TAB <b>4</b> with Fluoride Ions .....	52
2.3.9	X-Ray Structure Analysis of TAB <b>4</b> .....	53
2.3.10	Conclusions .....	55
2.4	AFM-Images of <i>poly-1</i> and <i>poly-4</i> .....	58
2.5	Conductivity Measurements .....	61
2.6	Conclusions .....	65
2.7	Literature .....	66
<b>3</b>	<b>Electron Deficient Conjugated Polymers</b> .....	<b>73</b>
3.1	Introduction.....	73
3.2	Electron Deficient Conjugated Borane Polymers.....	74

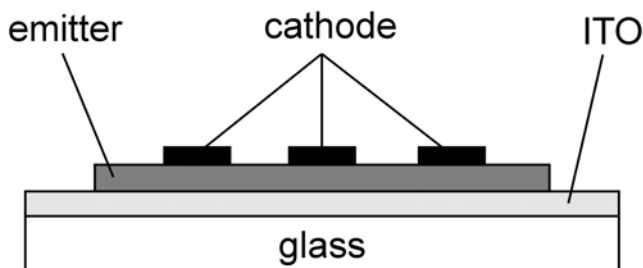
3.2.1	Synthesis of the Monomer.....	74
3.2.2	Cyclic Voltammetry.....	75
3.2.3	Absorption and Emission Spectroscopy .....	76
3.2.4	Conclusions.....	77
3.3	Electron Deficient Poly( <i>para</i> -phenylene)-Analogues Based on 4,4'- Bipyridinium (Viologen) .....	78
3.3.1	Synthesis of the Monomers.....	78
3.3.2	Cyclic Voltammetry.....	82
3.3.3	Absorption and Emission Spectroscopy .....	88
3.3.4	Conductivity Measurements .....	88
3.3.5	Conclusions.....	89
3.4	Literature.....	90
<b>4</b>	<b>Summary.....</b>	<b>93</b>
<b>5</b>	<b>Experimental Section .....</b>	<b>95</b>
5.1	Analytical Methods.....	95
5.2	Syntheses .....	104
5.2.1	General Experimental Procedures .....	104
5.2.2	Synthesis of the Carbazole Substituted Precursors .....	105
5.2.3	Synthesis of the Diphenylamino Precursor.....	111
5.2.4	Synthesis of the 2,5-Diaryl-1,3,4-oxadiazoles .....	114
5.2.5	Synthesis of the Triarylboranes.....	118
5.2.6	Synthesis of the <i>para</i> -Substituted 1,4-Bis(pyridinio)benzenes .....	125
5.3	Literature.....	132
	<b>Table of Formulas .....</b>	<b>134</b>
	<b>Appendix.....</b>	<b>136</b>
	Zusammenfassung .....	136
	Publikationen .....	138
	Lebenslauf .....	139
	Danksagung.....	140
	Erklärung .....	144

## 1 Introduction

In the past decades an enormous research as well as commercial interest has focused on the new field of conjugated organic electronics materials.<sup>[1-13]</sup> This interest, which has just recently received a new impulse thanks to the Nobel Prize in chemistry for Shirakawa, MacDiarmid and Heeger,<sup>[14-16]</sup> is due to the fact that these materials combine a number of interesting properties which give rise to a broad variety of new applications. Probably the most important feature of conjugated organic electronics materials is their ability to transport charges, i.e. they can be conductors or semiconductors.<sup>[12, 17]</sup> On the other hand these materials are organic molecules or polymers and thus offer the possibility to be designed in such a way as to perfectly fit the desired requirements.<sup>[2]</sup> In this context these materials are often described as synthetic metals.<sup>[12]</sup> Depending on their molecular weight and solubility, conjugated organic electronics materials can be easily processed by common techniques like organic chemical vapour deposition (OCVD)<sup>[18]</sup>, spin-coating<sup>[2]</sup> or simple ink-jet printing<sup>[15]</sup>. Owing to their mechanical stability these materials can even be deposited on flexible substrates. These features provide the possibility of producing “plastic organic electronics” at very low costs.<sup>[12, 15]</sup> Potential applications for polymeric materials include fully printed polymer field effect transistors (PFETs),<sup>[19-23]</sup> conjugated polymer photovoltaic cells,<sup>[24-26]</sup> organic light emitting diodes (OLED)<sup>[2, 27-29]</sup> and lasers<sup>[30-32]</sup> as well as polymer sensors, actors, batteries and components for fuel cells.<sup>[33]</sup> Low molecular weight compounds can be used in vapour-deposited thin-film transistors,<sup>[10]</sup> and as charge transporting or emitting molecular glasses in OLEDs,<sup>[13, 34]</sup> photovoltaic cells, photo copiers and laser printers.<sup>[9]</sup> Moreover, small conjugated molecules or oligomers can be designed in order to mimic the functionality of single electronic units like transistors, diodes, resistors and switches on a molecular scale.<sup>[17, 35]</sup> It is thus possible to further reduce the dimensions of these electronic components to the nanometre level.

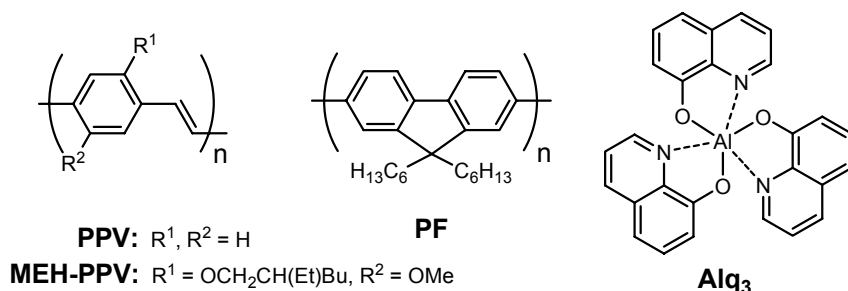
As mentioned above, one key application for conducting polymers, oligomers and conjugated small molecules is their use in OLEDs. Such light emitting devices with poly(*para*-phenylenevinylene) (PPV) as the emissive material have first been

described in 1990 by Friend et al.<sup>[27]</sup> and are of the general structure depicted in Scheme 1.1.



**Scheme 1.1:** General structure of a one-layer OLED by Friend.<sup>[27]</sup>

A simple one-layer OLED consists of an emitter material which is sandwiched between a transparent bottom electrode (anode) and a metal electrode (cathode) on top. Usually an indium tin oxide (ITO) coated glass substrate serves as a transparent anode whereas the cathode normally consists of metals with low work functions (Al, Mg, Ca). The emitter material can either be a polymer like PPV or polyfluorene (PF) or a low molecular weight compound such as tris(8-hydroxyquinolino)-aluminium (Alq<sub>3</sub>).<sup>[2, 13, 28]</sup> If an external field is applied between the two electrodes, positive and negative charges are injected at the anode and cathode, respectively. These charges recombine within the emission layer by formation of localised excited states (excitons) which can then decay radiatively (see Scheme 1.2, a)).<sup>[28, 36]</sup>

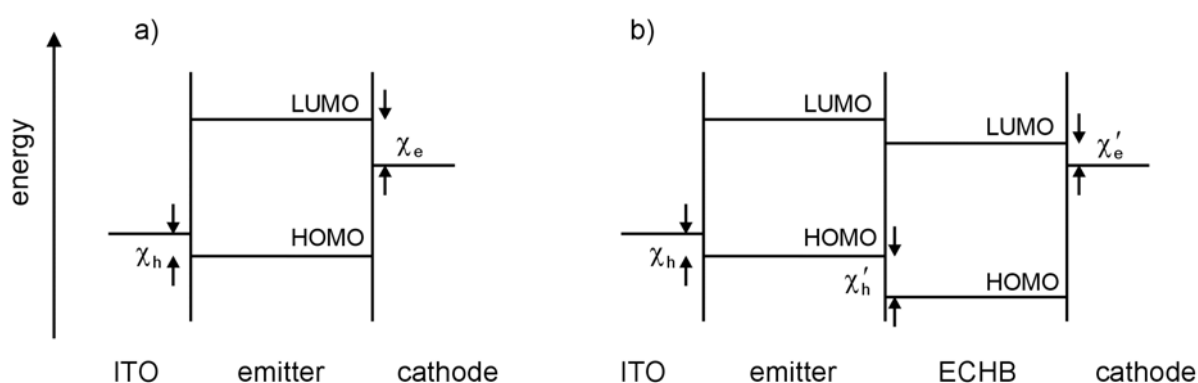


OLED displays have certain advantages compared to liquid crystal displays (LCD) and other display technologies.<sup>[37-40]</sup> OLED displays possess rather high power efficiencies because they are emissive displays and do not need an additional backplane illumination. Further advantages are fast response times (up to 10<sup>4</sup> times



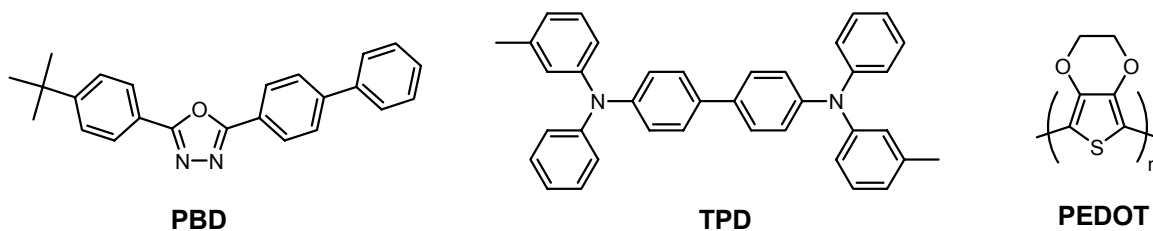
faster than LCD), high luminance at relatively low voltages, wide view angle and high contrast. Flexible and large area displays are also possible.

Despite these advantages the conventional one-layer OLED displays still have some drawbacks. One major problem is the unbalanced charge flow through the devices which leads to higher operating voltages and reduced lifetimes.<sup>[2]</sup> The difference between the amount of positive (holes) and negative (electrons) charge carriers injected into the device is mainly caused by a mismatch between the HOMO and LUMO levels of the emitter material and the Fermi level of the adjacent electrode (Scheme 1.2, a)). Moreover, holes possess a higher mobility than electrons in many emitter materials which leads to nonradiative neutralisation of the positive charges at the cathode.<sup>[41-43]</sup>



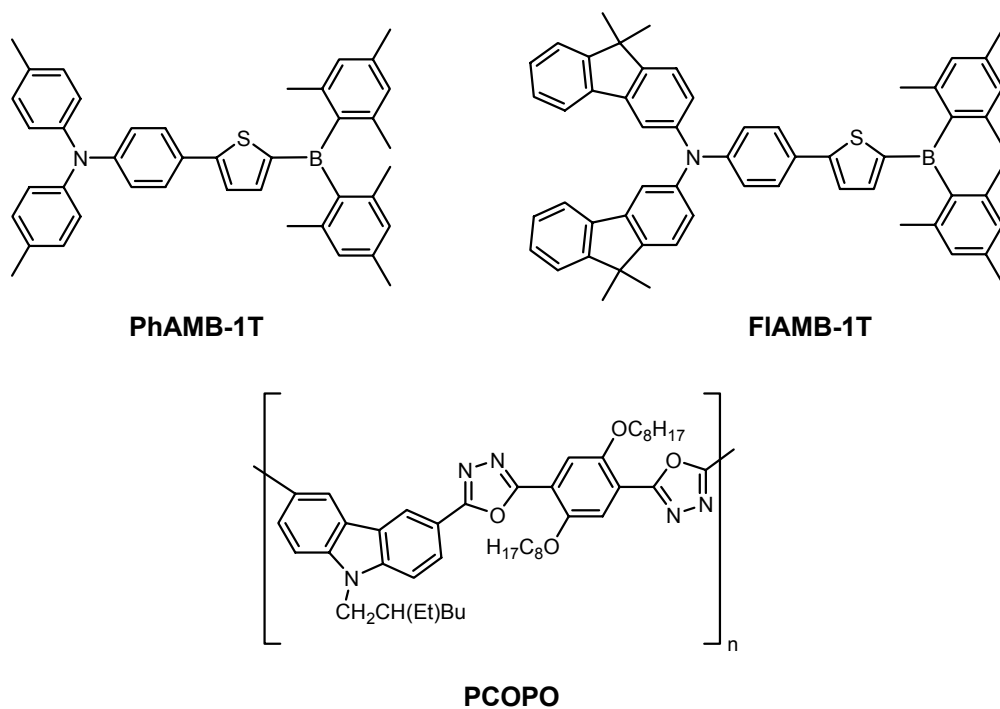
**Scheme 1.2:** Energy level diagram of an a) single-layer OLED and b) OLED with additional electron-conducting/hole-blocking layer (ECHB). The energy barriers for the injection of holes and electrons are denoted as  $\chi_h$  and  $\chi_e$ , respectively.

To circumvent this problem additional charge-injection layers between the emission layer and the corresponding electrodes may be introduced. Especially the insertion of a so-called electron-conducting/hole-blocking (ECHB) layer has proved to effectively inhibit the quenching of holes at the cathode (Scheme 1.2, b)).<sup>[2, 36]</sup> Materials with good electron transport properties are molecules or polymers with low-lying LUMO levels such as oxadiazoles (PBD), triazines, benzothiadiazoles, etc..<sup>[11, 34]</sup> For the improved injection of holes materials with high-lying HOMO levels are needed. Typical hole transporting materials (HTM) are aromatic amines like TPD or electron rich polymers like poly(ethylenedioxythiophene) (PEDOT).<sup>[44-46]</sup>



The aim of this work is to develop and characterise new  $\pi$ -conjugated charge-transport polymers especially for use in OLEDs and other optoelectronic thin-film devices. The desired materials are deposited onto platinum or ITO/glass surfaces by either oxidative or reductive electropolymerisation<sup>[3]</sup> of the corresponding monomer units. This method allows polymer formation from soluble low molecular weight precursors with the resultant polymer being almost insoluble in many organic solvents. It is thus possible to assemble multi-layer devices by successive deposition of different polymers without solubilising previously deposited films. Furthermore, electropolymerisation permits to directly control the extent of p- or n-doping of the polymer by the applied potential. The deposited conjugated polymers are characterised by means of cyclic voltammetry, UV/Vis/NIR-spectroelectrochemistry and conductivity measurements. Where appropriate, the polymer surface is studied by atomic force microscopy (AFM).

The first part of this work focuses on bipolar p-n diblock polymers which combine all three basic requirements for an OLED within one material: improved electron and hole transport as well as electroluminescence properties. Polymers (PCOPO)<sup>[47-49]</sup> as well as molecular materials (e. g. PhAMB-1T, FIAMB-1T)<sup>[50, 51]</sup> of this bipolar character have been described recently and have been demonstrated to effectively improve the performance of OLEDs.



Since oxadiazoles and triarylboranes are known to exhibit excellent electron-transport properties as well as photoluminescence in the visible region<sup>[34, 52]</sup> these chromophores are chosen as monomeric subunits for the desired polymers. Additional carbazole substituents allow for oxidative polymerisation of the monomers<sup>[53-58]</sup> and should provide the desired hole transporting properties of the resultant polymers.

The second part of this work aims at the synthesis and characterisation of purely electron conducting conjugated polymers. In order to serve as efficient ECHB materials these polymers have to exhibit high electron affinities and at the same time high ionisation potentials. These requirements are fulfilled by triarylboranes<sup>[52]</sup> and viologens<sup>[59, 60]</sup> which are thus chosen as the electron transporting subunits. The corresponding monomers have to be polymerised reductively because oxidative electropolymerisation would lead to polymers with additional p-type functionalities.

## Literature

- [1] S. A. Jenekhe, *Chem. Mater.* **2004**, *16*, 4381-4382.
- [2] A. Kraft, A. C. Grimsdale, A. B. Holmes, *Angew. Chem.* **1998**, *110*, 416-443.
- [3] J. Heinze, *Top. Curr. Chem.* **1990**, *152*, 1-47.
- [4] H. G. Kiess, *Conjugated Conducting Polymers*, Springer Verlag, Berlin, **1992**.
- [5] H. S. Nalwa, *Handbook of Organic Conductive Molecules and Polymers, Vol. 4*, Wiley, Chichester, **1997**.
- [6] G. Wegner, *Angew. Chem.* **1981**, *93*, 352-371.
- [7] K. Menke, S. Roth, *Chem. Unserer Zeit* **1986**, *20*, 1-10.
- [8] K. Menke, S. Roth, *Chem. Unserer Zeit* **1986**, *20*, 33-43.
- [9] P. Strohriegl, J. V. Grazulevicius, *Adv. Mater.* **2002**, *14*, 1439-1452.
- [10] T. W. Kelley, P. F. Baude, C. Gerlach, D. E. Ender, D. Muyres, M. A. Haase, D. E. Vogel, S. D. Theiss, *Chem. Mater.* **2004**, *16*, 4413-4422.
- [11] G. Hughes, M. R. Bryce, *J. Mater. Chem.* **2005**, *15*, 94-107.
- [12] M. Rehahn, *Chem. Unserer Zeit* **2003**, *37*, 18-30.
- [13] U. Mitschke, P. Bäuerle, *J. Mater. Chem.* **2000**, *10*, 1471-1507.
- [14] H. Shirakawa, *Angew. Chem.* **2001**, *113*, 2642-2648.
- [15] A. G. MacDiarmid, *Angew. Chem.* **2001**, *113*, 2649-2659.
- [16] A. J. Heeger, *Angew. Chem.* **2001**, *113*, 2660-2682.
- [17] R. L. Carroll, C. B. Gorman, *Angew. Chem. Int. Ed.* **2002**, *41*, 4379-4400.
- [18] O. Schäfer, A. Greiner, J. Pommerehne, W. Guss, H. Vestweber, H. Y. Tak, H. Bässler, C. Schmidt, G. Lüssem, *Synth. Met.* **1996**, *82*, 1-9.
- [19] J. Ficker, A. Ullmann, W. Fix, H. Rost, W. Clemens, *J. Appl. Phys.* **2003**, *94*, 2638-2641.
- [20] H. Rost, J. Ficker, J. S. Alonso, L. Leenders, I. McCulloch, *Synth. Met.* **2004**, *145*, 83-85.
- [21] J. Ficker, H. v. Seggern, H. Rost, W. Fix, W. Clemens, I. McCulloch, *Appl. Phys. Lett.* **2004**, *85*, 1377-1379.
- [22] W. Fix, A. Ullmann, J. Ficker, W. Clemens, *Appl. Phys. Lett.* **2002**, *81*, 1735-1737.

- [23] A. Knobloch, A. Manuelli, A. Berndts, W. Clemens, *J. Appl. Phys.* **2004**, *96*, 2286-2291.
- [24] C. J. Brabec, S. N. Sariciftci, *Monatsh. Chem.* **2001**, *132*, 421-431.
- [25] A. Cravino, S. N. Sariciftci, *J. Mater. Chem.* **2002**, *12*, 1931-1943.
- [26] K. M. Coakley, M. D. McGehee, *Chem. Mater.* **2004**, *16*, 4533-4542.
- [27] J. H. Burroughes, D. D. C. Bradley, A. R. Brown, R. N. Marks, K. Mackay, R. H. Friend, P. L. Burns, A. B. Holmes, *Nature* **1990**, *347*, 539-541.
- [28] R. H. Friend, R. W. Gymer, A. B. Holmes, J. H. Burroughes, R. N. Marks, C. Taliani, D. D. C. Bradley, D. A. Dos Santos, J. L. Brédas, M. Logdlund, W. R. Salaneck, *Nature* **1999**, *397*, 121-128.
- [29] D. Hertel, C. D. Müller, K. Meerholz, *Chem. Unserer Zeit* **2005**, *39*, 336-347.
- [30] M. D. McGehee, A. J. Heeger, *Adv. Mater.* **2000**, *12*, 1655-1668.
- [31] N. Tessler, D. J. Pinner, V. Cleave, P. K. H. Ho, R. H. Friend, G. Yahiolglu, P. Le Barny, J. Gray, M. de Souza, G. Rumbles, *Synth. Met.* **2000**, *115*, 57-62.
- [32] F. Hide, M. A. Diaz-Garcia, B. J. Schwartz, A. J. Heeger, *Acc. Chem. Res.* **1997**, *30*, 430-436.
- [33] H.-K. Roth, M. Schrödner, *Materialwissenschaft Und Werkstofftechnik* **2003**, *34*, 254-261.
- [34] A. P. Kulkarni, C. J. Tonzola, A. Babel, S. A. Jenekhe, *Chem. Mater.* **2004**, *16*, 4556-4573.
- [35] V. Balzani, A. Credi, F. M. Raymo, J. F. Stoddart, *Angew. Chem. Int. Ed.* **2000**, *39*, 3349-3391.
- [36] M. Deußen, H. Bäessler, *Chem. Unserer Zeit* **1997**, *31*, 76-86.
- [37] R. Scharf, *Physikalische Blätter* **1999**, *55*, 37-39.
- [38] R. Froböse, *Bild Wiss.* **2000**, *37*, 44-48.
- [39] S. W. Eder, W. Schulz, *VDI Nachrichten* **2004**, *23*.
- [40] O. Prache, *Displays* **2001**, *22*, 49-56.
- [41] J. R. Sheats, H. Antoniadis, M. Hueschen, W. Leonard, J. Miller, R. Moon, D. Roitman, A. Stocking, *Science* **1996**, *273*, 884-888.
- [42] P. W. M. Blom, M. J. M. deJong, J. J. M. Vleggaar, *Appl. Phys. Lett.* **1996**, *68*, 3308-3310.
- [43] N. C. Greenham, R. H. Friend, *Solid State Physics* **1995**, *49*, 1-149.

- [44] D. F. O'Brien, P. E. Burrows, S. R. Forrest, B. E. Koene, D. E. Loy, M. E. Thompson, *Adv. Mater.* **1998**, *10*, 1108-1112.
- [45] R. H. Friend, *Pure Appl. Chem.* **2001**, *73*, 425-430.
- [46] B. E. Koene, D. E. Loy, M. E. Thompson, *Chem. Mater.* **1998**, *10*, 2235-2250.
- [47] W.-L. Yu, H. Meng, J. Pei, S.-J. Chua, W. Huang, Y.-H. Lai, *Chem. Commun.* **1998**, *18*, 1957-1958.
- [48] W.-L. Yu, H. Meng, J. Pei, W. Huang, *J. Am. Chem. Soc.* **1998**, *120*, 11808-11809.
- [49] H. Meng, Z.-K. Chen, W. Huang, *J. Phys. Chem. B* **1999**, *103*, 6429-6433.
- [50] Y. Shirota, M. Kinoshita, T. Noda, K. Okumoto, T. Ohara, *J. Am. Chem. Soc.* **2000**, *122*, 11021-11022.
- [51] H. Doi, M. Kinoshita, K. Okumoto, Y. Shirota, *Chem. Mater.* **2003**, *15*, 1080-1089.
- [52] C. D. Entwistle, T. B. Marder, *Chem. Mater.* **2004**, *16*, 4574-4585.
- [53] M. M. Verghese, M. K. Ram, H. Vardhan, B. D. Malhotra, S. M. Ashraf, *Polymer* **1997**, *38*, 1625-1629.
- [54] S. Yapi Abe, J. C. Bernede, M. A. Delvalle, Y. Tregouet, F. Ragot, F. R. Diaz, S. Lefrant, *Synth. Met.* **2002**, *126*, 1-6.
- [55] H. Taoudi, J. C. Bernede, A. Bonnet, M. Morsli, A. Godoy, *Thin Solid Films* **1997**, *304*, 48-55.
- [56] J. Heinze, K. Hinkelmann, M. Dietrich, J. Mortensen, *Ber. Bunsenges.* **1985**, *89*, 1225-1229.
- [57] S. Cattarin, G. Mengoli, M. M. Musiani, B. Schreck, *J. Electroanal. Chem.* **1988**, *246*, 87-100.
- [58] E. Cloutet, C. Olivero, D. Ades, M.-C. Castex, A. Siove, *Polymer* **2002**, *43*, 3489-3495.
- [59] W. Sliwa, B. Bachowska, N. Zelichowicz, *Heterocycles* **1991**, *32*, 2241-2273.
- [60] A. Factor, G. E. Heinsohn, *J. Polym. Sci., Part B: Polym. Lett.* **1971**, *9*, 289-295.

## 2 Bipolar Polymers with Intrinsic Electron and Hole Transport Properties

### 2.1 Introduction

As discussed in Section 1 a basic problem of OLEDs is to achieve a balanced injection and flow of positive and negative charges through the emissive film of the device. This problem can be overcome by either usage of low work function cathode materials like Ca or Mg or by the insertion of additional charge-injection and transport layers. The first approach includes the need for difficult and expensive device encapsulation because both Ca and Mg are easily susceptible to atmospheric corrosion while the second possibility implies the deposition of additional layers which also increases the costs for device fabrication. A third approach which has already been pursued successfully<sup>[1]</sup> is to combine electron- and hole-transport properties and electroluminescence within one single layer by blending of n-type, p-type and emissive polymers. However, the problem of phase separation during device operation still remains a pretentious challenge.<sup>[2]</sup> In an ideal material the transport of positive and negative charge carriers as well as the emission of light should be combined within one molecule or polymer. Such a material has to include electron deficient (acceptor) and electron rich (donor) moieties and be capable of forming emissive excited states.<sup>[3-10]</sup>

Oxadiazoles are an important class of electron deficient heteroaromatic compounds and were first described as fluorescent components of liquid organic scintillators.<sup>[11, 12]</sup> The first 2,5-diaryl-1,3,4-oxadiazole which has been used successfully as an efficient ETM in OLEDs by Adachi et al. in 1989 is 5-(4-biphenyl)-2-(4-*tert*-butylphenyl)-1,3,4-oxadiazole (PBD).<sup>[13, 14]</sup> Stimulated by these promising results various molecular as well as polymeric 2,5-diaryl-1,3,4-oxadiazoles have been studied as ETMs and/or emitter materials in OLEDs.<sup>[2, 15-29]</sup>

In recent years, triarylboranes (TABs) have also attracted increasing interest due to their unique electrochemical and photophysical properties<sup>[30, 31]</sup>. From the viewpoint of electrochemistry these compounds are fairly good electron acceptors because of the vacant boron  $p_z$  orbital. Thus, TABs can easily be reduced to yield

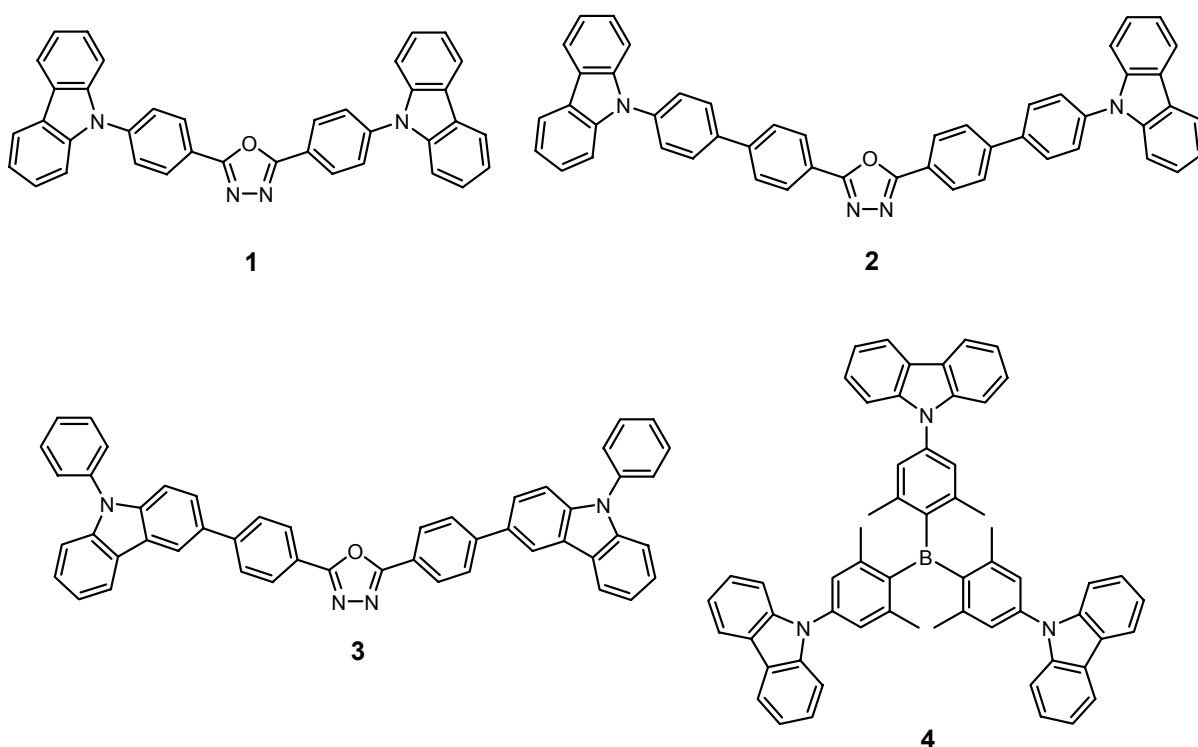
their corresponding radical anions. On the other hand, this electron deficiency facilitates the attack of nucleophiles and, therefore, bulky substituents such as methyl or isopropyl groups in *ortho*-position to the boron atom are necessary in order to provide kinetic stability. Furthermore, TABs exhibit a pronounced fluorescence in the visible region which can be tuned by additional substituents. High fluorescence quantum yields have been found for donor substituted TABs in particular<sup>[30]</sup>. Owing to these properties the dimesitylboryl group has often been used as the acceptor moiety in  $\pi$ -conjugated donor–acceptor chromophores.<sup>[32-36]</sup> Due to the above mentioned features TABs are used as emitting and/or charge-transport materials in optoelectronic devices such as organic light emitting diodes (OLED).<sup>[8, 9, 30, 31, 37-39]</sup> In particular the combination of TABs with (amino) donor moieties is a promising approach and several representatives of this type of compounds have already demonstrated their suitability for use in OLEDs.<sup>[8, 9, 40, 41]</sup>

As mentioned in Section 1 aromatic amines are widely used as efficient hole transport materials (HTM)<sup>[42-45]</sup>. However, triphenylamine and diphenylamino-substituted compounds can only be electropolymerised in special solvent/electrolyte systems<sup>[46]</sup> or by thin-layer cyclic voltammetry.<sup>[47]</sup> Carbazole<sup>[48-50]</sup> and *N*-phenyl-carbazole<sup>[51, 52]</sup> can be electropolymerised in different solvents under semi-infinite conditions and are thus chosen as electron donating substituents.

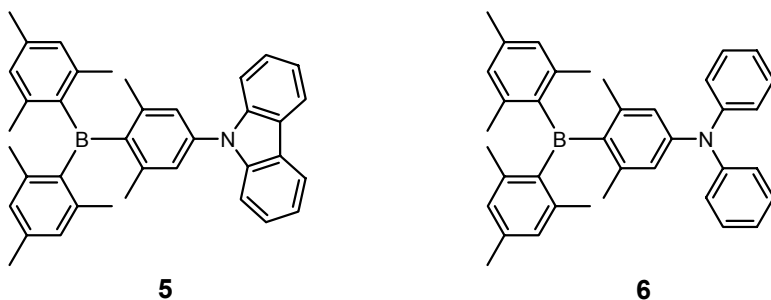
The subject of the first part of this work is therefore the synthesis of the carbazole substituted oxadiazoles **1–3** and the triarylborane **4** as monomeric precursors for bipolar conjugated polymers. These molecules are electropolymerised potentiodynamically in order to obtain the corresponding polymers which are characterised by cyclic voltammetry, UV/Vis/NIR-spectroelectrochemistry and conductivity measurements.

In order to systematically improve the performance of materials used in optoelectronic devices a detailed understanding of their basic electrochemical as well as photophysical properties is indispensable. In addition triarylboranes are isoelectronic to triphenylmethane cations and can therefore provide further information about this important class of dyes.





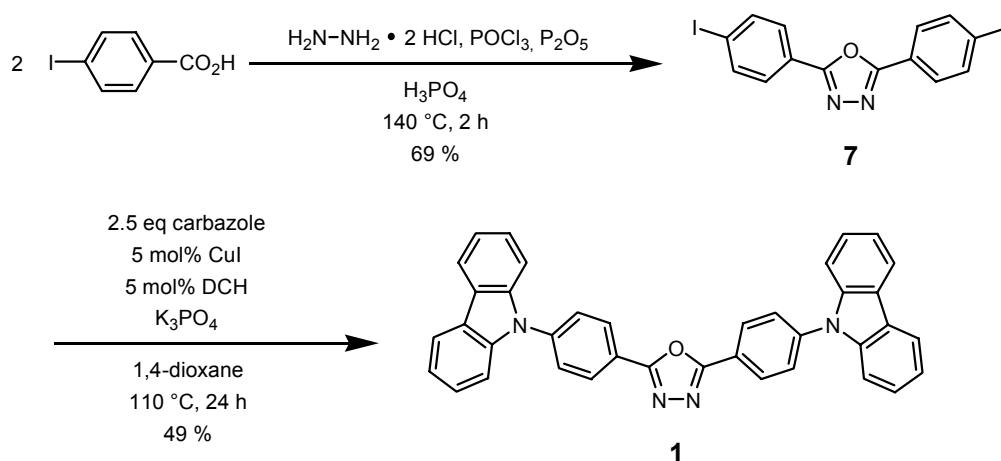
Although the electrochemistry<sup>[53-55]</sup> and photophysics<sup>[56-58]</sup> of simple triarylboranes such as triphenylborane or trimesitylborane have been subject of various publications in the past decades some aspects of the properties of their donor substituted analogues still demand further investigation. Especially the symmetry of the ground state, which has been studied intensively for triphenylborane and related model compounds<sup>[57, 59-62]</sup> as well as for triphenylmethane dyes,<sup>[63, 64]</sup> is still discussed controversially. Therefore, the TABs **5** and **6** are synthesised as model compounds of **4** to gain deeper insight into the electrochemical as well as photophysical properties of this class of compounds.



## 2.2 Bipolar Polymers Based on Carbazole-Substituted Oxadiazoles

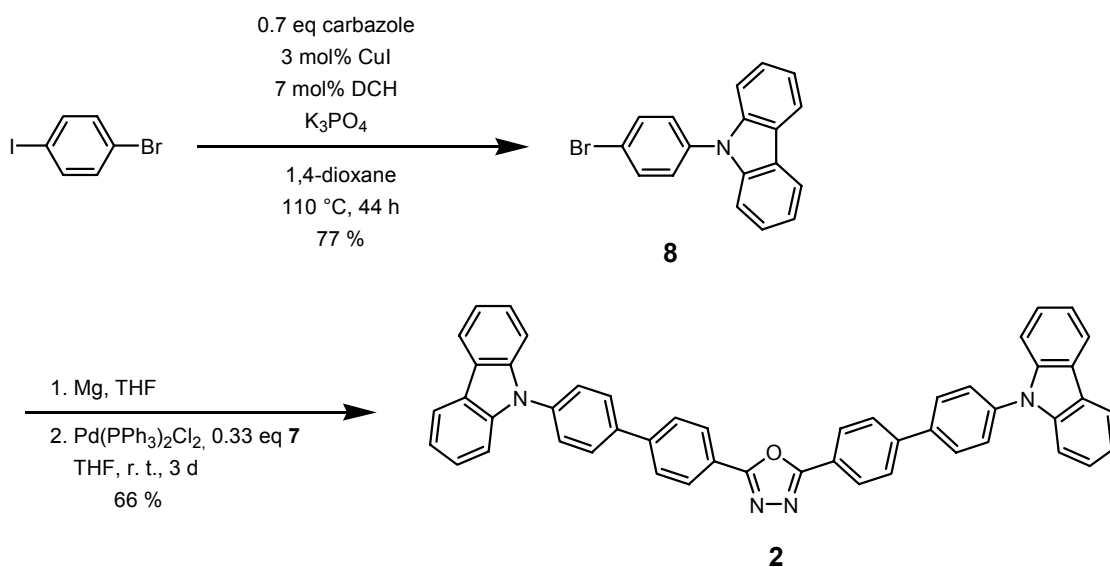
### 2.2.1 Synthesis of the Monomers

The oxadiazole precursor **7** was synthesised in a one-pot reaction according to Lagrenée et al.<sup>[65]</sup> in 69 % yield. Copper-catalysed coupling<sup>[66]</sup> of **7** with an excess of carbazole gave the oxadiazole **1** in 49 % yield (Scheme 2.1).



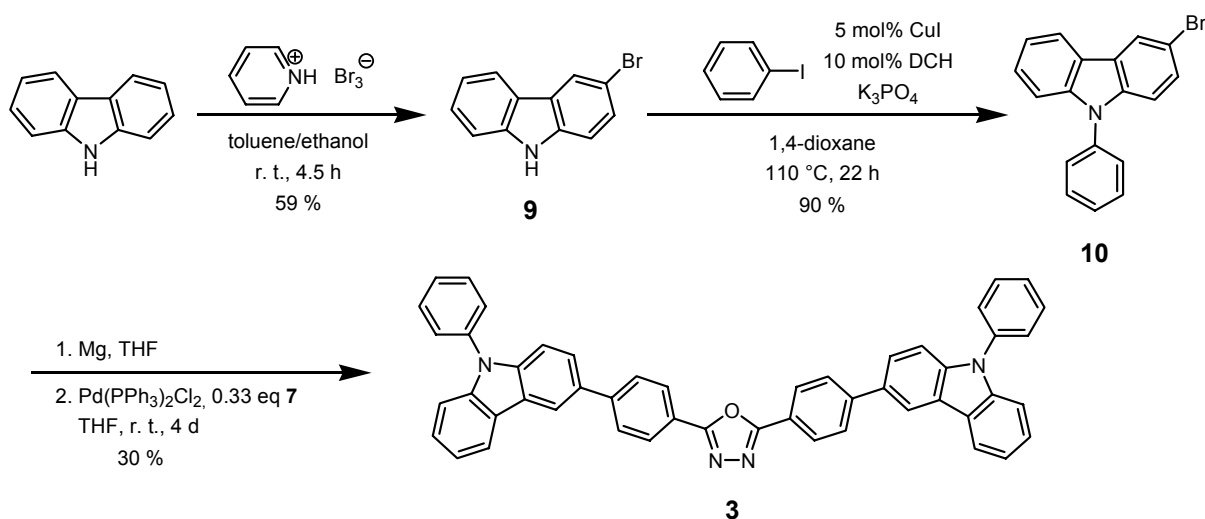
**Scheme 2.1:** Synthesis of the carbazole-substituted oxadiazole **1**.

9-(4-Bromophenyl)-9*H*-carbazole (**8**) was obtained by analogous copper-catalysed amination<sup>[66]</sup> of 1-bromo-4-iodobenzene with carbazole. Conversion of **8** into the Grignard reagent and subsequent Pd-catalysed cross-coupling with **7** afforded the oxadiazole compound **2** in 66 % yield (Scheme 2.2).



**Scheme 2.2:** Synthesis of the carbazole-substituted oxadiazole **2**.

The regioisomer of **8**, 3-bromo-9-phenyl-9*H*-carbazole (**10**) was synthesised by bromination of carbazole with pyridinium hydrobromide perbromide and subsequent copper-catalysed cross-coupling with an excess of iodobenzene. After conversion of **10** into the corresponding Grignard reagent the oxadiazole **3** was obtained by analogous Pd-catalysed cross-coupling with **7** in 30 % yield (Scheme 2.3).



**Scheme 2.3:** Synthesis of the carbazole-substituted oxadiazole **3**.

## 2.2.2 Cyclic Voltammetry

The redox behaviour of the three oxadiazoles **1–3** was investigated by cyclic voltammetry in CH<sub>2</sub>Cl<sub>2</sub> and THF using tetrabutylammonium hexafluorophosphate (TBAPF<sub>6</sub>) as the supporting electrolyte. The corresponding redox potentials are summarised in Table 2.1.

**Table 2.1:** Redox potentials of the oxadiazole monomers **1–3** (vs. Fc/Fc<sup>+</sup>).

	<b>1</b>	<b>2</b>	<b>3</b>
$E_{\text{ox}} / \text{mV}$ [a-c]	980	900	930
$E_{\text{red}} / \text{mV}$ [d]	-2410 [e]	-2340	-2490 [e]
$E_{\text{ox}} - E_{\text{red}} / \text{mV}$	3390	3240	3420

[a] 0.2 M CH<sub>2</sub>Cl<sub>2</sub>/TBAPF<sub>6</sub>, [b] peak potential of the chemically irreversible oxidation, [c] shoulder at lower potential indicates additional oxidation process, [d] 0.3 M THF/TBAPF<sub>6</sub>, [e] chemically irreversible.

All oxadiazole compounds **1–3** can be reduced electrochemically to their radical anions between -2340 mV and -2490 mV (vs. Fc/Fc<sup>+</sup>) in THF/TBAPF<sub>6</sub>. The reduction of **1** and **3** is chemically reversible at moderate to high scan rates ( $v > 250$  mV/s) but appears to be chemically irreversible at lower scan rates. This phenomenon might be due to the reaction of the radical anion species with traces of oxygen or moisture and/or the formation of ion pairs with the *n*Bu<sub>4</sub>N<sup>+</sup>-cation of the electrolyte. Similar effects have been observed recently for 2,5-diphenyl-1,3,4-oxadiazole.<sup>[67]</sup> However, the reduction of **2** is found to be fully reversible under semi-infinite conditions even at low scan rates. Moreover, a second reduction process can be observed at -2600 mV (see Figure 2.1).

The carbazole substituted oxadiazoles **1–3** are oxidised chemically irreversibly between 900–980 mV (vs. Fc/Fc<sup>+</sup>) in CH<sub>2</sub>Cl<sub>2</sub>/TBAPF<sub>6</sub> with a shoulder at slightly lower potential indicating an additional oxidation process (see Figure 2.2). The two superimposed oxidation signals observed in the cyclic voltammogram are associated with the subsequent oxidation of the two carbazole moieties. In **1** the difference between the two oxidation potentials can be estimated to be  $\Delta E_{\text{ox}} \approx 90$  mV which suggests a rather weak electronic interaction between the two carbazole nitrogen

redox centres. In **2** and **3** the shoulder of the oxidation signal is less pronounced because the distance between the carbazole redox centres is increased with respect to **1** and consequently the electronic interaction is lower.

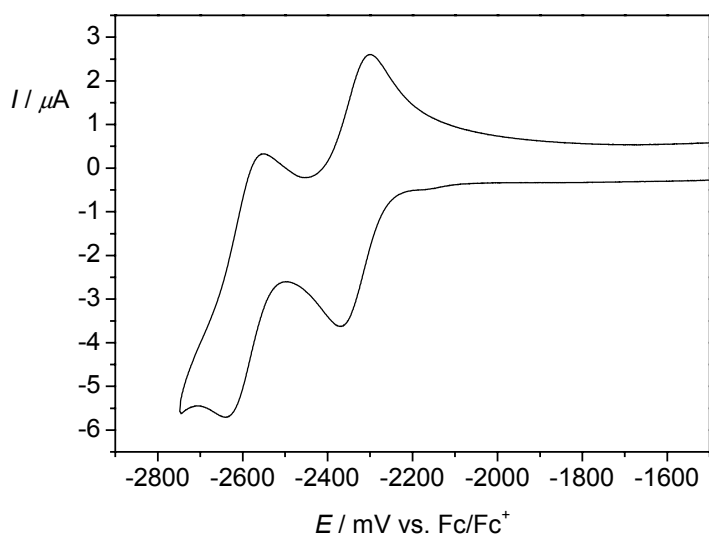


**Figure 2.1:** Cyclic voltammogram of **2** in 0.3 M THF/TBAPF<sub>6</sub>,  $\nu = 250$  mV/s.

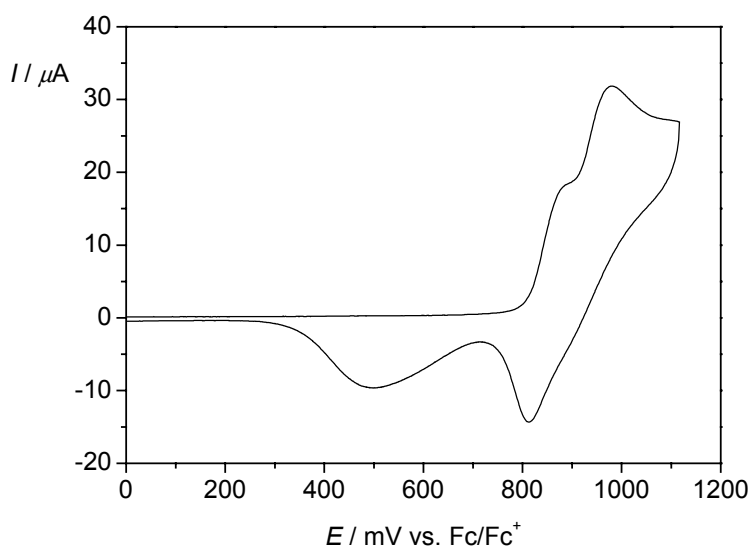


**Figure 2.2:** Cyclic voltammogram of **1** in 0.2 M CH<sub>2</sub>Cl<sub>2</sub>/TBAPF<sub>6</sub>,  $\nu = 100$  mV/s.

When the potential is scanned continuously between 0–1400 mV the peak current increases with each cycle and new redox signals appear at 550–650 mV and

900–950 mV for all three oxadiazoles **1–3**. This clearly indicates the formation of polymers on the electrode surface with 3,3'-carbazole dimers as the bridging unit between the oxadiazole centres (see below). A typical multi-sweep cyclic voltammogram is depicted in Figure 2.3 and a proposed mechanism for the oxidative polymerisation reaction<sup>[51, 68, 69]</sup> is given in Scheme 2.4.

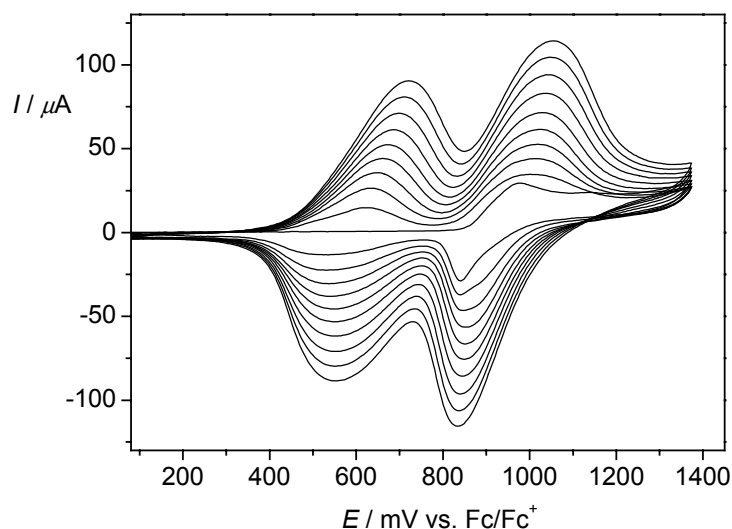
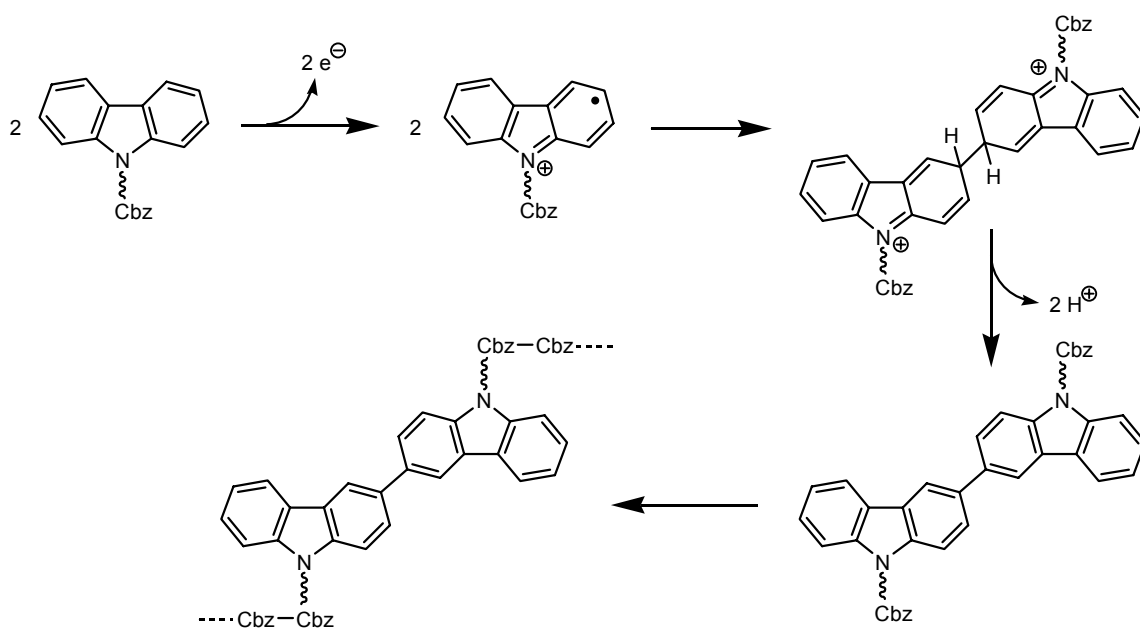


**Figure 2.3:** Multi-sweep cyclic voltammogram of **1** in 0.2 M CH<sub>2</sub>Cl<sub>2</sub>/TBAPF<sub>6</sub>,  $v = 100$  mV/s.



**Scheme 2.4:** Radical-radical coupling mechanism of the polymerisation of *N*-arylcarbazole compounds (Cbz = carbazole).<sup>[51]</sup>

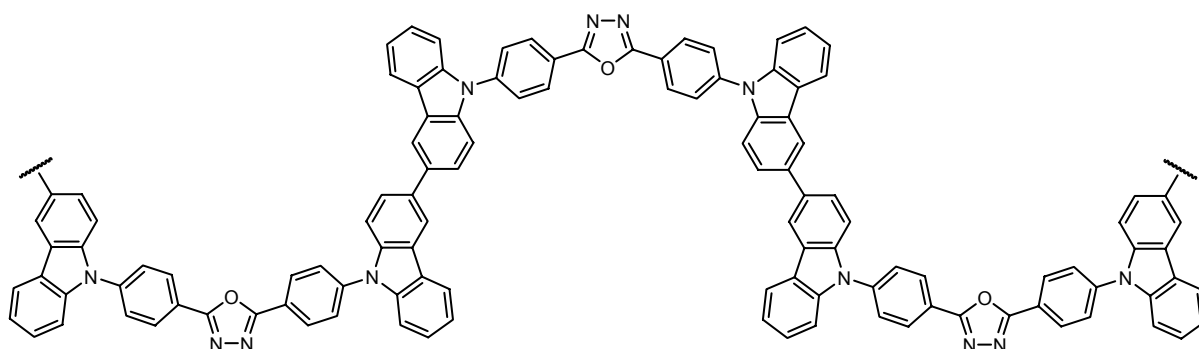
Cyclic voltammetry of the polymers was measured in monomer-free solutions of 0.2 M MeCN/TBAPF<sub>6</sub>. Due to their electron donor and acceptor functionalities all oxadiazole polymers can be both oxidised and reduced electrochemically. The corresponding redox potentials are summarised in Table 2.2.

**Table 2.2:** Redox potentials of the oxadiazole polymers *poly-1*, *poly-2* and *poly-3* (vs. Fc/Fc<sup>+</sup>).<sup>[a]</sup>

	<i>poly-1</i>	<i>poly-2</i>	<i>poly-3</i>
$E_{\text{ox}}^1 / \text{mV}$	740	650	670
$E_{\text{ox}}^2 / \text{mV}$	1030	940	960
$E_{\text{red}} / \text{mV}^{[b]}$	-2360	-2340	-2520 <sup>[c]</sup>

[a] 0.2 M MeCN/TBAPF<sub>6</sub>, [b] chemically irreversible, [c] peak potential of the irreversible reduction.

All polymers *poly-1–poly-3* show two discrete and fully reversible oxidation waves at 650–740 mV and 940–1030 mV in the cyclic voltammogram (Figure 2.4). A comparison with the electrochemical behaviour of end-capped 3,6-linked carbazole dimers and trimers<sup>[70]</sup> suggests, that no oligomeric or polymeric carbazole chains (which should possess broader and more complex oxidation signals) but only dimeric carbazole subunits are present in the polymers. Thus, the structure of the polymers is believed to be as exemplified below for *poly-1*.



The oxadiazole polymers can be reduced chemically irreversible between -2340 mV and -2520 mV (vs. Fc/Fc<sup>+</sup>). For *poly-1–poly-3* the peak current decreases with each additional redox cycle and after ca. 10–15 consecutive cycles the reduction signal disappears completely, while the oxidation signals can still be observed. It can thus be concluded, that during one redox cycle only the oxadiazole moieties are subject to

irreversible degradation whereas the carbazole dimer functionalities remain almost unaffected.

Another interesting feature of the electrochemical behaviour of all oxadiazole polymers *poly-1–poly-3* is provided by the irreversible redox signals at 360–530 mV and between -2040 mV and -2240 mV. When the potential (e. g. for *poly-1*) is scanned between 0–1300 mV several times, the sharp oxidation signal at 530 mV disappears after the first cycle. Upon consecutive reduction a new reduction signal at -2240 mV is observed which again disappears after the first reduction cycle. In the following oxidation scan the signal at 530 mV is recovered. A similar behavior is found for *poly-2* and *poly-3*, but the origin of this “switching” behavior remains obscure.

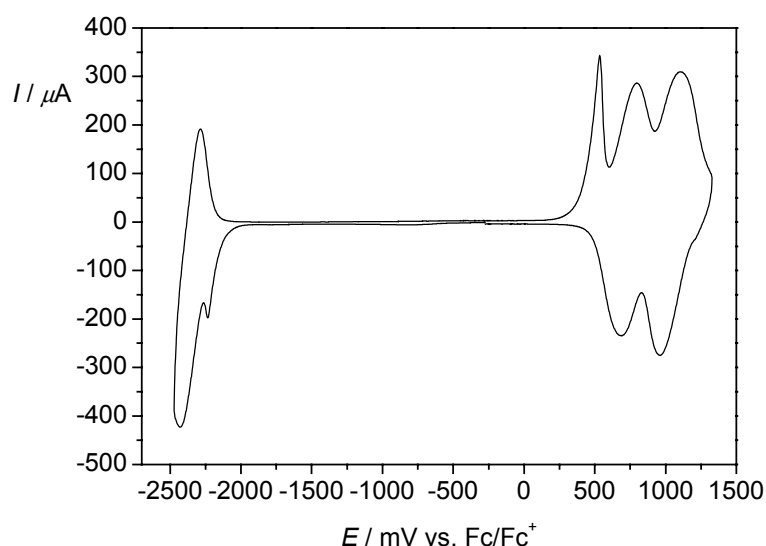


**Figure 2.4:** Cyclic voltammogram of *poly-1* in 0.2 M MeCN/TBAPF<sub>6</sub>,  $v = 250$  mV/s.



### 2.2.3 Spectroelectrochemistry

The spectroelectrochemical behaviour of all oxadiazole polymers *poly-1–poly-3* is nearly identical. Therefore, the spectra for the first and second oxidation of *poly-2* are shown below as a representative example (Figure 2.5).

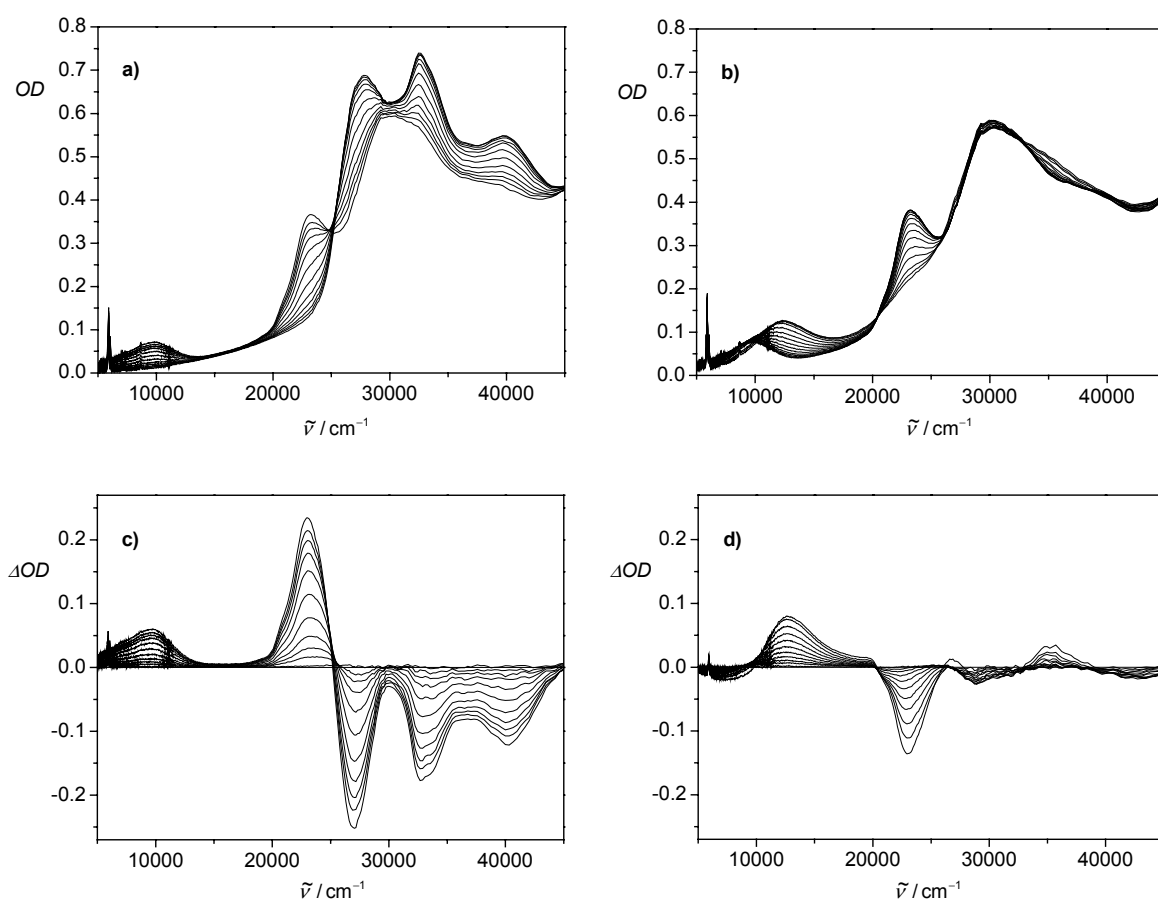
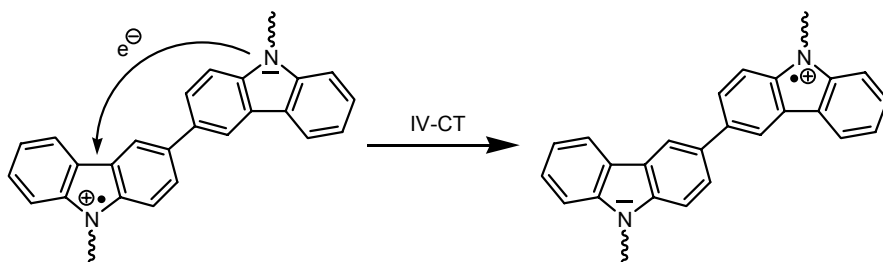


**Figure 2.5:** Spectroelectrochemistry of the first (a) and second (b) oxidation of *poly-2* in 0.2 M  $\text{CH}_2\text{Cl}_2$ . The corresponding difference spectra (c and d) were obtained by subtraction of the starting spectrum (at 0 mV and 800 mV, respectively) from each of the other spectra.

When *poly-2* is oxidised stepwise from 0 mV up to a potential corresponding to the first reversible oxidation wave (at 650 mV, see cyclic voltammetry), two new absorption bands at  $9900\text{ cm}^{-1}$  and  $23100\text{ cm}^{-1}$  can be observed which are characteristic for the radical cation of the *N*-phenylcarbazole-3,3'-dimer.<sup>[71]</sup> Such low-energy bands have often been assigned to polaron or bipolaron states in fully conjugated heterocycle polymers like polypyrrole.<sup>[72-77]</sup> However, in poly(*N*-alkyl-

carbazole)s<sup>[78]</sup> and 9,9'-dimethyl-3,3'-dicarbazolyl tetrafluoroborate<sup>[79]</sup> comparable absorption bands have been attributed to an intermolecular charge transfer between adjacent neutral and charged carbazole diades. In analogy to the structurally related tetraanisylbenzidine radical cation which also exhibits a low-energy transition at ca.  $6400\text{ cm}^{-1}$ ,<sup>[80]</sup> the absorption band at  $9900\text{ cm}^{-1}$  is believed to be due to an optically induced inter-valence charge-transfer (IV-CT) in the benzidine-like carbazole dimer subunits of *poly-2*, i.e. one electron is transferred from a neutral to a positively charged nitrogen atom (Scheme 2.5). The absorption band at  $23100\text{ cm}^{-1}$  might be interpreted in terms of a local HOMO–SOMO or SOMO–LUMO transition (radical band) in the carbazole radical cation units.



**Scheme 2.5:** Inter-valence charge-transfer (IV-CT) in the carbazole-dimer subunit.

When the potential is further increased until it reaches the second oxidation signal of *poly-2* (940 mV) the second nitrogen redox centre of the carbazole dimer subunits is oxidised. Consequently, the intensity of the IV-CT band decreases (Figure 2.5, b and d). The decrease of the IV-CT band is partly hidden due to the superposition of a new increasing absorption band at  $12700\text{ cm}^{-1}$ . Comparable results have been obtained recently for tetraanisylbenzidine and related bistriarylamine compounds.<sup>[80]</sup>

### 2.2.4 Absorption and Emission Spectroscopy

UV/Vis absorption and fluorescence spectra were measured for the oxadiazole compounds **1–3** in solvents of different polarity ranging from C<sub>6</sub>H<sub>12</sub> to MeCN. The corresponding absorption and emission maxima are listed in Table 2.3. With the exception of CH<sub>2</sub>Cl<sub>2</sub> the extinction coefficients could not be determined accurately due to the poor solubility of the oxadiazoles in most of the solvents.

**Table 2.3:** Absorption and fluorescence maxima of **1–3** in solvents of different polarity.

Solvent	$\tilde{\nu}_{\text{abs}} / \text{cm}^{-1}$			$\tilde{\nu}_{\text{fl}} / \text{cm}^{-1}$		
	<b>1</b>	<b>2</b>	<b>3</b>	<b>1</b>	<b>2</b>	<b>3</b>
MeCN	29300	29300	28800	22100	20600	22700
DMSO	29100	29100	28700	21800	20500	22500
CH <sub>2</sub> Cl <sub>2</sub>	29200	29200	28800	23800	22700	23300
THF	29300	29300	28700	24400	23300	23600
EtOAc	29300	29300	29000	24500	23500	24100
MTBE	29400	29200	29000	25300	24500	24500
<i>n</i> Bu <sub>2</sub> O	29300	29100	29000	26600	24600	25900
C <sub>6</sub> H <sub>12</sub>	28700	29400	29000	27100	26400	26300

A low-energy charge transfer (CT) band is observed in the UV/Vis absorption spectra at ca. 29000 cm<sup>-1</sup> for the compounds **1–3** in CH<sub>2</sub>Cl<sub>2</sub> (Figure 2.6). This CT band is superimposed by a local carbazole transition as shown by a comparison with the absorption spectrum of *N*-phenylcarbazole (Figure 2.6, bottom).<sup>[81]</sup>

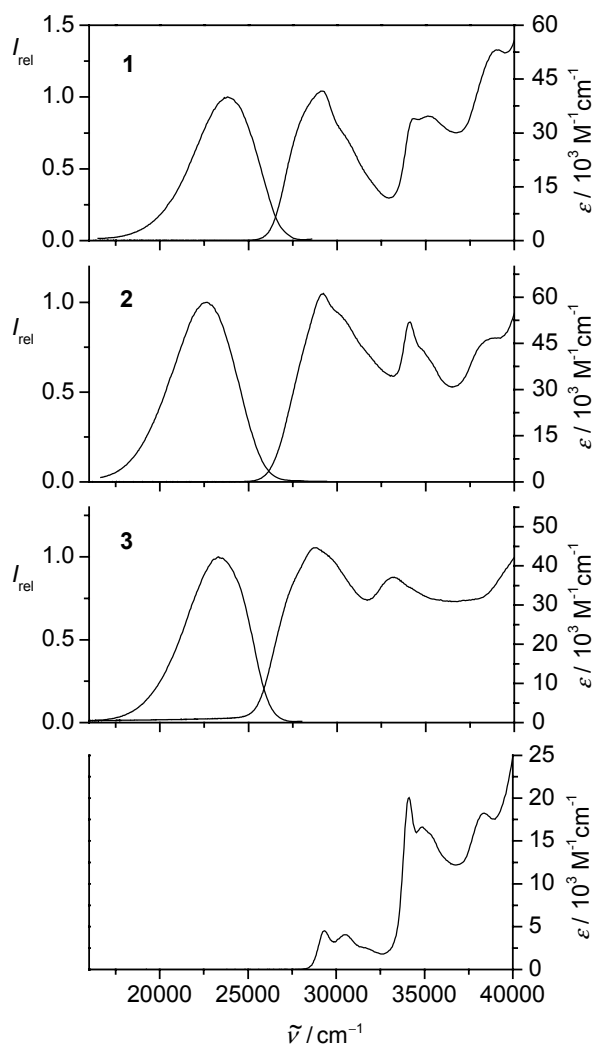


**Figure 2.6:** Absorption and fluorescence spectra of **1–3** and absorption spectrum of *N*-phenylcarbazole (bottom) in  $\text{CH}_2\text{Cl}_2$ .

While the spectral position of the CT absorption band is independent of the solvent polarity, a positive solvatochromic behaviour is observed for the emission of **1–3** (Figure 2.7). This implies that the excited CT state of the donor–acceptor chromophores has a significantly higher dipole moment than the ground state. The difference of the ground- and excited-state dipole moment  $|\Delta\bar{\mu}_{\text{eg}}|$  was estimated for all oxadiazoles **1–3** according to the method of Lippert and Mataga<sup>[82, 83]</sup>. Therefore, the Stokes-shift between the absorption and emission maximum ( $\tilde{\nu}_{\text{abs}} - \tilde{\nu}_{\text{fl}}$ ) in each solvent is plotted against the solvent polarity function

$(D-1)/(2D+1) - (n^2-1)/(2n^2+1)$  with the permittivity  $D$  and the refractive index  $n$  of the solvent (Figure 2.8).

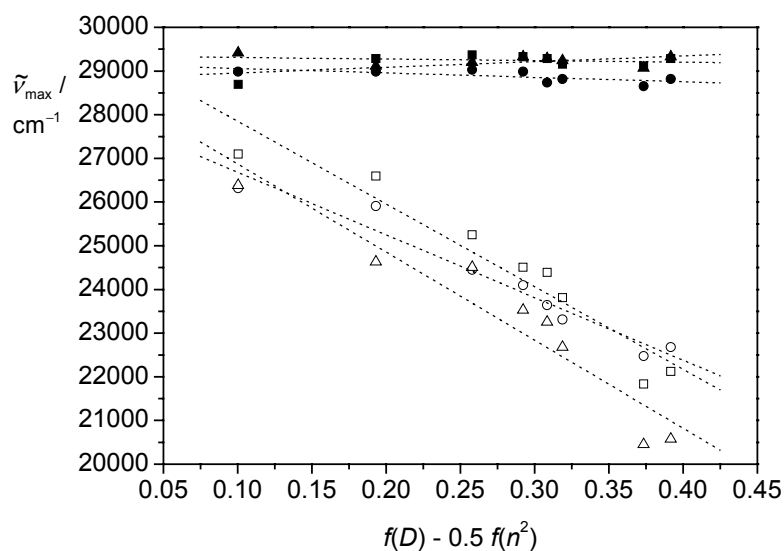


**Figure 2.7:** Absorption (filled symbols) and emission maxima (empty symbols) of **1** (squares), **2** (triangles) and **3** (circles) in solvents of different polarity ( $\text{C}_6\text{H}_{12}$ ,  $n\text{Bu}_2\text{O}$ , MTBE, EtOAc, THF,  $\text{CH}_2\text{Cl}_2$ , DMSO, MeCN).  $f(D) - 0.5f(n^2)$  is the solvent polarity function with  $f(D) = (D-1)/(2D+1)$  and  $f(n^2) = (n^2-1)/(2n^2+1)$ .

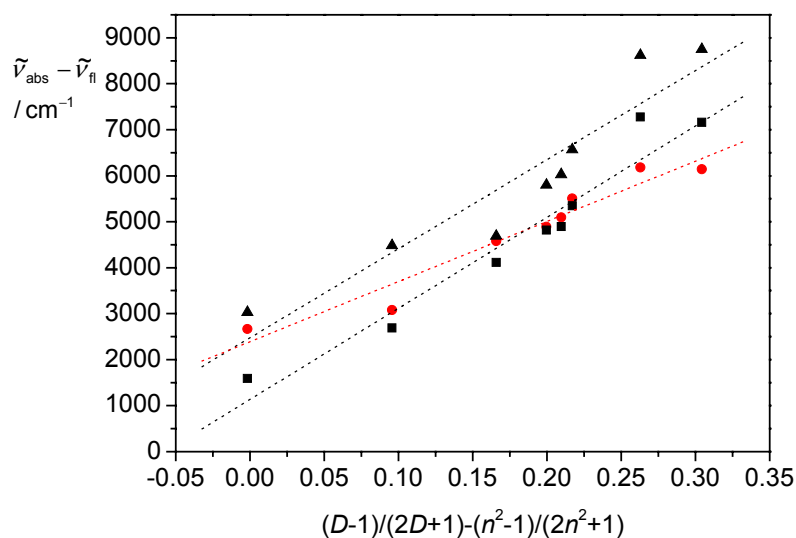


**Figure 2.8:** Plot of the Stokes-shift ( $\tilde{\nu}_{\text{abs}} - \tilde{\nu}_{\text{fl}}$ ) of **1** (squares), **2** (triangles) and **3** (circles) versus the solvent polarity function  $f(D) - f(n^2)$  with  $f(D) = (D-1)/(2D+1)$  and  $f(n^2) = (n^2-1)/(2n^2+1)$ .

The dipole-moment difference  $|\Delta\vec{\mu}_{\text{eg}}|$  can then be calculated from the slope of a linear regression of the corresponding data points using Equation 2-1.

$$hc(\tilde{\nu}_{\text{abs}} - \tilde{\nu}_{\text{fl}}) = hc(\tilde{\nu}_{\text{abs}}^{\text{vac}} - \tilde{\nu}_{\text{fl}}^{\text{vac}}) + \frac{2(\bar{\mu}_{\text{e}} - \bar{\mu}_{\text{g}})^2}{a_0^3} \left[ \frac{D-1}{2D+1} - \frac{n^2-1}{2n^2+1} \right] \quad (\text{eq. 2-1})$$

with the solvent-dependent maxima of the CT absorption and fluorescence ( $\tilde{\nu}_{\text{abs}}$  and  $\tilde{\nu}_{\text{fl}}$ ) and the corresponding values extrapolated to the gas-phase ( $\tilde{\nu}_{\text{abs}}^{\text{vac}}$  and  $\tilde{\nu}_{\text{fl}}^{\text{vac}}$ ). The effective radius of the Onsager cavity<sup>[84]</sup>,  $a_0$ , was obtained by calculating the Connolly solvent-excluded volume from an AM1-optimised geometry of the corresponding chromophore. The radius  $a_0$  was then calculated assuming a spherical volume for each molecule. By this method, the dipole-moment difference  $|\Delta\vec{\mu}_{\text{eg}}|$  between the ground and excited state of the oxadiazoles **1**, **2** and **3** was calculated to be 14 D, 16 D and 13 D, respectively.

## 2.2.5 Conclusions

According to their bipolar nature the oxadiazoles **1–3** can be both oxidised and reduced electrochemically. From the potentiodynamic oxidation of **1–3** it can be concluded that the electronic interaction between the two carbazole redox centres is comparably low, which is thought to arise from a twisted arrangement of the carbazole moieties and the phenylene spacers with respect to the oxadiazole ring. Taking the oxidation and reduction potentials of **1–3** as qualitative measures of the relative HOMO and LUMO energies, respectively, it can be rationalised from  $E_{\text{ox}} - E_{\text{red}}$  that the HOMO–LUMO gap in these compounds is almost identical. This is consistent with the virtually equal spectral positions of the CT absorption bands of **1–3** and suggests a similar electronic interaction of the carbazole donor and the oxadiazole acceptor for all three compounds. However, this is surprising in so far, as

one would expect a decreased interaction in **2** with respect to **1** due to the increased spacer length.

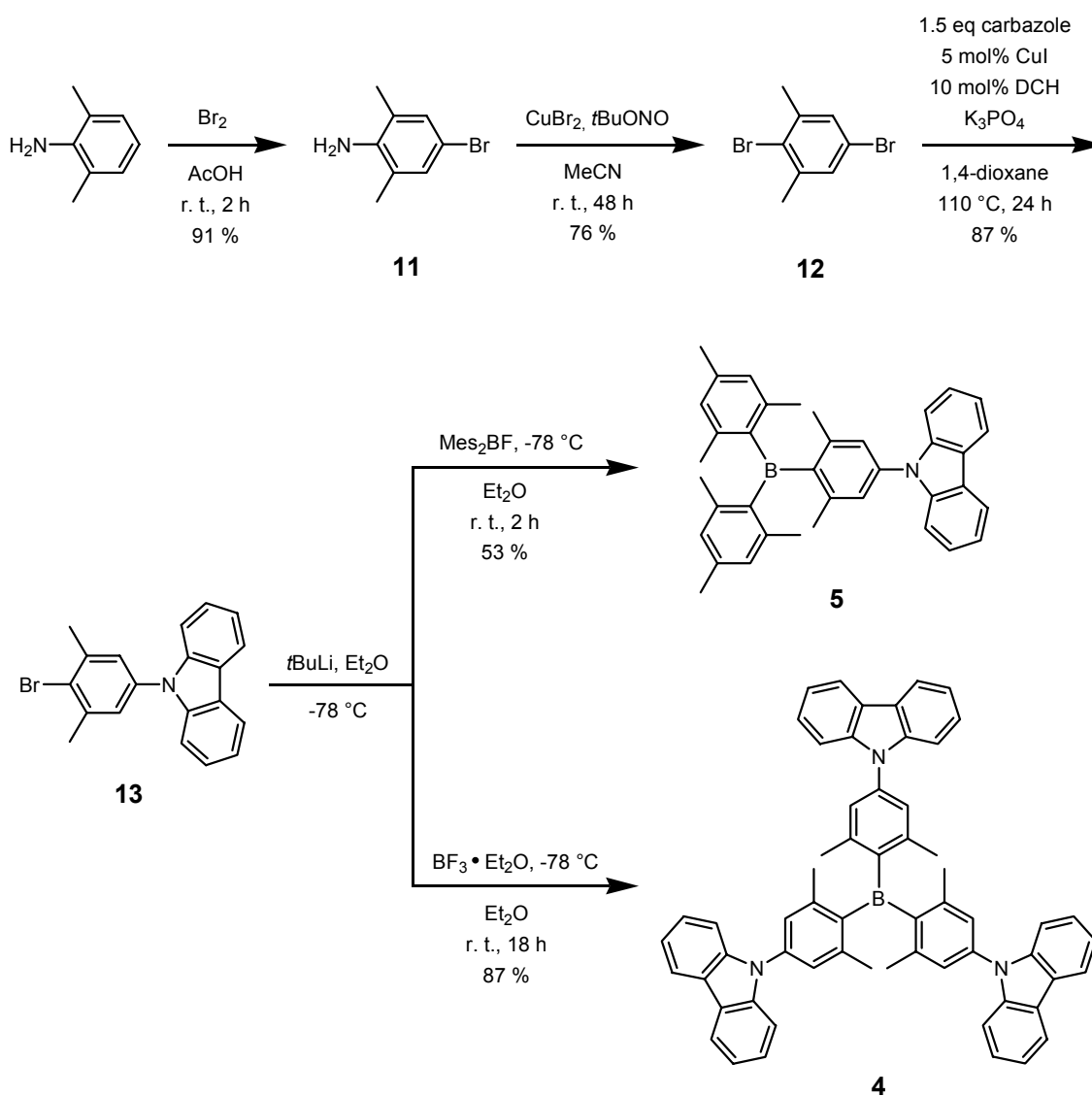
The bipolar nature of the monomers **1–3** is preserved in their corresponding polymers formed upon potentiodynamic oxidation. Although the oxidation of *poly-1–poly-3* is fully reversible, the oxadiazole polymers show only minor stability upon electrochemical n-doping. Moreover, the reduction of *poly-3* is completely irreversible which might be explained by the significantly higher (more negative) reduction potential compared to *poly-1* and *poly-2*. As the cyclic voltammogram of an end-capped 3,6-linked carbazole trimer has been demonstrated to be rather complex in contrast to its dimer analogue (which shows two discrete oxidation waves),<sup>[70]</sup> it can be concluded that in *poly-1–poly-3* the oxadiazole moieties are linked by carbazole dimer units and no oligomeric or polymeric carbazole chains are formed. A comparison of their spectroelectrochemical behaviour with the spectra of the radical cations of tetraanisylbenzidine<sup>[80]</sup> and the 3,3'-dimer of *N*-phenylcarbazole<sup>[71]</sup> further substantiates this hypothesis. Moreover, a dimerisation of the carbazole units instead of polymerisation has also been observed recently for the oxidative chemical polymerisation of 1,8-bis(*N*-carbazolyl)octane.<sup>[85]</sup> It can thus be concluded that the oxadiazole polymers have a linear structure as exemplified for *poly-1* in Section 2.2.2.

The linear optical properties of the oxadiazoles **1–3** are governed by a low-energy CT transition and a highly solvent-dependent fluorescence band. The positive solvatochromism of the emission is due to a high excited-state dipole moment as demonstrated by the Lippert–Mataga plots for the compounds **1–3**. The maxima of the CT absorption bands of **1–3** are independent of the solvent polarity indicating a ground-state polarisation close to zero.

## 2.3 Bipolar Polymers Based on Carbazole-Substituted Triarylboranes

### 2.3.1 Synthesis of the Monomers

The synthesis of TABs **4**, **5** and **6** is outlined in Scheme 2.6 and Scheme 2.7. The bromoaniline **11** was synthesised by bromination of xylidine in glacial acetic acid<sup>[86]</sup> and converted into the dibromo-*m*-xylene **12** in a Sandmeyer-like substitutive deamination reaction with *t*BuONO and CuBr<sub>2</sub>.<sup>[87]</sup>

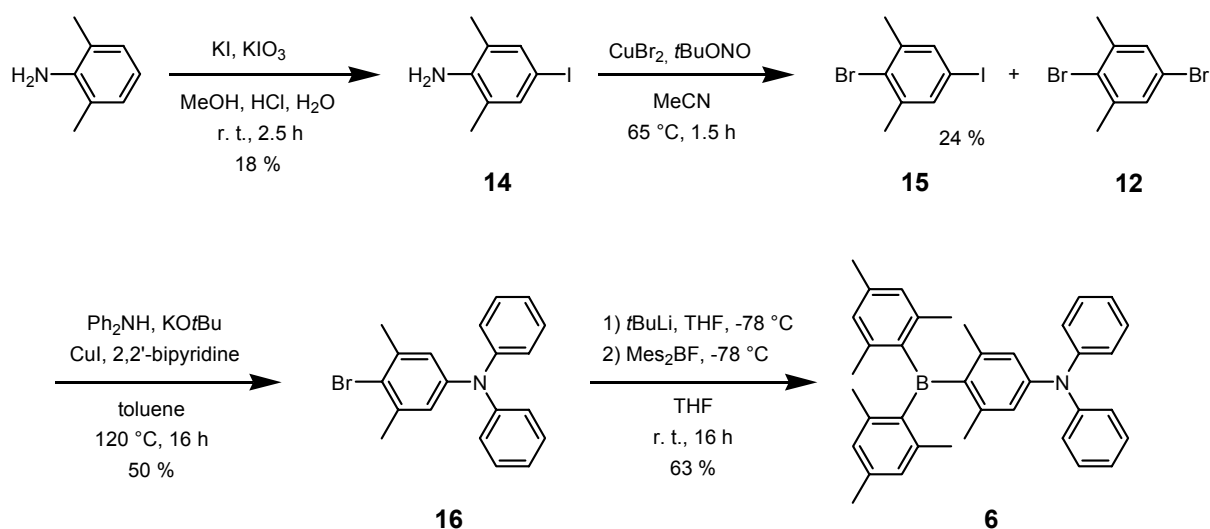


**Scheme 2.6:** Synthesis of the carbazole-substituted triarylboranes **4** and **5**.



The carbazole-substituted precursor **13** was prepared by copper-catalysed amination of **12** with carbazole.<sup>[66]</sup> Conversion into the corresponding aryllithium compound and reaction with either dimesitylboron fluoride or trifluoroborane diethyletherate in the appropriate stoichiometry yielded the TABs **4** and **5**, respectively.

The iodoaniline **14** was synthesised by iodination of xylidine with KI/KIO<sub>3</sub> according to a literature procedure.<sup>[88]</sup> Treatment of **14** with *t*BuONO and CuBr<sub>2</sub><sup>[87]</sup> yielded a 1:1 mixture of the desired bromo-iodo-*m*-xylene (**15**) and the dibromo-*m*-xylene (**12**). This mixture can be directly used in a copper-catalysed amination with diphenylamine to obtain the diphenylamino-substituted precursor **16**.<sup>[89]</sup> TAB **6** was then synthesised by lithiation of **16** with *t*BuLi and subsequent reaction of the aryllithium compound with dimesitylboron fluoride.



**Scheme 2.7:** Synthesis of the diphenylamino-substituted triarylborane **6**.

### 2.3.2 Cyclic Voltammetry

The redox properties of TABs **4–6** were studied by cyclic voltammetry. Due to their donor–acceptor character all compounds can be both oxidised and reduced electrochemically. The corresponding oxidation and reduction potentials are summarised in Table 2.4.

**Table 2.4:** Redox potentials of the TABs **4–6** and *poly-4* (vs. Fc/Fc<sup>+</sup>).

	<b>4</b>	<b>5</b>	<b>6</b>	<i>poly-4</i> <sup>[b]</sup>
$E_{\text{ox}}^1 / \text{mV}$	850 <sup>[a], [d], [e]</sup>	860 <sup>[a], [d]</sup>	470 <sup>[a], [f]</sup>	620
$E_{\text{ox}}^2 / \text{mV}$	-	-	-	830
$E_{\text{red}} / \text{mV}$	-2215 <sup>[c], [f]</sup>	-2480 <sup>[c]</sup>	-2580 <sup>[c], [f]</sup>	-2190 <sup>[f]</sup>

[a] 0.2 M CH<sub>2</sub>Cl<sub>2</sub>/TBAP, [b] 0.2 M MeCN/TBAP, [c] 0.3 M THF/TBAP, [d] peak potential of the irreversible oxidation, [e] shoulder at lower potential indicates multiple oxidation processes, [f] chemically irreversible.

Both redox processes of the diphenylamino-substituted TAB **6** appear to be chemically fully reversible under semi-infinite conditions but are in fact chemically irreversible under thin-layer conditions<sup>[90]</sup> as the peak current decreases upon repetitive potential cycling. Moreover, a second reversible oxidation process occurs at 290 mV in a multi-sweep CV experiment under thin-layer conditions. This indicates the formation of dimers or oligomers of **6** via the unsubstituted *para*-positions of the phenyl rings of the diphenylamino moiety. However, no indication for the formation of polymeric species was found. The reduction potential of **6** (-2.58 V vs. Fc/Fc<sup>+</sup> in THF) is in good agreement with that of [*p*-(dimethylamino)phenyl]dimesitylborane (**27**) (-2.16 V vs. SCE  $\cong$  -2.63 V vs. Fc/Fc<sup>+</sup> in DMF).<sup>[55]</sup> This is surprising in so far, as the  $\pi$ -conjugation between nitrogen and boron should be more effective in **27** because of the lack of two sterically demanding methyl groups. Therefore the electron affinity of **27** should be less than that of **6**. Obviously the N–B  $\pi$ - $\pi$  interaction is not the crucial factor to affect the electrochemical as well as the optical properties in this class of compounds. This is supported by the fact, that the CT absorption of **27** (28200 cm<sup>-1</sup> in C<sub>6</sub>H<sub>12</sub>)<sup>[55, 91]</sup> is significantly higher in energy than that of **6** (25300 cm<sup>-1</sup> in C<sub>6</sub>H<sub>12</sub>;

see below). On the other hand, the maximum of the CT absorption of [*p*-(diphenylamino)phenyl]dimesitylborane (**28**) in C<sub>6</sub>H<sub>12</sub> is found at 26500 cm<sup>-1</sup>.<sup>[33]</sup>

Carbazole-substituted TAB **5** is oxidised irreversibly at 860 mV under semi-infinite conditions and two new redox waves appear at 750 mV and 500 mV upon back reduction (Figure 2.9). This is in good agreement with the results obtained by Heinze et al. for the first oxidation cycle of *N*-phenylcarbazole.<sup>[51]</sup> Upon oxidation of the carbazole moiety the radical cation species form dimers which are immediately oxidised under the applied potential. In the backward scan the reduction of the dimers is observed as two new redox waves. In contrast to *N*-phenylcarbazole which polymerises upon multi-sweep oxidation in CH<sub>3</sub>NO<sub>2</sub>/tetrabutylammonium hexafluorophosphate (TBAPF<sub>6</sub>) to give *poly-N*-phenylcarbazole no such polymerisation was observed for compound **5** in CH<sub>2</sub>Cl<sub>2</sub>/tetrabutylammonium perchlorate (TBAP). This discrepancy most likely has its origin in the different solvent/electrolyte systems or in the higher monomer concentration that was used in case of *N*-phenylcarbazole. Unfortunately, **5** is almost insoluble in CH<sub>3</sub>NO<sub>2</sub> rendering it impossible to measure cyclic voltammetry in this solvent. In contrast to **6** the reduction of **5** is completely reversible even under thin-layer conditions.

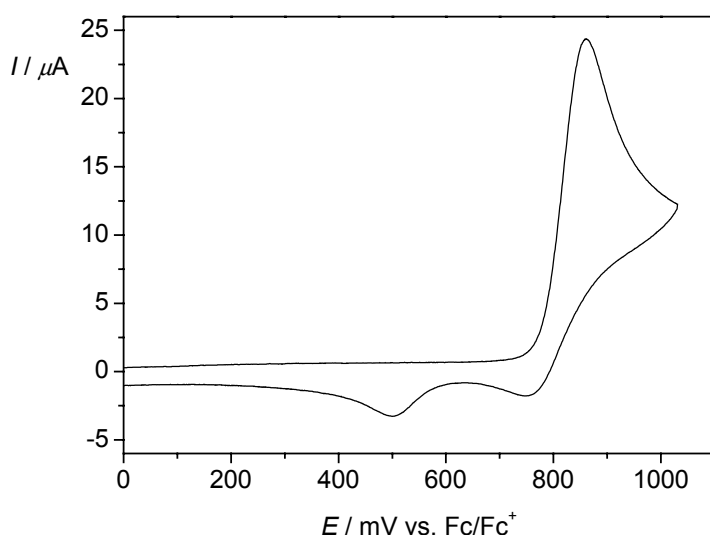


**Figure 2.9:** Cyclic voltammogram of **5** (0.64 mM) in 0.2 M CH<sub>2</sub>Cl<sub>2</sub>/TBAP,  $\nu = 100$  mV/s.

TAB **4** bearing three carbazole moieties is also oxidised irreversibly but upon multi-sweep oxidation the peak current increases with each cycle. Moreover, new

redox signals appear at ca. 500 mV and 780 mV (see Figure 2.10). This clearly indicates the formation of polymers on the electrode surface with 3,3'-carbazole dimers as the bridging unit between the triarylboron centres.

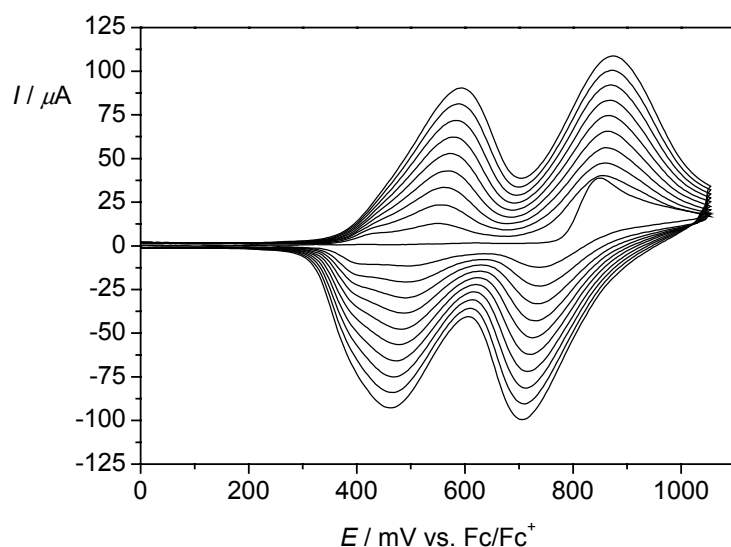


**Figure 2.10:** Multi-sweep CV of **4** (0.41 mM) in 0.2 M CH<sub>2</sub>Cl<sub>2</sub>/TBAP,  $\nu = 100$  mV/s, 10 cycles.

Cyclic voltammetry of *poly-4* was measured in a monomer-free solution of 0.2 M MeCN/TBAP (Figure 2.11). The fact that only two discrete oxidation waves are observed at 620 mV and 830 mV is a further hint that no oligomeric carbazole chains but only carbazole dimer units are present in the polymer (see Section 2.2.2). The reduction of *poly-4* was found to be chemically irreversible as the peak current decreases with each cycle upon multi-sweep reduction. However, only the triarylborane part of the polymer is affected by this degeneration process as the oxidation signals of the carbazole units can still be observed even after several reduction cycles. A similar “switching” behaviour as observed for the oxadiazole polymers *poly-1–poly-3* is provided by the irreversible redox signals at 310 mV and -2040 mV of *poly-4*. When the potential is scanned between 0 mV and 1000 mV several times, the oxidation signal at 310 mV disappears after the first cycle. Upon consecutive reduction a new signal is observed at -2040 mV which again disappears after the first reduction cycle. In the following oxidation scan the signal at 310 mV is recovered. This “switching” behaviour is most likely associated with the carbazole subunits of the polymer as it is observed in both oxadiazole and borane polymers.

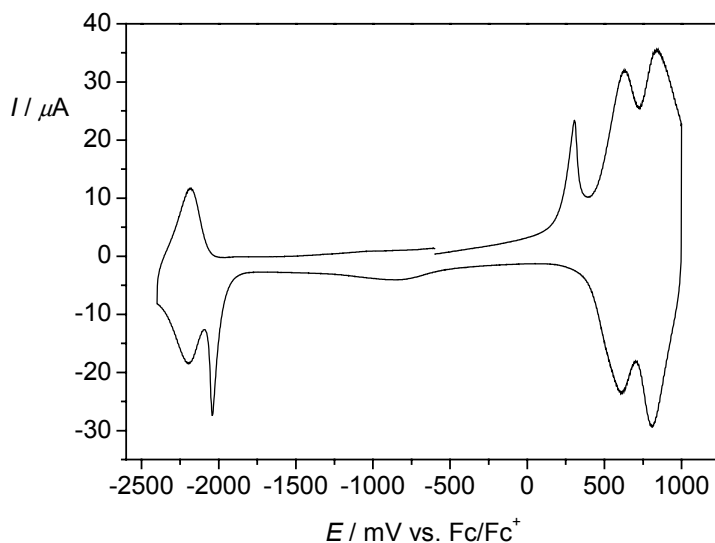


**Figure 2.11:** Cyclic voltammogram of *poly-4* in 0.2 M MeCN/TBAP,  $\nu = 250$  mV/s.

If one compares the reduction potentials of TAB **4** and **5** it surprises that **4** is reduced at 270 mV less negative than **5** although its three donor substituents should diminish the electrophilicity of the boron center. Obviously, the electron deficiency of the boron atom cannot be effectively stabilised by the amino donor because of the propeller-like distortion of the dimethylphenyl rings. Therefore, the inductive electron withdrawing effect of the more electronegative nitrogen atom exceeds its mesomeric donor effect. Hence, each additional carbazole moiety increases the electrophilicity of the boron center. This indicates that the  $\pi$ - $\pi$ -interaction between B and N is rather weak in this type of chromophore, which is also supported by the small ground-state dipole moments (see below).

### 2.3.3 Spectroelectrochemistry

The electrochromic behaviour of *poly-4* upon oxidation was studied by spectroelectrochemical measurements. The results are comparable to those obtained for the oxadiazole polymers *poly-1–poly-3* and the UV/Vis/NIR spectra of the “uncharged”, “semi-charged” and “fully charged” polymer (*poly-4*, *poly-4*<sup>n+</sup>, *poly-4*<sup>2n+</sup>) are given in Figure 2.12.

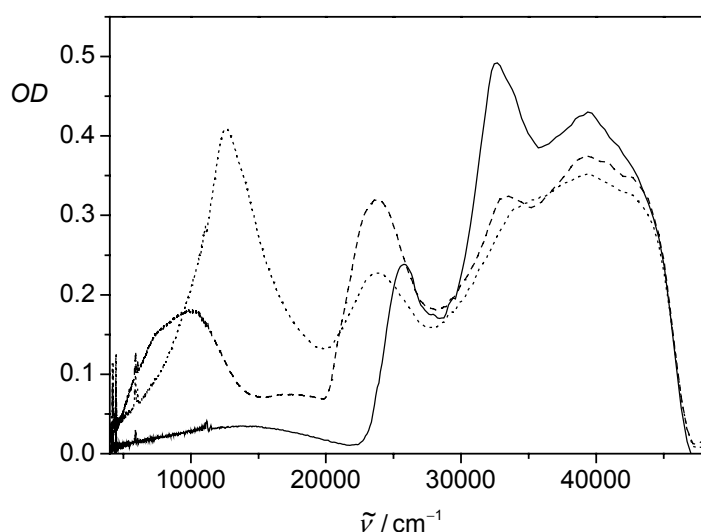


**Figure 2.12:** UV/Vis/NIR spectra of *poly-4* at 0 mV (solid line), at 620 mV (dashed line) and at 830 mV (dotted line).

In analogy to its oxadiazole pendants the “semi-charged” polymer (at the first oxidation at  $E = 620$  mV) exhibits a low-energy IV-CT absorption band at ca.  $10000\text{ cm}^{-1}$  and an additional band at  $23700\text{ cm}^{-1}$ . As expected an increase of the potential up to the second oxidation signal ( $E = 830$  mV) is accompanied by a decrease of the IV-CT band. Moreover, the emergence of a new absorption band at  $12600\text{ cm}^{-1}$  can be observed.

### 2.3.4 Absorption and Emission Spectroscopy

The UV/Vis absorption spectra of the TABs **4**, **5** and **6** are characterised by a low-energy charge transfer band at  $26000\text{ cm}^{-1}$ ,  $27600\text{ cm}^{-1}$  and  $25300\text{ cm}^{-1}$  in  $\text{C}_6\text{H}_{12}$  respectively (Figure 2.13).

The carbazole-substituted TABs **4** and **5** exhibit a very intense narrow absorption band at about  $34100\text{ cm}^{-1}$  with the molar extinction coefficient of **4** being about three times as high as that of **5**. This band can be attributed to a local carbazole transition. Furthermore, the CT absorption band of **5** is shifted to higher wavenumbers with respect to **4** which leads to a superposition of the CT absorption band and the carbazole bands at  $29400\text{ cm}^{-1}$  and  $30700\text{ cm}^{-1}$ .

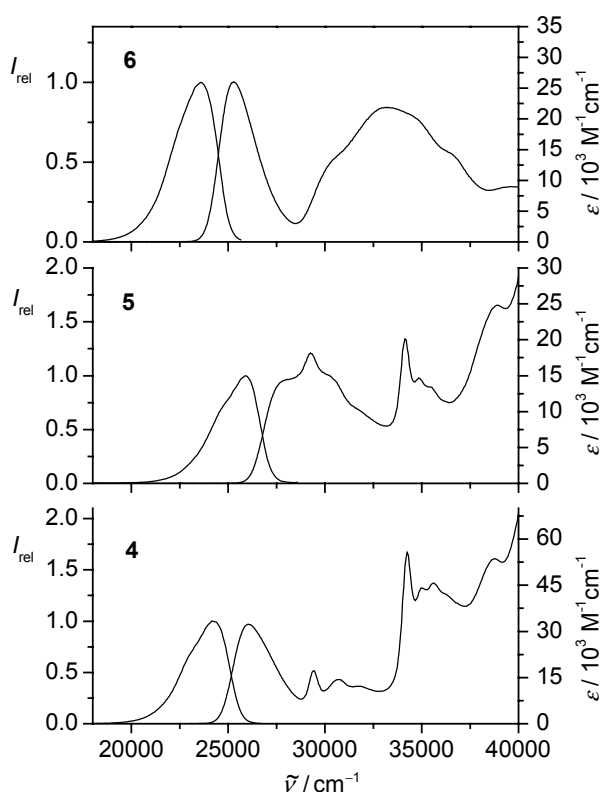
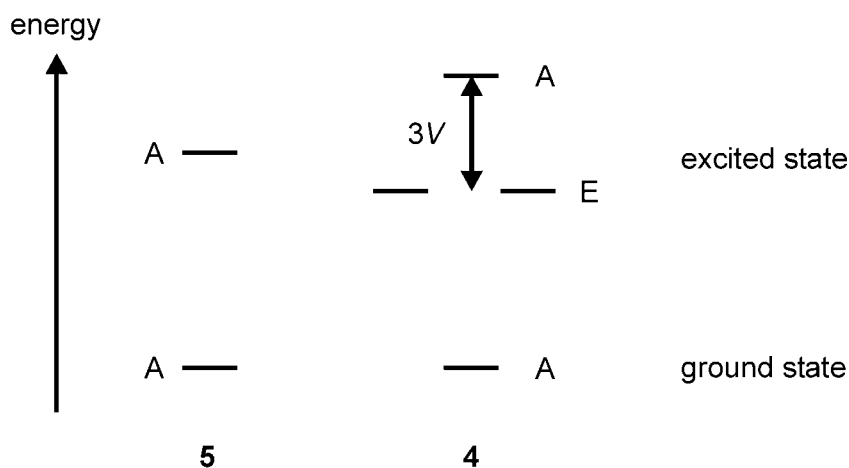


**Figure 2.13:** UV/Vis absorption and emission spectra of **4–6** in  $\text{C}_6\text{H}_{12}$ .

Similar effects have been observed recently for tricyanovinyl-substituted triaryl amines and were explained in terms of electronic coupling between the subchromophores of the molecules.<sup>[92]</sup> If one presumes  $D_3$  symmetry for **4** the dipole–dipole interaction

between the transition moments of the subchromophores of **4** leads to a splitting of the excited states into a degenerate *E* state and an *A* state as outlined in Scheme 2.8.<sup>[93]</sup>



**Scheme 2.8:** Excited-state splitting of **4** with respect to **5**. The coupling integral  $V$  is a measure for the electronic interaction between the subchromophores in **4**.

This interaction is associated with an exchange of excitation energy from one subchromophore to another.<sup>[93]</sup> Provided that the orbital overlap of the three subchromophores of **4** is weak, the coupling integral  $V_{pq}$  between the transition moments of the subchromophores  $p$  and  $q$  can be approximated by the point-dipole–point-dipole model<sup>[93]</sup> (Equation 2-2) within the framework of the exciton coupling theory.<sup>[93-95]</sup>

$$V_{pq} = \mu_{0a}^{(p)} \mu_{0a}^{(q)} R_{pq}^{-3} \{ \mathbf{e}_p \cdot \mathbf{e}_q - 3(\mathbf{e}_p \cdot \mathbf{e}_{pq})(\mathbf{e}_q \cdot \mathbf{e}_{pq}) \} \quad (\text{eq. 2-2})$$

In Equation 2-2  $\mu_{0a}^{(p)}$  and  $\mu_{0a}^{(q)}$  denote the transition moments of the subchromophores  $p$  and  $q$ , respectively. The parameter  $R_{pq}$  defines the distance between the centres of the two transition moments and was calculated as the distance between the midpoints of two B–N distances (5.0 Å) of an AM1-optimised geometry of **4**;  $\mathbf{e}_p$ ,  $\mathbf{e}_q$  and  $\mathbf{e}_{pq}$  denote the unit vectors of  $\mu_{0a}^{(p)}$ ,  $\mu_{0a}^{(q)}$  and  $R_{pq}$ , respectively. Taking the transition moment of the model compound **5** (3.30 D) as the corresponding value for  $\mu_{0a}^{(p)}$  and  $\mu_{0a}^{(q)}$ , a value of  $V_{pq} \approx 800 \text{ cm}^{-1}$  (in  $\text{C}_6\text{H}_{12}$ ) was calculated for **4** which is in qualitative agreement with the observed shift of the CT absorption band of



$\Delta\tilde{\nu} = 1600 \text{ cm}^{-1}$  in the same solvent. It should be noted, that the exciton coupling theory can only provide a rough approximation of  $V$  as small changes in  $R_{\text{pq}}$  have an enormous impact on the calculated value of  $V$ . Moreover, the estimation of  $\mu_{0a}$  of the single chromophore **5** bears some inaccuracy as will be discussed below.

UV/Vis absorption and fluorescence spectra of the TABs **4**, **5** and **6** were measured in a series of solvents with different polarity ranging from  $\text{C}_6\text{H}_{12}$  to MeCN. The corresponding absorption and fluorescence maxima are summarised in Table 2.5.

**Table 2.5:** Absorption and fluorescence maxima of **4–6** in solvents of different polarity.

Solvent	$\tilde{\nu}_{\text{abs}} / \text{cm}^{-1} (\epsilon / 10^3 \text{ M}^{-1} \text{ cm}^{-1})$			$\tilde{\nu}_{\text{fl}} / \text{cm}^{-1}$		
	<b>4</b>	<b>5</b> <sup>[a]</sup>	<b>6</b>	<b>4</b>	<b>5</b>	<b>6</b>
MeCN	27200 (17.5)	29500 (13.3)	25800 (19.8)	20100	21800	19300
DMSO	26900 (22.9)	29100 (20.1)	25400 (18.2)	19700	21900	19500
$\text{CH}_2\text{Cl}_2$	26900 (25.6)	29000 (15.2)	25600 (18.5)	21800	23300	20600
THF	26700 (25.8)	28900 (16.7)	25400 (20.6)	21600	23300	21100
EtOAc	26800 (25.9)	28900 (15.6)	25700 (20.6)	21700	23600	21100
MTBE	26500 (26.6)	28600 (15.0)	25500 (21.4)	22400	24400	21800
$n\text{Bu}_2\text{O}$	26400 (29.9)	28300 (17.0)	25400 (22.7)	23400	25000	22700
$\text{C}_6\text{H}_{12}$	26000 (30.5)	27600 (13.5)	25300 (26.0)	24200	25900	23600

[a] Extinction coefficients of **5** were estimated from the mirror image of the corresponding reduced fluorescence spectra (see below).

For all compounds the emission band shows a pronounced positive solvatochromism with increasing solvent polarity (Figure 2.14) which is due to a large excited-state dipole moment of the fluorescent state. On the other hand, the maximum of the CT absorption band of all three TABs is marginally shifted to higher energies with increasing solvent polarity (negative solvatochromism).

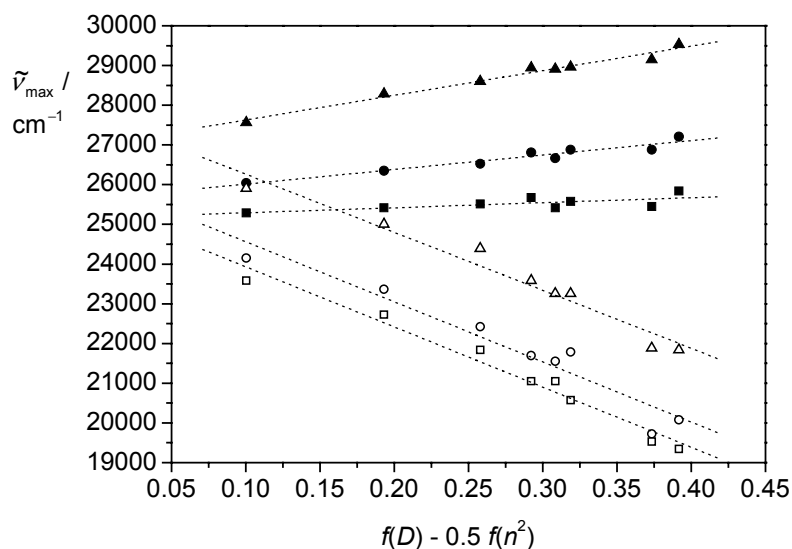


**Figure 2.14:** Absorption (filled symbols) and emission maxima (empty symbols) of **4** (circles), **5** (triangles) and **6** (squares) in solvents of different polarity ( $C_6H_{12}$ ,  $nBu_2O$ , MTBE, EtOAc, THF,  $CH_2Cl_2$ , DMSO, MeCN).  $f(D) - 0.5 f(n^2)$  is the solvent polarity function with  $f(D) = (D - 1)/(2D + 1)$  and  $f(n^2) = (n^2 - 1)/(2n^2 + 1)$ .

Similar effects have been reported for the fluorescence of related donor-substituted tridurylboranes, however, no solvatochromism was found for the absorption of these chromophores.<sup>[96, 97]</sup> It is interesting to note, that in the study of Yamaguchi et al.<sup>[96]</sup> a hypsochromic shift of approximately  $1200\text{ cm}^{-1}$  was also observed between the amino-substituted tris(phenylethynyl)durylborane and its one-dimensional linear analogue. This phenomenon was explained by the authors in terms of the extended  $\pi$ -conjugation of the two-dimensional chromophore, but may also have similar reasons (exciton coupling) as discussed above for the TABs **4** and **5**.

An unusual negative solvatochromic behaviour, as observed for the absorption of the TABs **4–6**, has been reported before for acceptor-substituted carbazole derivatives<sup>[98, 99]</sup> and may have different reasons: a) the ground-state dipole moment  $\bar{\mu}_g$  is larger than the excited-state dipole moment  $\bar{\mu}_e$ , b)  $\bar{\mu}_g$  and  $\bar{\mu}_e$  have opposite directions or c) the ground-state dipole moment cannot be treated as a point-dipole situated in the centre of the Onsager cavity<sup>[84]</sup> which would be a prerequisite for the validity of the Onsager–Lippert–Mataga model.<sup>[84, 99]</sup> Possibility a) would be in contrast to the solvent dependence of the emission which suggests a large excited-state dipole moment. In the case of the  $C_2$  symmetric molecules **5** and **6** c) seems to

be unlikely as well because both  $\bar{\mu}_g$  and  $\bar{\mu}_e$  should be located on the long axis of symmetry between the boron and nitrogen atom and should therefore lie in the centre of the Onsager cavity. Hence, the requirements for the validity of the Onsager–Lippert–Mataga model should be fulfilled. In order to validate possibility b) the CT absorption bands of the TABs **4** and **6**<sup>[100]</sup> were analysed using Jortner’s theory.<sup>[101-103]</sup> This model combines an average molecular vibration which is treated quantum-mechanically with a classical solvent coordinate.<sup>[104]</sup> The parameters for the inner-sphere and outer-sphere reorganisation energy ( $\lambda_v$  and  $\lambda_o$ , respectively) as well as the parameters for the average molecular vibrational mode  $\tilde{\nu}_v$  and the difference of the free energy between the diabatic ground and excited state  $\Delta G^{00}$  (Equation 2-3) were obtained from least-squares fits of the CT absorption bands of **4** and **6** in different solvents.

$$\varepsilon = \frac{8N\pi^3}{3000h \ln 10} n \tilde{\nu} \mu_{eg}^2 \sum_{j=0}^{\infty} \frac{e^{-S} S^j}{j!} \sqrt{\frac{1}{4\pi\lambda_o RT}} \exp\left[-\frac{(j\tilde{\nu}_v + \lambda_o - \tilde{\nu} + \Delta G^{00})^2}{4\pi\lambda_o RT}\right] \quad (\text{eq. 2-3})$$

with the Huang–Rhys factor  $S = \frac{\lambda_v}{\tilde{\nu}_v}$

A typical fit of the CT absorption band of **6** is depicted in Figure 2.15. In Figure 2.16 the resulting parameters are plotted against the solvent polarity function  $(D - 1)/(2D + 1) - 0.5 (n^2 - 1)/(2n^2 + 1)$ , in which  $D$  and  $n$  denote the permittivity and the refractive index of the solvent, respectively.

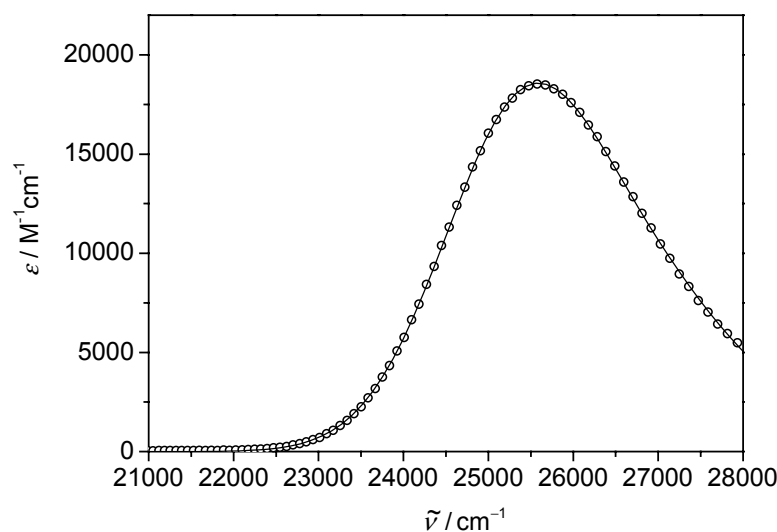


**Figure 2.15:** Typical Jortner-fit (solid line) of the CT absorption band of **6** in  $\text{CH}_2\text{Cl}_2$  (circles).

As expected from the positive solvatochromism of the emission,  $\Delta G^{00}$  of **4** and **6** decreases with increasing solvent polarity due to the highly polar nature of the excited state. Concomitantly, an increase of the solvent reorganisation energy  $\lambda_o$  with the solvent polarity is observed. It can be rationalised from Figure 2.16 that in the case of **6**  $\Delta G^{00}$  is slightly overcompensated by  $\lambda_o$  which gives a direct explanation for the weak hypsochromic shift of the CT absorption band described above. In the case of **4** the difference between the absolute values of the slopes of  $\Delta G^{00}$  and  $\lambda_o$  is even higher and thus the negative solvatochromism of **4** is more pronounced (see Figure 2.14). The inner-sphere reorganisation energy  $\lambda_v$  has only a weak but systematic solvent dependence for both compounds with a positive slope for **4** and a negative slope for **6** (see Figure 2.16). However, the energy of the average molecular vibrational mode  $\tilde{\nu}_v$  slightly increases for both **4** and **6** with increasing solvent polarity.

Additionally, the dipole moments of the ground state and the differences between the ground- and excited-state dipole moments of the TABs **4**, **5** and **6** were estimated by electrooptical absorption measurements (EOAM) in 1,4-dioxane as previously described.<sup>[105]</sup> The results are summarised in Table 2.6.

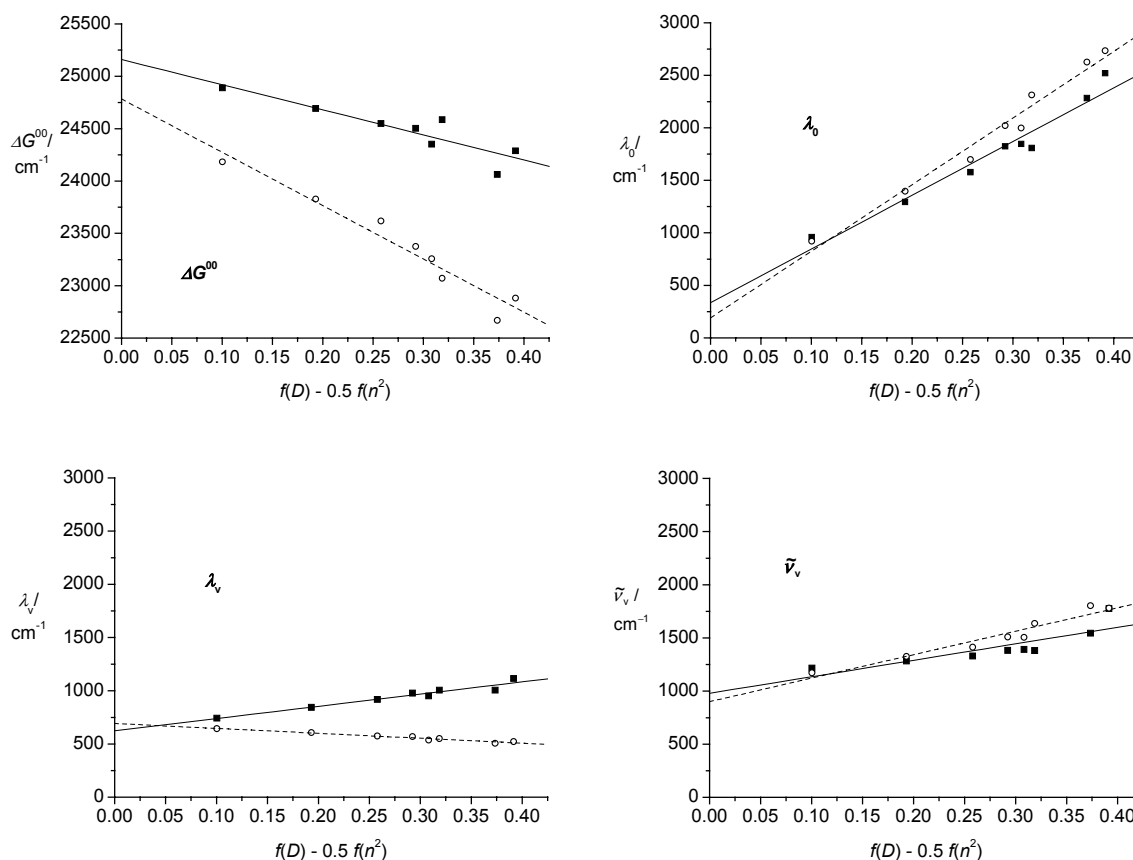


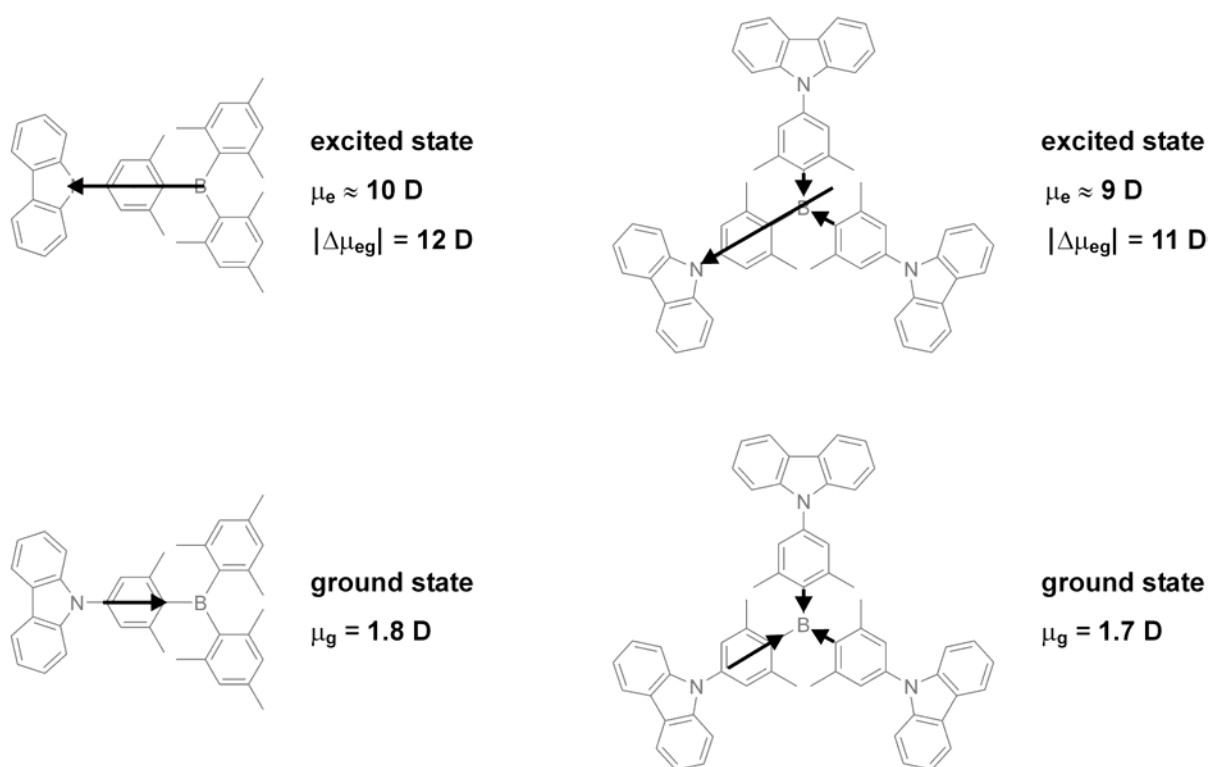
**Figure 2.16:** Plots of  $\Delta G^{00}$ ,  $\lambda_0$ ,  $\lambda_v$  and  $\tilde{\nu}_v$  versus the solvent polarity function  $f(D) - 0.5 f(n^2)$  for **4** (filled squares) and **6** (open circles) with  $f(D) = (D - 1)/(2D + 1)$  and  $f(n^2) = (n^2 - 1)/(2n^2 + 1)$ .

**Table 2.6:** Adiabatic dipole moments of the ground state and the differences between the adiabatic ground- and excited-state dipole moments of **4**, **5** and **6** estimated by electrooptical absorption measurements (EOAM).

	<b>4</b>	<b>5</b>	<b>6</b>
$\bar{\mu}_g / D$ ( $10^{-30}$ Cm)	1.7 (5.6) $\pm 0.06$ (0.2)	1.8 (6.1) $\pm 0.27$ (0.9)	0.57 (1.9) $\pm 0.15$ (0.5)
$ \Delta\bar{\mu}_{eg}  / D$ ( $10^{-30}$ Cm)	11 (37) $\pm 0.18$ (0.6)	12 (40) $\pm 1.1$ (3.7)	11 (36) $\pm 0.84$ (2.8)

For the TABs **5** and **6** the EOAM reveal a ground-state dipole moment of  $\bar{\mu}_g = 1.8$  D and  $\bar{\mu}_g = 0.6$  D respectively and a dipole-moment difference of  $|\Delta\bar{\mu}_{eg}| = 11$ – $12$  D. Comparable values for the ground-state dipole moments of both compounds **5** and **6**

were obtained by AM1-calculations ( $\bar{\mu}_g = 1.8$  D and  $\bar{\mu}_g = 0.4$  D, respectively) with the dipole vector pointing from the nitrogen (negative end) to the boron (positive end). That means that upon excitation of **5** and **6** the direction of the dipole-moment vector reverses (see Scheme 2.9) because charge is transferred from the nitrogen to the boron centre. As a consequence the solvent molecules have an energetically very unfavourable orientation after excitation into the Franck–Condon state causing a distinct increase of the outer-sphere reorganisation energy  $\lambda_o$  especially in polar solvents. This, in turn, causes the observed negative solvatochromism as discussed above.



**Scheme 2.9:** Schematic representation of the ground- and excited-state dipole moments of **5** and **4**. The length of the arrows is not to scale with the absolute values of the dipole moments.

Relatively small ground-state dipole moments have been reported earlier by Marder et al. for related donor–phenyl–B(Mes)<sub>2</sub> compounds like [*p*-(dimethylamino)phenyl]-dimesitylborane (**27**) ( $\bar{\mu}_g = 3.0$  D).<sup>[106, 107]</sup> However, a positive solvatochromic behaviour was observed for the CT-absorption band of **27**, which implies that—in contrast to **5** and **6**—the dipole-moment vector is not reversed but retains its original

direction upon excitation of **27**. It can thus be concluded that in the sterically less hindered chromophore **27** the ground-state polarisation is dominated by mesomeric effects leading to a charge-separated quinoidal character with a (partially) negative boron and a positive nitrogen. In **5** and **6**, because of the less effective  $\pi$ -conjugation, the ground-state polarisation is mainly influenced by inductive effects, i.e. boron is a  $\sigma$ -donor and nitrogen is a  $\sigma$ -acceptor. This leads to an inversed orientation of the ground-state dipoles in the TABs **5** and **6** with respect to **27**.

For the two-dimensional TAB **4** a more sophisticated explanation of the experimental results is needed. The ground-state dipole moment of  $\bar{\mu}_g = 1.7$  D estimated by EOAM suggests a lower symmetry than  $D_3$  in the ground state (Scheme 2.9) where two branches of the molecule contribute only marginally to the overall ground-state dipole moment. This unsymmetrical contribution of the three subchromophores of **4** might be caused by different torsion angles of the carbazole planes with respect to the phenyl rings leading to a smaller ground-state polarisation in two of the three branches. If one assumes that the charge-transfer excitation is mainly localised on one branch of the molecule (which is supported by the high excited-state dipole moment, see above) and that the contribution of the other two branches can be neglected, the overall excited-state dipole moment will be governed by the excited-state dipole moment of only one subchromophore. Furthermore, it seems very likely that an excitation also leads to a dipole inversion in this subchromophore as calculated for the model compound **5**. This dipole inversion in one subchromophore will presumably cause an increase in the outer-sphere reorganisation energy  $\lambda_o$  which is thought to be the reason for the negative solvatochromism of the CT absorption band of the three TABs **4–6**.

For comparison, the difference of the ground- and excited-state dipole moment  $|\Delta\bar{\mu}_{eg}|$  was estimated according to the method of Lippert and Mataga<sup>[82, 83, 108]</sup> for all TABs **4–6**. Therefore, the Stokes-shift between the absorption and emission maximum ( $\tilde{\nu}_{abs} - \tilde{\nu}_{fl}$ ) in each solvent is plotted against the solvent polarity function  $(D - 1)/(2D + 1) - (n^2 - 1)/(2n^2 + 1)$ . The dipole-moment difference  $|\Delta\bar{\mu}_{eg}|$  can then be calculated from the slope of a linear regression of the corresponding data points using Equation 2-1 (see above). The effective radius of the Onsager cavity,  $a_o$ , was

obtained by calculating the Connolly solvent-excluded volume from an AM1-optimised geometry as outlined for the oxadiazoles **1–3**. By this method, the dipole-moment difference  $|\Delta\bar{\mu}_{\text{eg}}|$  between the ground and excited state of the TABs **4**, **5** and **6** was calculated to be 17 D, 15 D and 14 D, respectively. These values are in good agreement with those estimated by EOAM, taking into account that  $|\Delta\bar{\mu}_{\text{eg}}| \propto a_0^3$  and therefore small changes in  $a_0$  have an enormous impact on  $|\Delta\bar{\mu}_{\text{eg}}|$ . However, the estimation of  $a_0$  is to a certain extent arbitrary.<sup>[82, 84]</sup>

The transition moments of the CT absorption of the TABs **4**, **5** and **6** were calculated from the integrals of the reduced absorption bands in each solvent according to Equation 2-4<sup>[109]</sup>

$$\mu_{\text{eg}}^2 = \frac{3hc\varepsilon_0 \ln 10}{2000\pi^2 N} \frac{9n}{(n^2 + 2)^2} \int \varepsilon / \tilde{\nu} d\tilde{\nu} \quad (\text{eq. 2-4})$$

with the refractive index  $n$  and the molar extinction coefficient  $\varepsilon$ .

In the case of TAB **5**—because the CT absorption band of **5** is superimposed by a local carbazole transition—the integral  $\int \varepsilon / \tilde{\nu} d\tilde{\nu}$  was determined with the help of the reduced fluorescence spectrum under the assumption, that the reduced absorption and fluorescence spectra exhibit a mirror image relationship<sup>[109]</sup> (Figure 2.17). It should be noted here that this method implies some inaccuracy, because the intensity of the fluorescence has to be adjusted in order to fit the CT absorption band. For comparison, the transition moments of the fluorescence were calculated from the fluorescence rate constants  $k_f$  (see below) using the Strickler–Berg relationship<sup>[110]</sup> (Equation 2-5)

$$\mu_{\text{fl}}^2 = \frac{3h\varepsilon_0}{16 \times 10^6 \pi^3} \frac{9}{n(n^2 + 2)^2} \frac{g_e}{g_g} \frac{\int \tilde{\nu}^{-3} I_f d\tilde{\nu}}{\int I_f d\tilde{\nu}} k_f \quad (\text{eq. 2-5})$$

with  $n$  being the refractive index of the solvent and  $g_e$  and  $g_g$  being the degeneracy of the excited state and the ground state, respectively.  $I_f$  denotes the intensity of the



fluorescence against the wavenumber ( $I_f = I_\lambda \times \lambda^2$ ). The resulting transition moments of the absorption and fluorescence are summarised in Table 2.7.

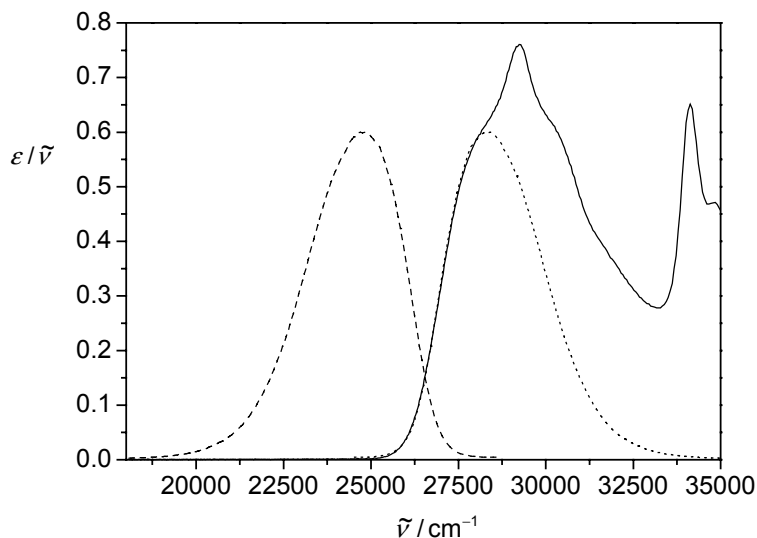


**Figure 2.17:** Reduced absorption (solid line) and fluorescence (dashed line) spectra of **5** in  $n\text{Bu}_2\text{O}$ . The integral of the reduced absorption band  $\int \epsilon / \tilde{\nu} d\tilde{\nu}$  was calculated from the mirror image of the reduced fluorescence spectrum (dotted line).

**Table 2.7:** Transition moments of the CT absorption and fluorescence of the TABs **4**, **5** and **6**.

Solvent	$\mu_{\text{eg}} / \text{D}$			$\mu_{\text{fl}} / \text{D}$		
	<b>4</b>	<b>5</b>	<b>6</b>	<b>4</b>	<b>5</b>	<b>6</b>
MeCN	3.82	3.91	4.34	4.47	4.41	4.11
DMSO	4.43	4.53	3.95	4.52	4.76	4.08
$\text{CH}_2\text{Cl}_2$	4.72	3.82	3.99	4.54	4.62	4.10
THF	4.81	4.02	4.12	4.88	4.80	4.59
EtOAc	4.88	3.92	4.19	4.68	5.05	4.64
MTBE	4.86	3.73	4.16	5.29	5.06	4.30
$n\text{Bu}_2\text{O}$	5.00	3.90	4.14	5.55	4.94	4.53
$\text{C}_6\text{H}_{12}$	4.71	3.30	4.14	5.95	5.47	4.75

In a molecular aggregate of  $N$  identical subchromophores,  $\mu_{\text{eg}}^2$  (which is proportional to the oscillator strength) should be  $N$  times as high as in the single

chromophore, provided that the electronic interaction between the subchromophores is weak.<sup>[111]</sup> However, comparison of the  $\mu_{\text{eg}}^2$  values of **5** (as the single chromophore) and **4** (as the trimer of **5**) reveals that  $\mu_{\text{eg}}^2$  of **4** is only 1–2 times as high as  $\mu_{\text{eg}}^2$  of **5**. This discrepancy supports the above-stated suggestion that in **4** two of the chromophore branches are twisted, which should lead to a significantly decreased absorption intensity and consequently to lower  $\mu_{\text{eg}}^2$  values.

Differences between  $\mu_{\text{eg}}^2$  and  $\mu_{\text{fl}}^2$  of a chromophore can be regarded as an indication for a structural relaxation between the absorption and the emission process. For the amino-substituted TAB **6**  $\mu_{\text{fl}}^2$  is only somewhat higher than  $\mu_{\text{eg}}^2$  suggesting only a small structural reorganisation. In the case of the carbazole-substituted TABs **4** and **5**  $\mu_{\text{fl}}^2$  is significantly higher than  $\mu_{\text{eg}}^2$  especially in solvents of low polarity. This is evidence for a distinct structural relaxation which is thought to arise from a rotation of the carbazole moiety around the phenyl C–N bond.

The fluorescence quantum yield of the TABs **4–6** was determined in a series of solvents of different polarity (see Table 2.8). All TABs exhibit rather high fluorescence quantum yields as expected for this type of donor–acceptor chromophore.<sup>[30]</sup> An unexpected solvent dependence is observed especially for TAB **5**, for which  $\Phi_{\text{f}}$  increases significantly with increasing solvent polarity. This phenomenon can be explained by a decrease of  $k_{\text{nr}}$  as determined from fluorescence decay measurements (see below). However, from the solvent dependence of the fluorescence (decreasing emission energy with increasing solvent polarity) one would expect an opposite behaviour, because a lowering of  $\Delta G^{00}$  should cause an increase of  $k_{\text{nr}}$  (energy gap law<sup>[112]</sup>) and consequently a decrease of  $\Phi_{\text{f}}$  with increasing solvent polarity.

**Table 2.8:** Fluorescence quantum yields  $\Phi_f$ , fluorescence lifetimes  $\tau$  and rate constants for the fluorescent and nonradiative deactivation processes,  $k_f$  and  $k_{nr}$  of the TABs **4**, **5** and **6**.

Solvent	<b>4</b>			<b>5</b>			<b>6</b>					
	$\Phi_f$	$\tau / 10^{-9} \text{ s}$	$k_f / 10^8 \text{ s}^{-1}$	$k_{nr} / 10^7 \text{ s}^{-1}$	$\Phi_f$	$\tau / 10^{-9} \text{ s}$	$k_f / 10^8 \text{ s}^{-1}$	$k_{nr} / 10^7 \text{ s}^{-1}$	$\Phi_f$	$\tau / 10^{-9} \text{ s}$	$k_f / 10^8 \text{ s}^{-1}$	$k_{nr} / 10^7 \text{ s}^{-1}$
MeCN	0.58	11.1	0.521	3.82	0.94	7.14	1.31	0.869	0.82	10.3	0.794	1.78
DMSO	0.67	9.88	0.677	3.35	- <sup>[a]</sup>	6.55	- <sup>[a]</sup>	- <sup>[a]</sup>	1.00	9.64	1.03	- <sup>[b]</sup>
CH <sub>2</sub> Cl <sub>2</sub>	0.45	5.56	0.806	9.92	0.83	4.05	2.05	4.24	1.00	9.11	1.10	- <sup>[b]</sup>
THF	0.50	5.79	0.856	8.73	0.82	3.82	2.15	4.67	1.00	7.11	1.41	- <sup>[b]</sup>
EtOAc	0.44	5.83	0.751	9.64	0.80	3.52	2.27	5.71	1.00	7.44	1.34	- <sup>[b]</sup>
MTBE	0.41	3.84	1.06	15.4	0.63	2.53	2.48	14.8	0.96	7.47	1.29	0.533
<i>n</i> Bu <sub>2</sub> O	0.36	2.61	1.40	24.4	0.54	1.99	2.71	23.3	0.89	5.19	1.71	2.18
C <sub>6</sub> H <sub>12</sub>	0.39	2.08	1.86	29.5	0.62	1.65	3.78	22.8	0.77	3.54	2.18	6.43

[a] fluorescence quantum yield not measurable; [b]  $k_{nr} < 10^5 \text{ s}^{-1}$ .

### 2.3.5 Time-resolved Fluorescence Spectroscopy

The fluorescence lifetimes  $\tau$  of the TABs **4**, **5** and **6** were determined by fluorescence decay measurements in a series of solvents with different polarity ranging from C<sub>6</sub>H<sub>12</sub> to MeCN. In Figure 2.18 the fluorescence decay of **4** in DMSO and the corresponding mono-exponential fit are illustrated.

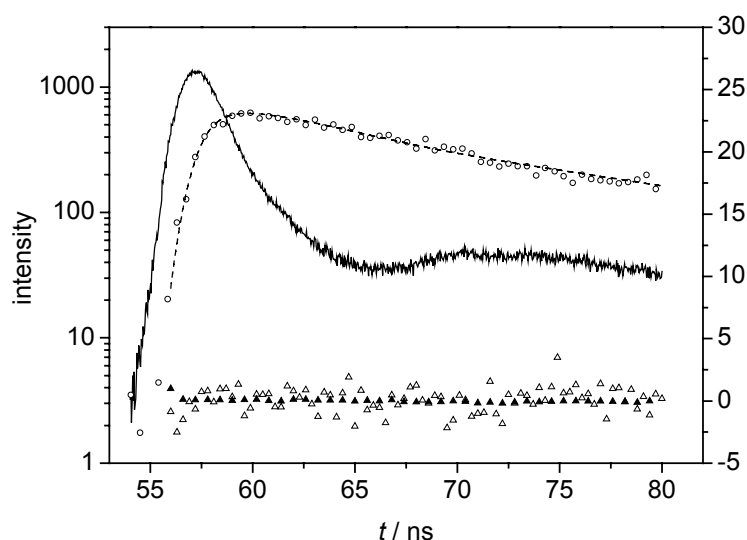


**Figure 2.18:** Fluorescence decay (empty circles), mono-exponential fit (dotted line) and instrument response (solid line) of **4** in DMSO. The residuals (empty triangles) and the autocorrelation (filled triangles) are a measure for the quality of the fit.

The rate constants for the fluorescent and nonradiative deactivation processes,  $k_f$  and  $k_{nr}$ , were calculated according to the Equations 2-6 and 2-7.

$$k_f = \frac{\Phi_f}{\tau} \quad (\text{eq. 2-6})$$

$$k_{nr} = \frac{1}{\tau} - k_f \quad (\text{eq. 2-7})$$

The results are summarised in Table 2.8. All compounds exhibit fluorescence lifetimes in the range of 2–10 ns with a pronounced solvent dependence. Surprisingly,  $\tau$  increases with decreasing emission energy (increasing solvent

polarity). Accordingly, an opposite behaviour is also found for  $k_{nr}$  which decreases with decreasing emission energy. The origin of this unexpected behaviour remains unclear. The solvent dependence of  $k_f$  (decreasing with decreasing emission energy) is in qualitative agreement with the Strickler–Berg equation (see above) which predicts a relationship of  $k_f \propto \tilde{\nu}_f^3$ .

### 2.3.6 Polarised Steady-State Fluorescence Spectroscopy

Fluorescence-anisotropy measurements were performed on the carbazole-substituted TABs **4** and **5** in a sucrose-octaacetate (SOA) matrix at room temperature. SOA, which has a polarity similar to  $n\text{Bu}_2\text{O}$ , is known to form a rigid glass after melting and cooling<sup>[113]</sup> thus hindering rotational diffusion of the solute. This is a prerequisite to measure the limiting anisotropy  $r_0$  which is related to the angle  $\beta$  between the transition moments of the absorption and emission. From Equation 2-8 a maximum anisotropy of 0.40 is obtained for a parallel orientation of the transition moments ( $\beta = 0^\circ$ ) whereas for perpendicular orientation ( $\beta = 90^\circ$ ) the minimum value is -0.20.<sup>[114]</sup>

$$r_0 = 0.4 \frac{3 \cos^2 \beta - 1}{2} \quad (\text{eq. 2-8})$$

The results of the fluorescence-anisotropy measurements are given in Figure 2.19. The emission anisotropy of the  $C_2$  symmetric compound **5** is constant over the whole wavelength region, which means that only one transition ( $S_1 \rightarrow S_0$ ) contributes to the emission band. The excitation anisotropy is low for the high-energy transition at  $34100 \text{ cm}^{-1}$ , indicating that the transition moments of the absorption and emission are not collinear. This is not surprising, as the absorption process at this spectral position is associated with a local carbazole transition involving a completely different transition-moment vector than for the emissive CT state. For lower excitation energies the anisotropy increases and reaches a maximum value of 0.30 at the low-

energy side of the absorption spectrum ( $S_0 \rightarrow S_1$  transition). At this spectral position the excitation and emission involve the same electronic transition resulting in a parallel orientation of the corresponding transition moments. The fact, that the excitation anisotropy does not reach the theoretical maximum value of 0.40 may indicate that there is still a small contribution from higher-energy (carbazole) transitions due to the overlap of the corresponding absorption bands (Figure 2.13).

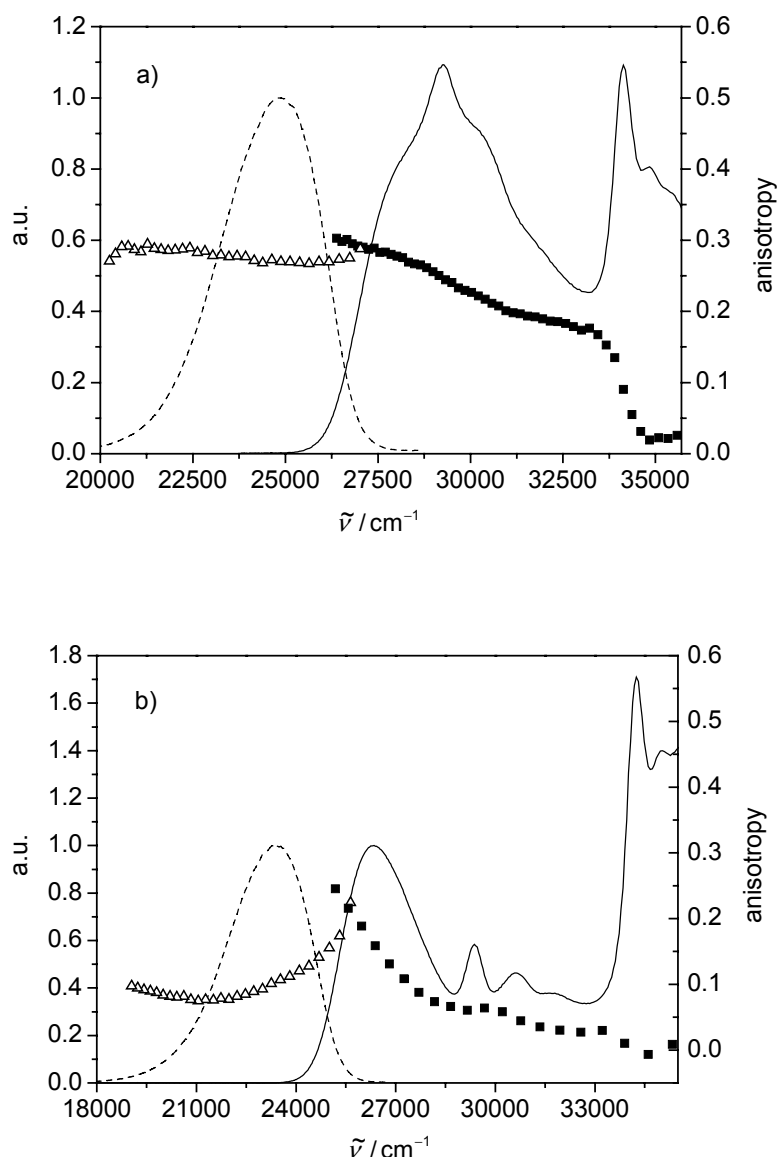
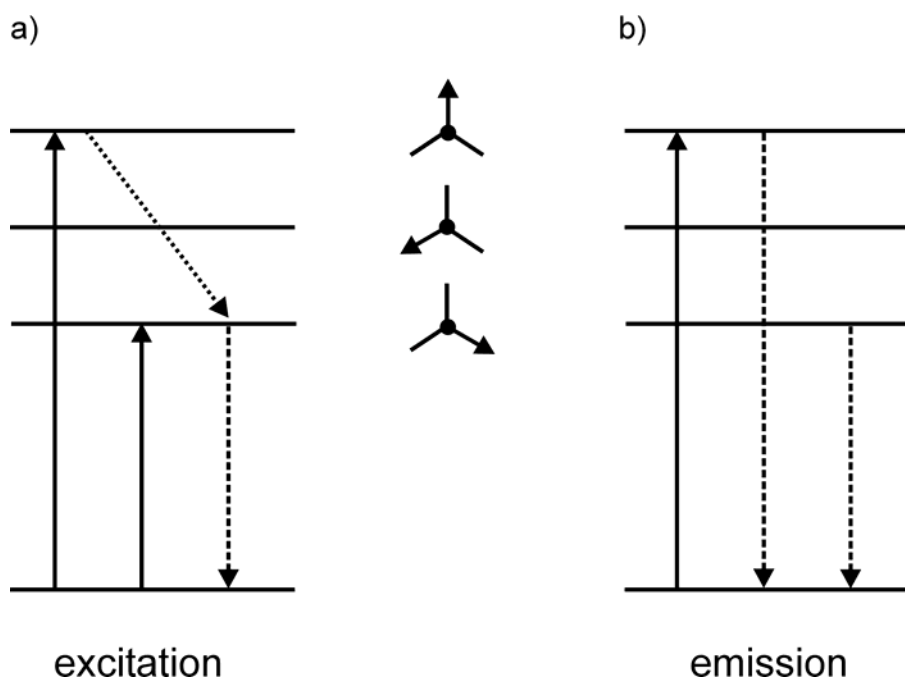


**Figure 2.19:** Anisotropy of the excitation (filled squares) and the emission (empty triangles) of a) **5** and b) **4** in a sucrose-octaacetate matrix at room temperature. The corresponding nonpolarised absorption (—) and emission (---) spectra of **5** and **4** in  $n\text{Bu}_2\text{O}$  are added for comparison.

In case of the  $D_3$  symmetric TAB **4** the excitation anisotropy is low ( $< 0.1$ ) over a wide spectral range but increases significantly for the low-energy CT transition. This red-edge excitation effect has been observed before<sup>[115, 116]</sup> and is due to an intramolecular excitation transfer between the three chromophore subunits of **4** in combination with symmetry breaking of the molecule. For molecules with a three-fold symmetry (e.g. triphenylene) where the transition moments are arranged within one plane, the additivity law of anisotropy yields a value of  $r_0 = 0.1$ .<sup>[117]</sup> This is, because after excitation the energy can be transferred among the three branches and the emission may occur from each of the three degenerate excited states with the same probability but with different transition-dipole orientations. In cases where the symmetry of the molecule is broken and, hence, the formerly degenerate states are split, the emission will preferably occur from that branch with the lowest excited-state energy (Scheme 2.10, a)) provided that the energy transfer is fast within the excited-state lifetime. The consequence of this dipole-relaxation process is that for higher excitation energies the absorption and emission processes involve electronic transitions with different transition-dipole orientations resulting in a low anisotropy. On the other hand, if the excitation occurs on the low-energy side of the spectrum, the energy transfer to other branches would be an uphill process. Therefore, absorption and emission involve the same transitions with identical dipole orientations resulting in an increase of the anisotropy. This phenomenon has already been observed and described in detail by De Schryver and co-workers.<sup>[116]</sup>

For the emission anisotropy an almost mirror-image behaviour with respect to the excitation anisotropy is observed (Figure 2.19). On the low-energy side of the fluorescence spectrum the emission anisotropy is small and increases towards higher emission frequencies. This wavelength dependence also gives rise to time-dependent relaxation processes<sup>[114]</sup> and can be explained in a similar way (Scheme 2.10, b)). As the excitation occurs at the high-energy side of the spectrum ( $27000\text{ cm}^{-1}$ ) it can be assumed that the energetically higher-lying states are excited with a higher probability. At higher emission energies predominantly that part of the emission is observed which originates from the higher-energy excited states. In this case the transition-dipole orientations of the absorption and emission are parallel, resulting in a high anisotropy value. At lower energies the emission of the relaxed

states is detected and hence absorption and emission involve different transition-dipole orientations. Therefore, the anisotropy decreases. In agreement with the estimated ground-state dipole moment of **4** the anisotropy measurements also show that **4** adopts an asymmetric structure in SOA in the ground state.



**Scheme 2.10:** Proposed electronic transitions and transition-dipole orientations of the non-degenerate excited states in **4** upon symmetry breaking. a) excitation anisotropy at a fixed emission wavelength; b) emission anisotropy at fixed excitation wavelength.

It should be noted, that for the excitation anisotropy of triphenylene contrary results have been reported in literature. Leroy and Lami observed an increase of the anisotropy upon red-edge excitation of triphenylene in glycerol at 203 K.<sup>[118]</sup> This phenomenon has been explained in terms of intramolecular excitation-transfer in combination with symmetry breaking of the molecule. Hall, Valeur and Weber however, were not able to reproduce these results.<sup>[117]</sup> They observed a constant value of the excitation polarisation of  $p_0 = 0.136$  (similar to  $r_0 = 0.095$ ) in a propylene glycol matrix at  $-70^\circ\text{C}$  without any red-edge excitation effect. In order to check the validity of the interpretation of our experimental results we also determined the anisotropy of triphenylene in a sucrose-octaacetate matrix at room temperature. We tried to stick as close as possible to the procedures described by Hall, Valeur and



Weber; especially the purification of triphenylene was done accurately. Surprisingly, we observed the same effect as Leroy and Lami. This leads us to the assumption, that the glass matrix plays a critical role in these experiments, as it may have a great impact on the symmetry of the solute.

### 2.3.7 Solid-State Fluorescence of *poly-4* on ITO-coated Glass

Fluorescence spectroscopy was measured for a film of *poly-4* deposited on an ITO-coated glass substrate by potentiodynamic electropolymerisation. The fluorescence spectrum of *poly-4* is depicted in Figure 2.20 together with an absorption spectrum of the polymer on a platinum disc electrode obtained from the spectroelectrochemistry measurements.

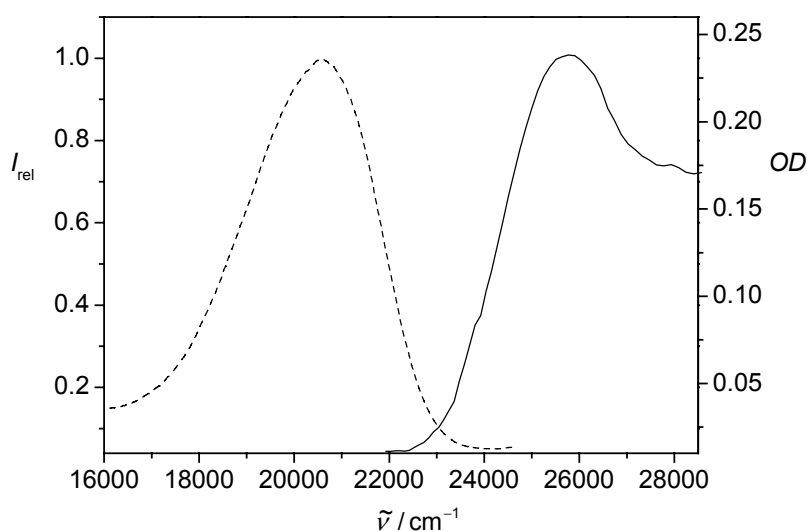


**Figure 2.20:** Absorption spectrum (solid line) of a *poly-4* film on a platinum disc electrode (Figure 2.12) and corresponding fluorescence of a *poly-4* film on an ITO-coated glass substrate.

An intense fluorescence band is observed at  $20600 \text{ cm}^{-1}$  upon optical excitation of *poly-4*. This emission energy is comparable to those of the monomeric TAB **4** in polar solvents like MeCN or DMSO.

### 2.3.8 Titration of TAB 4 with Fluoride Ions

It is known that lewis acidic trialkyl- and triarylboranes are easily attacked by nucleophiles leading to the formation of tetra-coordinate organoborates. However, if the boron atom is surrounded by sterically demanding substituents like mesityl or anthryl it can only be attacked by very small nucleophiles like the fluoride ion. It has been demonstrated recently that trianthryl- and trimesitylborane derivatives can effectively bind fluoride ions with a high selectivity compared to other anions like  $\text{AcO}^-$ ,  $\text{OH}^-$ ,  $\text{Cl}^-$  or  $\text{Br}^-$ .<sup>[119-121]</sup> Moreover, this binding process can be fully reversed by the addition of water or stronger fluoride scavengers like  $\text{BF}_3 \cdot \text{Et}_2\text{O}$ . This makes trianthryl- and trimesitylborane derivatives highly potent candidates for selective fluoride-ion sensing applications.

A solution of TAB 4 in THF ( $46.8 \mu\text{M}$ ) was titrated with a 1.0 mM solution of tetrabutylammonium fluoride (TBAF) in THF. As the addition of fluoride to the boron atom of 4 leads to a decrease of the CT absorption band the complexation reaction can easily be monitored by UV/Vis spectroscopy (Figure 2.21).

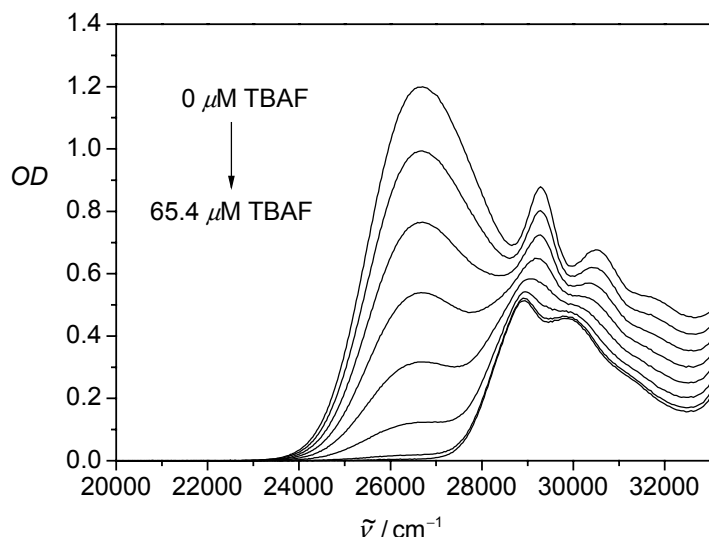


**Figure 2.21:** UV/Vis spectra of the titration of TAB 4 ( $46.8 \mu\text{M}$ ) with fluoride ions.

The binding constant  $K_b$  of the complexation reaction was determined by Levenberg–Marquardt least-squares fitting of the experimental spectra with the global-analysis

software SPECFIT/32™.<sup>[122]</sup> A value of  $\log K_b = 5.58 \pm 0.11$  was obtained for a 1:1 complex of **4** and  $F^-$  corresponding to  $K_b = 3.78 \times 10^5 \text{ M}^{-1}$ . This is in excellent agreement with previously reported values for trianthrylboranes ( $K_b \approx 3 \times 10^5 \text{ M}^{-1}$ ) and related dibenzoboroles ( $K_b \approx 1 \times 10^6 \text{ M}^{-1}$ ).<sup>[119, 120]</sup> As expected, the CT absorption band of TAB **4** is fully restored by the addition of water probably because of the strong  $\text{HO-H}\cdots\text{F}^-$  hydrogen-bond.

### 2.3.9 X-Ray Structure Analysis of TAB **4**

Single crystals of **4** were obtained by slow evaporation of a  $\text{CDCl}_3$  solution and analysed by single crystal X-ray diffraction. Crystallographic data of the single crystal and selected bond lengths and angles of the molecular structure of **4** are summarised in Table 2.9 and Table 2.10, respectively. A plot of the molecular structure of **4** is depicted in Figure 2.22.

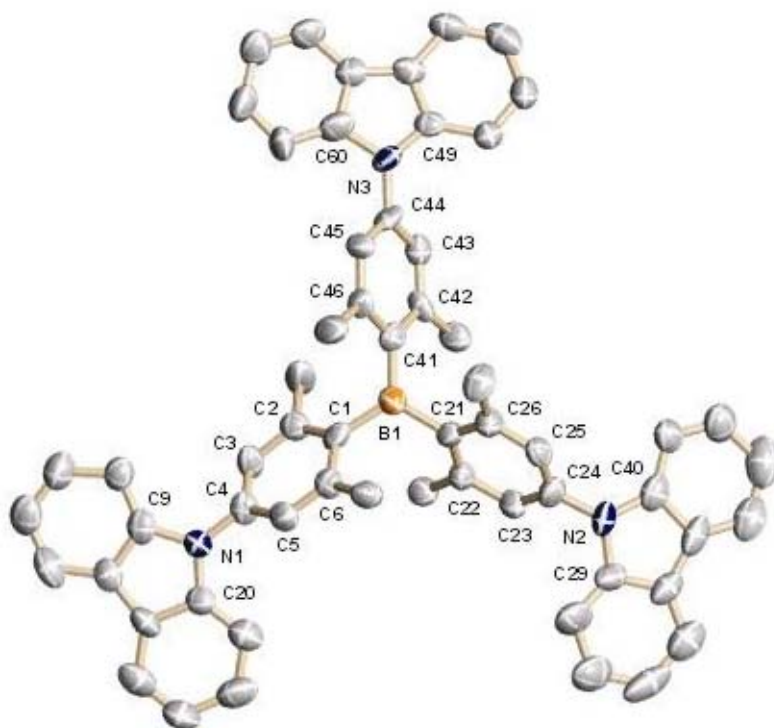


**Figure 2.22:** Molecular structure of **4** with thermal ellipsoids drawn at 50% probability.

**Table 2.9:** Crystallographic data of **4**.

Crystal system	monoclinic
Space group	P2 <sub>1</sub> /c
<i>a</i> , <i>b</i> , <i>c</i> / Å	24.5, 8.26, 26.1
$\alpha$ , $\beta$ , $\gamma$ / °	90.0, 96.1, 90.0
<i>V</i> / Å <sup>3</sup>	5259.2
<i>Z</i>	5
$\rho_{\text{calc}}$ / g cm <sup>-1</sup>	1.339
<i>GoF</i>	0.685
<i>R</i> ( <i>F</i> ), <i>I</i> > 2 $\sigma$ ( <i>I</i> )	0.060
<i>wR</i> ( <i>F</i> <sup>2</sup> ), all data <sup>[a]</sup>	0.187

**Table 2.10:** Selected bond distances, bond angles and dihedral angles of the molecular structure of **4**.

bond distance / Å		bond angle / °		dihedral angle / °	
B1–C1	1.576(6)	C1–B1–C21	117.7(3)	C2–C1–B1–C41	48.9
B1–C21	1.590(5)	C1–B1–C41	122.1(3)	C22–C21–B1–C1	53.8
B1–C41	1.574(5)	C21–B1–C41	120.2(3)	C42–C41–B1–C21	54.8
C4–N1	1.423(5)	C4–N1–C9	125.7(3)	C3–C4–N1–C9	-52.5
C24–N2	1.426(5)	C4–N1–C20	125.8(3)	C23–C24–N2–C29	-49.0
C44–N3	1.434(4)	C9–N1–C20	108.4(3)	C43–C44–N3–C49	-43.1
C1–C2	1.422(5)	C24–N2–C29	125.1(3)		
C2–C3	1.391(5)	C24–N2–C40	124.6(3)		
C3–C4	1.385(5)	C29–N2–C40	108.1(3)		
C4–C5	1.377(5)	C44–N3–C49	125.4(3)		
C5–C6	1.379(5)	C44–N3–C60	125.2(3)		
C6–C1	1.417(5)	C49–N3–C60	108.7(3)		

From Table 2.10 it can be deduced that the boron atom in **4** is surrounded by the three adjacent phenyl carbon atoms in a perfectly trigonal planar fashion with a sum of angles of 360 °. The three carbazole nitrogen atoms are only slightly pyramidalised

[a] The *wR*(*F*<sup>2</sup>) factor of the full matrix least-squares refinement is comparably high due to disordered CDCl<sub>3</sub> molecules in the crystal lattice.

with the sum of angles for N1, N2 and N3 being 359.9 °, 357.8 ° and 359.3 °, respectively. The B–C bond lengths and the torsion angles of the phenyl rings with respect to the BC<sub>3</sub>-plane are in excellent agreement with those of trimesitylborane<sup>[61]</sup> and related TABs with three sterically demanding substituents.<sup>[62, 96]</sup> The C<sub>boron</sub>–C<sub>ortho</sub> bonds (e. g. C1–C2 and C6–C1) are considerably lengthened compared to the other phenyl C–C bonds, which is due to the steric congestion around the boron atom. However, no indication for a quinoidal distortion can be observed in any of the three subchromophores, which is in contrast to the molecular structures of donor-substituted phenyldimesitylboranes (e. g. [*p*-(dimethylamino)phenyl]-dimesitylborane (**27**)) reported by Marder and co-workers.<sup>[106, 107]</sup> In these chromophores the donor-substituted phenyl ring is twisted only 20–30 ° out of the BC<sub>3</sub>-plane and exhibits a significant quinoidal distortion suggesting a pronounced B–N  $\pi$ – $\pi$ -interaction in the ground state. This again substantiates the hypothesis, that this  $\pi$ – $\pi$ -interaction is rather weak in the TABs **4**, **5** and **6**.

### 2.3.10 Conclusions

It has been demonstrated that the carbazole substituted TAB **4** can be polymerised by potentiodynamic electropolymerisation to form an electroactive film on the electrode surface. The resulting polymer can be switched electrochemically between a neutral, oxidised and reduced form by applying the appropriate potential. The p-doping process is completely reversible; however, the polymer shows only minor stability upon n-doping. In contrast to TAB **4** the linear TABs **5** and **6** only tend to form dimers upon electrochemical oxidation. Thus, it can be concluded that (in analogy to the oxadiazole polymers *poly-1*–*poly-3*) in *poly-4* the triarylborane moieties are linked by carbazole dimer units and no oligomeric or polymeric carbazole chains are formed. This is supported by the cyclic voltammetry measurements which show only two discrete oxidation signals for *poly-4*. According to the triply carbazole-functionalised monomer TAB **4** it can be assumed that the structure of *poly-4* is highly cross-linked.

Films of *poly-4* on an ITO-coated glass substrate show intense fluorescence in the blue-green region upon optical excitation. It can thus be assumed that *poly-4* might also exhibit electroluminescent properties as demonstrated recently for molecular triarylboranes.<sup>[8, 9, 40, 41]</sup>

The B–N  $\pi$ – $\pi$ -interaction in the triarylboranes **4–6** is rather weak as demonstrated by cyclic voltammetry, EOAM, and AM1 computations. Thus, the ground state of these molecules can be described by a benzoid rather than a quinoid structure. This is confirmed by the molecular structure of TAB **4** determined by single crystal X-ray diffraction. Moreover, the small ground-state polarisation leads to an “inverse” ground-state dipole moment with a partially negatively charged nitrogen and a positively charged boron atom. Because the  $S_0 \rightarrow S_1$  transition involves a charge transfer from the nitrogen to the boron atom the dipole-moment vector is inverted upon CT excitation. Jortner’s theory has been applied successfully to show that this dipole inversion causes a significant increase in the reorganisation energy of the surrounding solvent molecules leading to the observed negative solvatochromism of the CT absorption bands of the TABs **4–6**.

Since triphenylborane and related TABs have been shown to adopt a propeller-shaped ground-state geometry with a three-fold symmetry,<sup>[59-62]</sup> TAB **4** was expected also to possess a similar ground-state structure with  $D_3$  symmetry. On the other hand, it has been demonstrated recently that the ground-state symmetry of various triphenylmethane dyes like parafuchsin or crystal violet is lowered by an interaction of one amino group with the solvent or counter ion.<sup>[63]</sup> The EOAM and polarised steady-state fluorescence spectroscopy reveal that the ground state of **4** in solution is symmetry broken although the dimethylphenyl rings are most likely surrounding the boron atom in a propeller-like fashion with local  $D_3$  symmetry. It can be hypothesised that the lowering of the ground-state symmetry is due to the rotation of two carbazole moieties around the C–N bond which is supported by the relatively low  $\mu_{eg}^2$  values of **4** compared to **5**. Although the existence of two rotational isomers (a symmetrical and an unsymmetrical propeller form) has been suggested for tris(*p*-dimethylaminophenyl)borane<sup>[57]</sup> this explanation is rather unlikely for **4** because of the steric congestion around the boron atom. From the solvatochromic shift of the

emission of **4** it can be concluded that the degeneracy of the excited  $E$  state (for a hypothetical  $D_3$  symmetry) is released by Jahn–Teller distortion.

The results of the fluorescence-anisotropy measurements clearly indicate that excitation energy can be transferred amongst the three subchromophores of **4**. This energy transfer can be rationalised in terms of transition dipole–dipole interactions between the chromophore subunits. Exciton coupling theory was used to qualitatively and quantitatively analyse the extent of the subchromophore interaction.

TAB **4** was shown to serve as an effective fluoride-ion sensor in solution with a comparably high binding constant. The binding event can be monitored by UV/Vis spectroscopy as the addition of fluoride to the boron atom of **4** causes a significant decrease of the CT absorption band. It can be assumed that these fluoride sensing properties can also be found in *poly-4* and that the binding event might also influence the redox behaviour of the polymer.

In conclusion it was shown that symmetry breaking may have a profound influence on the spectral properties of supposedly symmetric chromophores. These effects might be even stronger in a solid state environment as found in e.g. OLEDs.

## 2.4 AFM-Images of *poly-1* and *poly-4*

AFM measurements were performed on electropolymerised films of *poly-1* and *poly-4* on indium tin oxide (ITO) coated glass sheets (Merck). The thickness of the polymer film was controlled by varying the number of consecutive redox cycles during potentiodynamic polymerisation. In Figure 2.23 a tapping-mode AFM image of a bare ITO glass sheet is shown.

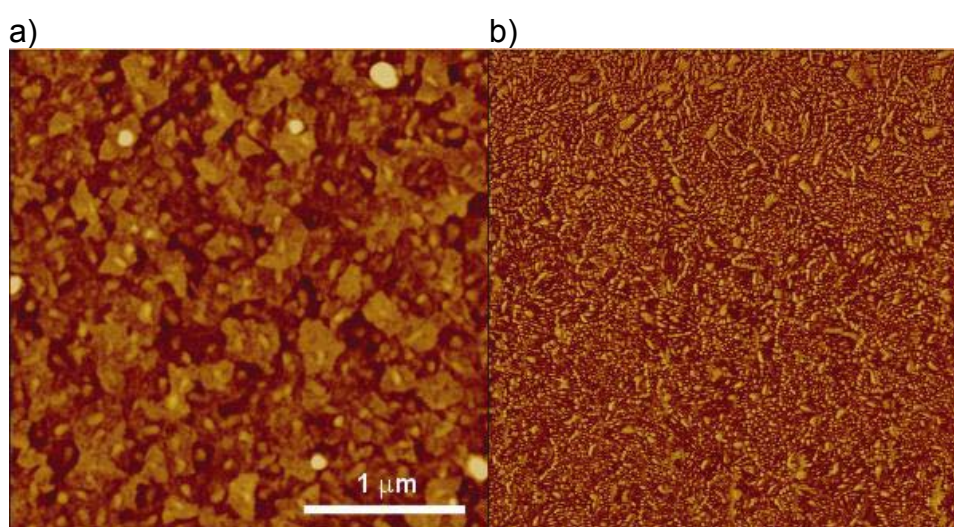


**Figure 2.23:** AFM height (a) and phase (b) images of indium tin oxide (ITO) coated glass sheets (Merck). In a) and b) the z scale is 30 nm and 60 °, respectively.

In order to determine the thickness of the polymers each film was scratched with a pair of tweezers. A cross section of the resulting scratch was scanned and the mean step height between ITO and the polymer was determined (Figure 2.25). Figure 2.24 illustrates an AFM image of a scratched film of *poly-1* on ITO. The structure of the bare ITO (left) is clearly visible.



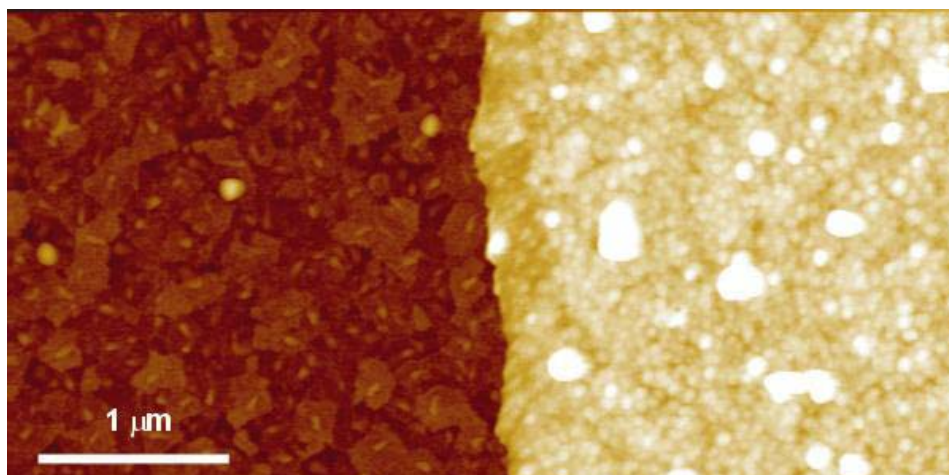


**Figure 2.24:** AFM image of a scratch in *poly-1* (right) on ITO (left). The z scale is 200 nm.

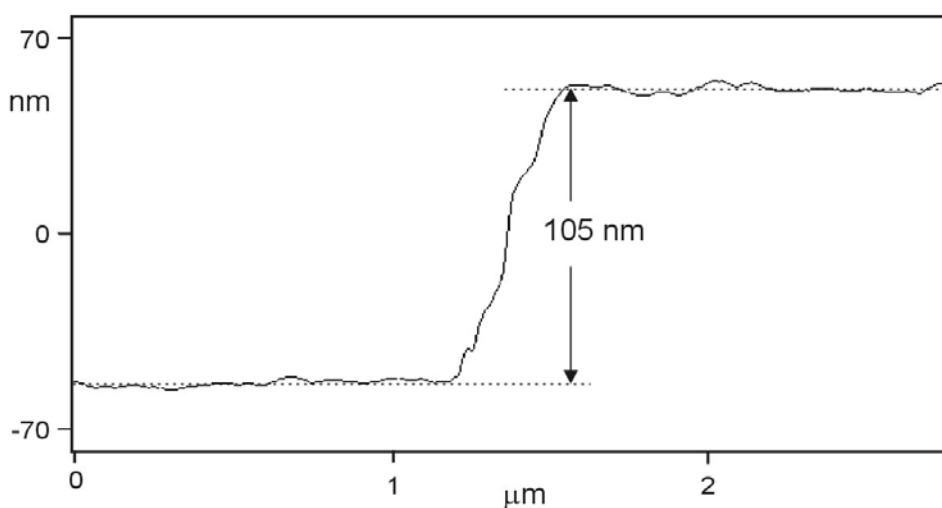


**Figure 2.25:** AFM cross section of a scratch in *poly-4*.

Table 2.11 summarises the estimated polymer-film thickness of *poly-1* and *poly-4* depending on the number of polymerisation redox cycles. A doubling of the oxidation cycles from 5 to 10 does not increase the thickness of *poly-1* significantly whereas it causes an increase from 64 nm to 105 nm for *poly-4*. This might be due to a lower conductivity of *poly-1* which would hinder the oxidation of monomers with increasing polymer thickness. However, in the CV (see Figure 2.3) the oxidation current increases almost linearly even after 10 redox cycles which suggests a steady polymer growth during polymerisation. Another explanation could be, that *poly-1* possesses a higher solubility than *poly-4*, and hence more polymer is removed by

washing the ITO glass sheets with methylene chloride after polymerisation (see experimental section). This would be in agreement with the proposed structures of *poly-1* (linear) and *poly-4* (cross-linked).

**Table 2.11:** Polymer-film thickness of *poly-1* and *poly-4* depending on the number of polymerisation redox cycles.

redox cycles	thickness / nm	
	<i>poly-1</i>	<i>poly-4</i>
5	25	64
10	30	105

The film surface of both *poly-1* and *poly-4* is unstructured with the overall roughness being significantly higher for *poly-1*. A typical AFM image of *poly-4* (10 cycles) on ITO-coated glass is depicted in Figure 2.26.

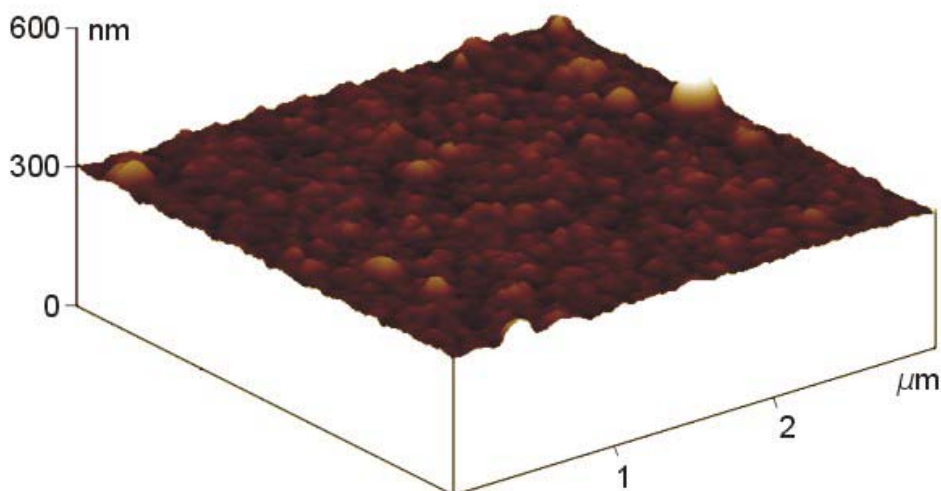


**Figure 2.26:** AFM image of *poly-4* on ITO-coated glass.

## 2.5 Conductivity Measurements

Besides the charge carrier mobility  $\mu$  the conductivity  $\sigma$  of a material is one important criterion to describe its ability to transport charges. The simplest method to determine the conductivity of a bulk material is the so-called two-point measurement. Therefore, a constant dc voltage is applied between two contacts and the resistance  $R$  is obtained from the measured current flow through the material. The conductivity  $\sigma$  can then be calculated from Equation 2-9,

$$\sigma = \frac{1}{R} \frac{d}{A} \quad (\text{eq. 2-9})$$

with the length  $d$  and the cross-sectional area  $A$  of a cylindrical or cubic material (e.g. copper wire, ohmic resist). However, the drawback of this technique is that an additional potential drop occurs at the contact/material interface, i.e. one measures not only the desired bulk resistance  $R_b$  but also the contact resistance  $R_c$ . This problem can be circumvented by using the so-called four-point measurement. Therefore, a constant known current is passed through the material at two contacts 1 and 2 (Figure 2.27). This induces a potential drop over the bulk material which can be measured between two additional contacts 3 and 4 without any current flow. From the applied current and the measured potential drop one can calculate the desired bulk resistance,  $R_b$ .

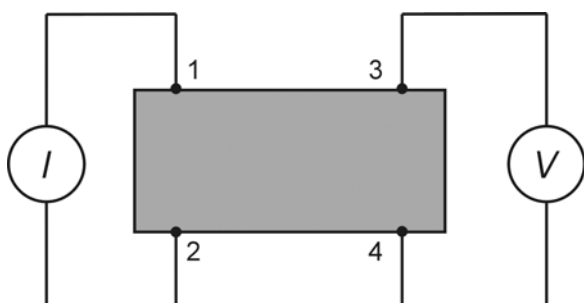


**Figure 2.27:** Conductivity measurement of a bulk material with the four-point method.

A very common method to measure the conductivity of thin semiconducting sheets is the van der Pauw technique.<sup>[123, 124]</sup> With this four-point method various permutations of the applied dc current ( $I_{12}, I_{24}, \dots$ ) and the induced potential drop ( $V_{34}, V_{13}, \dots$ ) have to be measured in order to obtain the sheet resistance  $R_s$  from which the conductivity  $\sigma$  can be calculated. Moreover, the van der Pauw method can be used for the estimation of the charge carrier mobility  $\mu$  by applying an external magnetic field orthogonal to the plane of the semiconductor sheet (Hall Effect).

A technique, which combines the advantages of the four-point method with the concept of interdigitated electrodes (commonly used for two-point conductivity measurements) has been reported recently.<sup>[125]</sup> With this method both  $R_b$  and  $R_c$  of thin films can be determined in separate experiments.

Porter and Vaid described a two-point method in which the contact resistance can be obtained by extrapolation of the measured total resistance.<sup>[126]</sup> They used a Delrin block with a cylindrical hole and two copper cylinders of the same diameter. Pellets of the material to be studied were pressed between the two copper cylinders within the Delrin block and the total resistance ( $R_t$ ) was determined as a function of the amount of substance. Extrapolation of  $R_t$  to a hypothetical zero mass of substance (for which  $R_b = 0$ ) yielded the contact resistance and consequently the desired bulk resistance of the material.

For the conductivity measurements of the oxadiazole polymers *poly-1–poly-3* and the borane polymer *poly-4* a two-point method using platinum two-band electrodes (TBEs) was used (experimental section).<sup>[127]</sup> The corresponding polymers have to be deposited onto the TBEs by electropolymerisation in order to bridge the two platinum electrodes which are separated by an insulating Mylar<sup>®</sup> spacer of defined thickness  $d$ . The conductivity  $\sigma$  can be calculated from the measured two-point resistance and the geometrical parameters of the TBE and the polymer film. As the thickness of the polymer on the electrode is particularly difficult to determine it is more convenient to estimate the conductivity relative to that of a known polymer (e.g. polypyrrole).<sup>[127]</sup> In analogy to the method of Porter and Vaid (see above) the contact resistance can be determined by extrapolation of  $R_t$  to  $d = 0$ .

In order to test the quality of the constructed TBEs the conductivity of polypyrrole was determined with a TBE20 (20  $\mu\text{m}$  Mylar<sup>®</sup> spacer). Pyrrole was

deposited galvanostatically onto the TBE20 and the drain current  $I_d$  ( $E_d = 10$  mV) was measured as a function of the applied gate potential  $E_g$  (Figure 2.28). Although the maximum drain current was found to be ca. 10 times lower as reported in literature, the results are in excellent qualitative agreement with those published by Zotti and co-workers.<sup>[127]</sup> In particular, the drain current was found to scale linearly with the applied drain potential and changed its sign upon reversing the polarity of  $E_d$ .

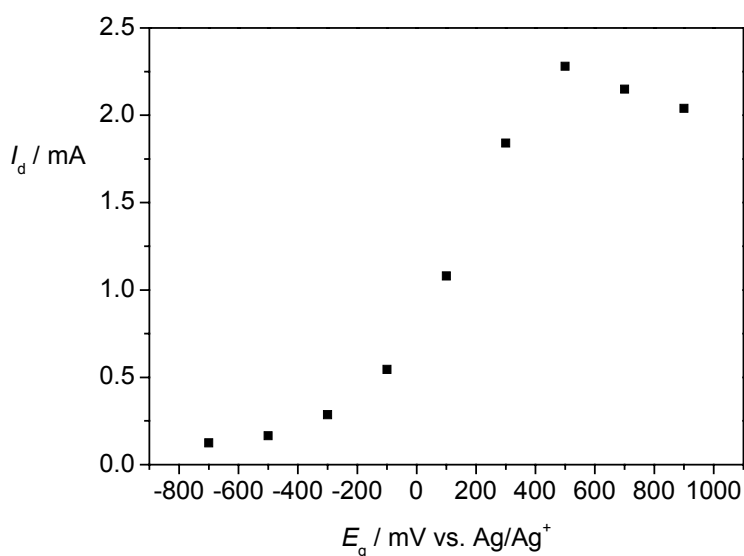


**Figure 2.28:** Drain current  $I_d$  versus gate potential  $E_g$  of a polypyrrole film deposited onto a 20  $\mu\text{m}$  platinum two-band electrode ( $E_d = 10$  mV).

TAB **4** was electropolymerised onto a TBE20 in a similar manner by galvanostatic deposition. However, a lower current density of 0.2 mA/cm<sup>2</sup> was applied owing to the low concentration of **4** in benzonitrile. In contrast to polypyrrole no stable limiting resistance was attained during deposition (Figure 2.29). Thus, the measurements were performed at a minimum resistance reached after 50 minutes deposition time.

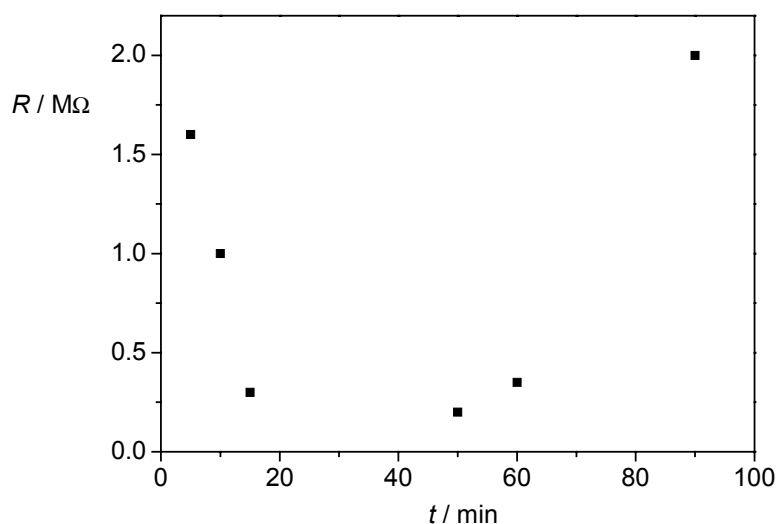


**Figure 2.29:** Measured resistance  $R$  between the TBE20 contacts as a function of the deposition time  $t$  for the galvanostatic polymerisation of TAB 4.

A plot of the drain current  $I_d$  ( $E_d = 10$  mV) as a function of the applied gate potential  $E_g$  of a *poly-4* film is outlined in Figure 2.30. As expected  $I_d$  is low for the uncharged polymer and increases significantly when *poly-4* is oxidised ( $E_g \sim 1200$  mV vs.  $Ag/Ag^+$ ). However, the overall current is about four orders of magnitude lower than that measured for polypyrrole. Moreover, no linear relationship between  $I_d$  and  $E_d$  is observed and the sign of  $I_d$  is not reversed upon changing the polarity of  $E_d$ . Similar results have been obtained for the oxadiazole polymers *poly-1–poly-3* which renders a reliable and reproducible determination of their conductivities impossible. The low  $I_d$  values can either be due to a low intrinsic conductivity of the studied polymers or may be caused by a high contact resistance ( $R_c$ ) between the polymers and the platinum electrodes. However, an accurate determination of  $R_c$  was not possible because of the unreliable estimation of  $I_d$ .

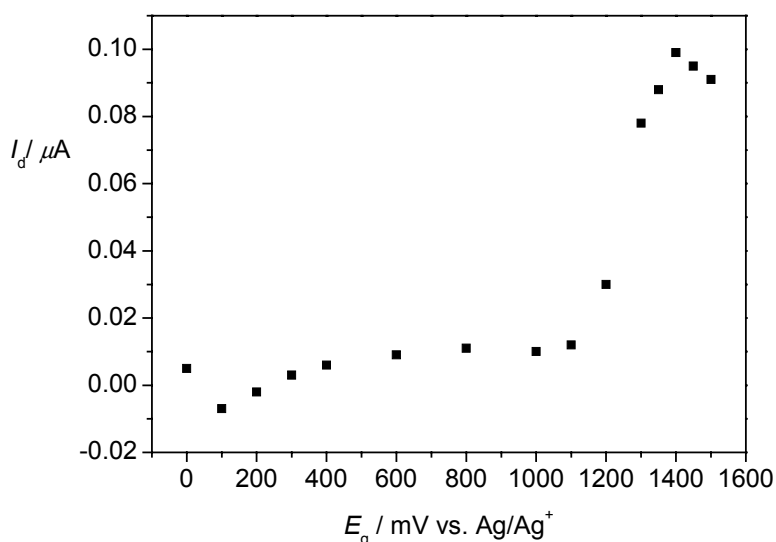


**Figure 2.30:** Drain current  $I_d$  versus gate potential  $E_g$  of a *poly-4* film measured with a TBE20 platinum electrode ( $E_d = 10$  mV).

## 2.6 Conclusions

In Section 2 of this work it was demonstrated that oxadiazoles and triarylboranes bearing two or three carbazole functionalities can be electropolymerised to give bipolar electroactive films on an electrode surface. These polymer films can be both oxidised and reduced electrochemically with the n-doping process causing an irreversible deterioration of the polymer acceptor units. AFM measurements reveal that the thickness of *poly-4* can be controlled to a certain extent by the number of consecutive polymerisation redox cycles while the thickness of *poly-1* reaches a limiting value of 30 nm after only a few cycles. The overall surface roughness of *poly-1* was found to be significantly higher than that of *poly-4*.

The conductivity of *poly-1–poly-4* was shown to increase significantly upon p-doping the polymers. However, the applied method for the conductivity measurements was not suitable to obtain reliable absolute values of  $\sigma$ . Conductivity measurements of the negatively charged polymers were not possible because of the minor stability of all polymers upon n-doping.

As demonstrated by fluorescence spectroscopy, *poly-4* is capable of forming emissive excited states in the solid state which suggests that this polymer might be effectively used as an emitter and/or charge transport material in OLEDs.

## 2.7 Literature

- [1] S.-H. Jin, W.-H. Kim, I.-S. Song, S.-K. Kwon, K.-S. Lee, E.-M. Han, *Thin Solid Films* **2000**, *363*, 255-258.
- [2] A. P. Kulkarni, C. J. Tonzola, A. Babel, S. A. Jenekhe, *Chem. Mater.* **2004**, *16*, 4556-4573.
- [3] Y. Zhang, Y. Hu, H. Li, L. Wang, X. Jing, F. Wang, D. Ma, *J. Mater. Chem.* **2003**, *13*, 773-777.
- [4] Z. Peng, Z. Bao, M. E. Galvin, *Chem. Mater.* **1998**, *10*, 2086-2090.
- [5] W.-L. Yu, H. Meng, J. Pei, S.-J. Chua, W. Huang, Y.-H. Lai, *Chem. Commun.* **1998**, *18*, 1957-1958.
- [6] W.-L. Yu, H. Meng, J. Pei, W. Huang, *J. Am. Chem. Soc.* **1998**, *120*, 11808-11809.
- [7] H. Meng, Z.-K. Chen, W. Huang, *J. Phys. Chem. B* **1999**, *103*, 6429-6433.
- [8] Y. Shirota, M. Kinoshita, T. Noda, K. Okumoto, T. Ohara, *J. Am. Chem. Soc.* **2000**, *122*, 11021-11022.
- [9] H. Doi, M. Kinoshita, K. Okumoto, Y. Shirota, *Chem. Mater.* **2003**, *15*, 1080-1089.
- [10] M. Kawamoto, H. Mochizuki, T. Ikeda, H. Iino, J.-i. Hanna, *J. Phys. Chem. B* **2005**, *109*, 9226-9230.
- [11] F. N. Hayes, B. S. Rogers, D. G. Ott, *J. Am. Chem. Soc.* **1955**, *77*, 1850-1852.
- [12] D. G. Ott, V. N. Kerr, F. N. Hayes, E. Hansbury, *J. Org. Chem.* **1960**, *25*, 872-873.
- [13] C. Adachi, T. Tsutsui, S. Saito, *Appl. Phys. Lett.* **1989**, *55*, 1489.
- [14] C. Adachi, T. Tsutsui, S. Saito, *Appl. Phys. Lett.* **1990**, *56*, 799.
- [15] G. Hughes, M. R. Bryce, *J. Mater. Chem.* **2005**, *15*, 94-107.



- [16] S. J. Chung, K. Y. Kwon, S. W. Lee, J. I. Jin, C. H. Lee, C. E. Lee, Y. Park, *Adv. Mater.* **1998**, *10*, 1112-1116.
- [17] B. Schulz, Y. Kaminorz, L. Brehmer, *Synth. Met.* **1997**, *84*, 449-450.
- [18] Y. Liu, G. Yu, H. Li, H. Tian, D. Zhu, *Thin Solid Films* **2002**, *417*, 107-110.
- [19] K. R. J. Thomas, J. T. Lin, Y.-T. Tao, C.-H. Chuen, *Chem. Mater.* **2004**, *16*, 5437-5444.
- [20] J. H. Kim, J. H. Park, H. Lee, *Chem. Mater.* **2003**, *15*, 3414-3416.
- [21] S.-H. Jin, M.-Y. Kim, J. Y. Kim, K. Lee, Y.-S. Gal, *J. Am. Chem. Soc.* **2004**, *126*, 2474-2480.
- [22] Q. Pei, Y. Yang, *Chem. Mater.* **1995**, *7*, 1568-1575.
- [23] W. Huang, H. Meng, W.-L. Yu, J. Gao, A. J. Heeger, *Adv. Mater.* **1998**, *10*, 593-596.
- [24] Z. Peng, Z. Bao, M. E. Galvin, *Adv. Mater.* **1998**, *10*, 680-684.
- [25] H. Tokuhisa, M. Era, T. Tsutsui, *Adv. Mater.* **1998**, *10*, 404-407.
- [26] T. Tsutsui, E.-i. Aminaka, H. Tokuhisa, *Synth. Met.* **1997**, *85*, 1201-1204.
- [27] M. Guan, Z. Q. Bian, Y. F. Zhou, F. Y. Li, Z. J. Li, C. H. Huang, *Chem. Commun.* **2003**, 2708-2709.
- [28] E. Buchwald, M. Meier, S. Karg, P. Pösch, H.-W. Schmidt, P. Strohrriegel, W. Rieß, M. Schwoerer, *Adv. Mater.* **1995**, *7*, 839-842.
- [29] X.-C. Li, F. Cacialli, M. Giles, J. Grüner, R. H. Friend, A. B. Holmes, S. C. Moratti, T. M. Yong, *Adv. Mater.* **1995**, *7*, 898-900.
- [30] C. D. Entwistle, T. B. Marder, *Chem. Mater.* **2004**, *16*, 4574-4585.
- [31] C. D. Entwistle, T. B. Marder, *Angew. Chem. Int. Ed.* **2002**, *41*, 2927-2931.
- [32] Z.-q. Liu, Q. Fang, D. Wang, D.-x. Cao, G. Xue, W.-t. Yu, H. Lei, *Chem. Eur. J.* **2003**, *9*, 5074-5084.
- [33] J. C. Doty, B. Babb, M. E. Glogowski, J. L. Williams, P. J. Grisdale, *J. Organomet. Chem.* **1972**, *38*, 229-236.
- [34] Z. Yuan, N. J. Taylor, Y. Sun, T. B. Marder, I. D. Williams, L. T. Cheng, *J. Organomet. Chem.* **1993**, *449*, 27-37.
- [35] Z. Yuan, J. C. Collings, N. J. Taylor, T. B. Marder, C. Jardin, J. F. Halet, *J. Solid State Chem.* **2000**, *154*, 5-12.
- [36] M. E. Glogowski, J. L. R. Williams, *J. Organomet. Chem.* **1981**, *216*, 1-8.

- [37] Y. Shirota, *J. Mater. Chem.* **2000**, *10*, 1-25.
- [38] T. Noda, Y. Shirota, *J. Am. Chem. Soc.* **1998**, *120*, 9714-9715.
- [39] M. Kinoshita, H. Kita, Y. Shirota, *Adv. Funct. Mater.* **2002**, *12*, 780-786.
- [40] W.-L. Jia, D.-R. Bai, T. McCormick, Q.-D. Liu, M. Motala, R.-Y. Wang, C. Seward, Y. Tao, S. Wang, *Chem. Eur. J.* **2004**, *10*, 994-1006.
- [41] W.-L. Jia, X. D. Feng, D.-R. Bai, Z. H. Lu, S. Wang, G. Vamvounis, *Chem. Mater.* **2005**, *17*, 164-170.
- [42] B. E. Koene, D. E. Loy, M. E. Thompson, *Chem. Mater.* **1998**, *10*, 2235-2250.
- [43] D. F. O'Brien, P. E. Burrows, S. R. Forrest, B. E. Koene, D. E. Loy, M. E. Thompson, *Adv. Mater.* **1998**, *10*, 1108-1112.
- [44] P. Strohriegel, J. V. Grazulevicius, *Adv. Mater.* **2002**, *14*, 1439-1452.
- [45] U. Mitschke, P. Bäuerle, *J. Mater. Chem.* **2000**, *10*, 1471-1507.
- [46] A. Petr, C. Kvarnstrom, L. Dunsch, A. Ivaska, *Synth. Met.* **2000**, *108*, 245-247.
- [47] C. Lambert, G. Nöll, *Synth. Met.* **2003**, *139*, 57-62.
- [48] M. M. Verghese, M. K. Ram, H. Vardhan, B. D. Malhotra, S. M. Ashraf, *Polymer* **1997**, *38*, 1625-1629.
- [49] S. Yapi Abe, J. C. Bernede, M. A. Delvalle, Y. Tregouet, F. Ragot, F. R. Diaz, S. Lefrant, *Synth. Met.* **2002**, *126*, 1-6.
- [50] H. Taoudi, J. C. Bernede, A. Bonnet, M. Morsli, A. Godoy, *Thin Solid Films* **1997**, *304*, 48-55.
- [51] J. Heinze, K. Hinkelmann, M. Dietrich, J. Mortensen, *Ber. Bunsenges.* **1985**, *89*, 1225-1229.
- [52] S. Cattarin, G. Mengoli, M. M. Musiani, B. Schreck, *J. Electroanal. Chem.* **1988**, *246*, 87-100.
- [53] T. J. DuPont, J. L. Mills, *J. Am. Chem. Soc.* **1975**, *97*, 6375-6382.
- [54] J. E. Leffler, G. B. Watts, T. Tanigaki, E. Dolan, D. S. Miller, *J. Am. Chem. Soc.* **1970**, *92*, 6825-6830.
- [55] W. Kaim, A. Schulz, *Chem. Ber.* **1989**, *122*, 1863-1868.
- [56] B. G. Ramsey, *J. Phys. Chem.* **1966**, *70*, 611-618.
- [57] D. S. Miller, J. E. Leffler, *J. Phys. Chem.* **1970**, *74*, 2571-2574.
- [58] H. Slama, C. Bräuchle, J. Voitlander, *Chem. Phys. Lett.* **1983**, *102*, 307-311.
- [59] H. C. Brown, S. Sujishi, *J. Am. Chem. Soc.* **1948**, *70*, 2793-2802.

- [60] T. J. Weismann, J. C. Schug, *J. Chem. Phys.* **1964**, *40*, 956.
- [61] J. F. Blount, P. Finocchiaro, D. Gust, K. Mislow, *J. Am. Chem. Soc.* **1973**, *95*, 7019-7029.
- [62] S. Toyota, M. Asakura, M. Oki, F. Toda, *Bull. Chem. Soc. Jpn.* **2000**, *73*, 2357-2362.
- [63] H. B. Lueck, J. L. McHale, W. D. Edwards, *J. Am. Chem. Soc.* **1992**, *114*, 2342-2348.
- [64] L. M. Lewis, G. L. Indig, *Dyes Pigm.* **2000**, *46*, 145-154.
- [65] F. Bentiss, M. Lagrenée, *J. Heterocycl. Chem.* **1999**, *36*, 1029-1032.
- [66] A. Klapars, J. C. Antilla, X. Huang, S. L. Buchwald, *J. Am. Chem. Soc.* **2001**, *123*, 7727-7729.
- [67] L. Kress, A. Neudeck, A. Petr, L. Dunsch, *J. Electroanal. Chem.* **1996**, *414*, 31-40.
- [68] G. Sabouraud, S. Sadki, N. Brodie, *Chem. Soc. Rev.* **2000**, *29*, 283-293.
- [69] E. M. Genies, G. Bidan, A. F. Diaz, *J. Electroanal. Chem.* **1983**, *149*, 101.
- [70] M. Kozaki, K. Okada, *Synth. Met.* **2001**, *119*, 177-178.
- [71] M. Oyama, J. Matsui, *Bull. Chem. Soc. Jpn.* **2004**, *77*, 953-957.
- [72] J. L. Brédas, J. C. Scott, K. Yakushi, G. B. Street, *Physical Review B: Condensed Matter and Materials Physics* **1984**, *30*, 1023-1025.
- [73] J. L. Brédas, G. B. Street, *Acc. Chem. Res.* **1985**, *18*, 309-315.
- [74] A. O. Patil, A. J. Heeger, F. Wudl, *Chem. Rev.* **1988**, *88*, 183-200.
- [75] G. Zotti, G. Schiavon, *Synth. Met.* **1989**, *30*, 151-158.
- [76] G. Appel, O. Böhme, R. Mikalo, D. Schmeißer, *Chem. Phys. Lett.* **1999**, *313*, 411-415.
- [77] G. A. Sotzing, J. L. Reddinger, A. R. Katritzky, J. Soloducho, R. Musgrave, J. R. Reynolds, P. J. Steel, *Chem. Mater.* **1997**, *9*, 1578-1587.
- [78] Y. Pelous, G. Froyer, D. Adès, C. Chevrot, A. Siove, *Polym. Commun.* **1990**, *31*, 341-342.
- [79] S. T. Wellinghoff, Z. Deng, T. J. Kedrowski, S. A. Dick, S. A. Jenekhe, H. Ishida, *Mol. Cryst. Liq. Cryst.* **1984**, *106*, 289-304.
- [80] C. Lambert, G. Nöll, *J. Am. Chem. Soc.* **1999**, *121*, 8434-8442.
- [81] S. M. Bonesi, R. Erra-Balsells, *Journal of Luminescence* **2001**, *93*, 51-74.

- [82] E. Lippert, *Z. Naturforsch., A: Phys. Sci.* **1955**, *10*, 541-545.
- [83] N. Mataga, Y. Kaifu, M. Koizumi, *Bull. Chem. Soc. Jpn.* **1955**, *28*, 690-691.
- [84] L. Onsager, *J. Am. Chem. Soc.* **1936**, *58*, 1486-1493.
- [85] E. Cloutet, C. Olivero, D. Ades, M.-C. Castex, A. Siove, *Polymer* **2002**, *43*, 3489-3495.
- [86] J. H. de Groot, K. Dillingham, H. Deuring, H. J. Haitjema, F. J. van Beijma, K. Hodd, S. Norrby, *Biomacromolecules* **2001**, *2*, 1271-1278.
- [87] M. P. Doyle, B. Siegfried, J. F. Dellaria, Jr., *J. Org. Chem.* **1977**, *42*, 2426-2431.
- [88] S. Adimurthy, G. Ramachandraiah, P. K. Ghosh, A. V. Bedekar, *Tetrahedron Lett.* **2003**, *44*, 5099-5101.
- [89] A. A. Kelkar, N. M. Patil, R. V. Chaudhari, *Tetrahedron Lett.* **2002**, *43*, 7143-7146.
- [90] R. Carlier, J. Simonet, *Bull. Soc. Chim. Fr.* **1988**, *5*, 831-833.
- [91] M. E. Long, *Journal of Luminescence* **1978**, *16*, 177-189.
- [92] C. Lambert, W. Gaschler, E. Schmäzlin, K. Meerholz, C. Bräuchle, *J. Chem. Soc., Perkin Trans. 2* **1999**, 577-587.
- [93] M. Kasha, H. R. Rawls, M. A. El-Bayoumi, *Pure Appl. Chem.* **1965**, *11*, 371-392.
- [94] E. G. McRae, M. Kasha in *Physical Processes in Radiation Biology* (Eds.: L. Augenstein, R. Mason, B. Rosenberg), Academic Press, New York, **1964**, pp. 23-42.
- [95] M. S. Gudipati, *J. Phys. Chem.* **1994**, *98*, 9750-9763.
- [96] S. Yamaguchi, T. Shirasaka, K. Tamao, *Org. Lett.* **2000**, *2*, 4129-4132.
- [97] W.-L. Jia, D. Song, S. Wang, *J. Org. Chem.* **2003**, *68*, 701-705.
- [98] G. Meshulam, G. Berkovic, Z. Kotler, A. Ben-Asuly, R. Mazor, L. Shapiro, V. Khodorkovsky, *Synth. Met.* **2000**, *115*, 219-223.
- [99] A. Kapturkiewicz, J. Herbich, J. Karpiuk, J. Nowacki, *J. Phys. Chem. A* **1997**, *101*, 2332-2344.
- [100] A similar analysis was not possible for **5** because of the overlap of the CT absorption band with local carbazole transitions.

- [101] S. F. Nelsen, M. T. Ramm, J. J. Wolff, D. R. Powell, *J. Am. Chem. Soc.* **1997**, *119*, 6863-6872.
- [102] J. Cortes, H. Heitele, J. Jortner, *J. Phys. Chem.* **1994**, *98*, 2527-2536.
- [103] I. R. Gould, D. Noukakis, L. Gomez-Jahn, R. H. Young, J. L. Goodman, S. Farid, *Chem. Phys.* **1993**, *176*, 439-456.
- [104] P. Y. Chen, T. J. Meyer, *Chem. Rev.* **1998**, *98*, 1439-1477.
- [105] R. Wortmann, P. Krämer, C. Glania, S. Lebus, N. Detzer, *Chem. Phys.* **1993**, *173*, 99-108.
- [106] Z. Yuan, N. J. Taylor, T. B. Marder, I. D. Williams, S. K. Kurtz, L.-T. Cheng in *Organic Materials for Non-linear Optics II* (Eds.: R. A. Hann, D. Bloor), The Royal Society of Chemistry, Cambridge, **1991**, pp. 190-196.
- [107] Z. Yuan, C. D. Entwistle, J. C. Collings, D. Albesa-Jove, A. S. Batsanov, J. A. K. Howard, H. M. Kaiser, D. E. Kaufmann, S.-Y. Poon, W.-Y. Wong, C. Jardin, S. Fathallah, A. Boucekkine, J.-F. Halet, T. B. Marder, *Chem. Eur. J.*, submitted.
- [108] J. Herbich, A. Kapturkiewicz, *J. Am. Chem. Soc.* **1998**, *120*, 1014-1029.
- [109] J. B. Birks, *Photophysics of Aromatic Molecules*, Wiley, New York, **1970**.
- [110] S. J. Strickler, R. A. Berg, *J. Chem. Phys.* **1962**, *37*, 814-822.
- [111] S. Gnanakaran in *Resonance Energy Transfer* (Eds.: D. L. Andrews, A. A. Demidov), Wiley, New York, **1999**, pp. 323-328.
- [112] R. Englman, J. Jortner, *Mol. Phys.* **1970**, *18*, 145-164.
- [113] G. J. Cox, J. H. Ferguson, M. L. Dodds, *J. Ind. Eng. Chem.* **1933**, *25*, 968-970.
- [114] J. R. Lakowicz, *Principles of Fluorescence Spectroscopy*, 2nd ed., Kluwer Academic/Plenum Publishers, New York, **1999**.
- [115] A. A. Demidov, D. L. Andrews, *Photochem. Photobiol.* **1996**, *63*, 39-52.
- [116] W. Verbouwe, M. Van der Auweraer, F. C. De Schryver, J. J. Piet, J. M. Warman, *J. Am. Chem. Soc.* **1998**, *120*, 1319-1324.
- [117] R. D. Hall, B. Valeur, G. Weber, *Chem. Phys. Lett.* **1985**, *116*, 202-205.
- [118] E. Leroy, H. Lami, *Chem. Phys. Lett.* **1976**, *41*, 373-377.
- [119] S. Yamaguchi, S. Akiyama, K. Tamao, *J. Am. Chem. Soc.* **2001**, *123*, 11372-11375.

- [120] S. Yamaguchi, T. Shirasaka, S. Akiyama, K. Tamao, *J. Am. Chem. Soc.* **2002**, *124*, 8816-8817.
- [121] Y. Kubo, M. Yamamoto, M. Ikeda, M. Takeuchi, S. Shinkai, S. Yamaguchi, K. Tamao, *Angew. Chem. Int. Ed.* **2003**, *42*, 2036-2040.
- [122] R. A. Binstead, B. Jung, A. D. Zuberbühler, SPECFIT/32<sup>TM</sup> V3.0.33, Program for Multivariate Data Analysis, 1993, Spectrum Software Associates, Marlborough (USA).
- [123] L. J. v. d. Pauw, *Philips Tech. Rev.* **1958**, *20*, 220-224.
- [124] <http://www.eeel.nist.gov/812/intr.htm>
- [125] Q. Hao, V. Kulikov, V. M. Mirsky, *Sensors and Actuators B* **2003**, *94*, 352-357.
- [126] W. W. Porter III, T. P. Vaid, *J. Org. Chem.* **2005**, *70*, 5028-5035.
- [127] G. Schiavon, S. Sitran, G. Zotti, *Synth. Met.* **1989**, *32*, 209-217.

## 3 Electron Deficient Conjugated Polymers

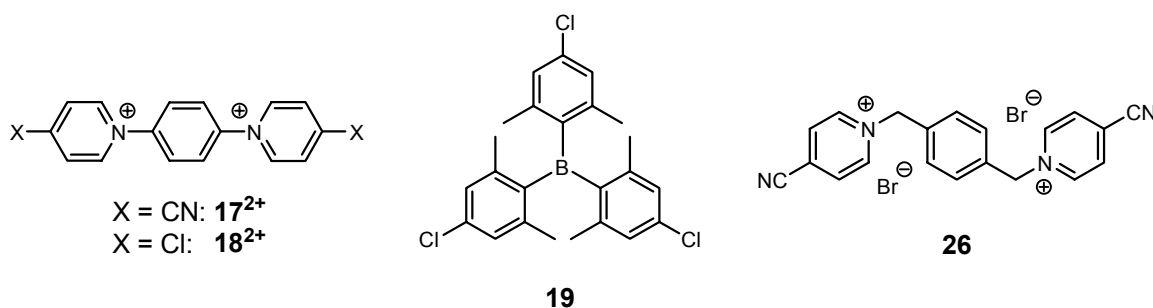
### 3.1 Introduction

Intense research efforts have been devoted to the synthesis and investigation of new electron-conducting organic materials in the past decade.<sup>[1, 2]</sup> The use of these materials as electron-conducting/hole-blocking (ECHB) layers in OLEDs<sup>[3]</sup> or as electron acceptors in bilayer organic photovoltaic cells<sup>[4]</sup> are only two of numerous possible applications.

Triarylboranes are good electron acceptors and can easily be reduced to yield their corresponding radical anions due to their vacant boron  $p_z$  orbital. Thus, TABs have been successfully used as electron-transport or hole-blocking materials in OLEDs (Section 2).<sup>[5-7]</sup> However, the use of TABs in optoelectronic devices has mainly concentrated on monomeric species and examples of conjugated polymers containing boron in their backbone are rather scarce.<sup>[8-13]</sup>

Another important class of electron conducting materials are  $N,N'$ -alkylated or arylated 4,4'-bipyridinium compounds, also known as viologens.<sup>[14]</sup> The simplest and probably the most intensively studied viologen is the  $N,N'$ -dimethyl-4,4'-bipyridinium dication (paraquat,  $PQ^{2+}$ ). Besides its herbicidal activity<sup>[15]</sup>  $PQ^{2+}$  has a relatively high electron affinity and can be reversibly reduced to yield its radical cation and the neutral form at comparably low potentials ( $E_{red}^1 = -0.58$  V,  $E_{red}^2 = -0.96$  V vs.  $Fc/Fc^+$ ).<sup>[16, 17]</sup>  $PQ^{2+}$  and related viologens have been explored as electron mediators in photoreactions,<sup>[18]</sup> as redox-active components in "molecular switches"<sup>[19]</sup> and in porphyrin–viologen systems designed to mimic electron-transfer processes of the photosynthetic reaction centre.<sup>[14, 20, 21]</sup> Moreover, viologens have been incorporated into redox-active polymers, either as part of the main chain<sup>[14, 22-26]</sup> or as pendant side chains.<sup>[27]</sup> However, with the exception of a PPV-analogous viologen-polymer studied by Merz and Reitmeier,<sup>[24]</sup> the  $\pi$ -conjugation in the backbone of these polymers is always interrupted by  $CH_2$ -groups or longer alkyl chains. Similar polymers and oligomers containing single pyridinio-moieties in the main chain were synthesised by various research groups but no electrochemical data were reported.<sup>[28-31]</sup>

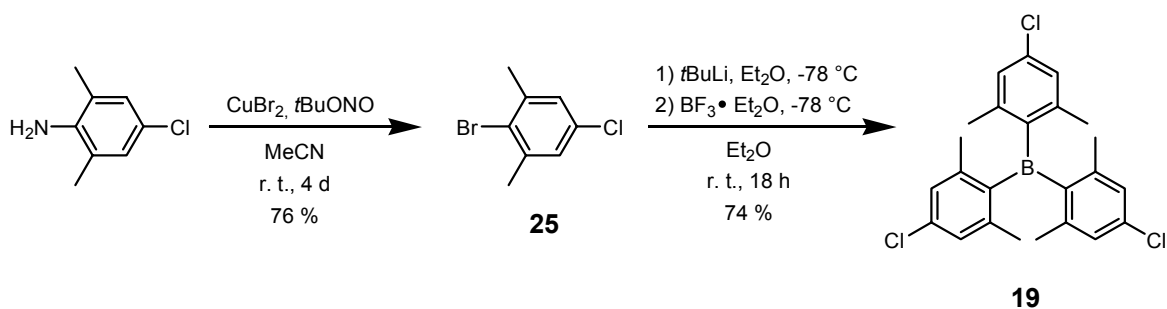
Since it is known that 4-cyano-pyridinium salts<sup>[22, 23, 32]</sup> and 2,5-dichlorobenzonitrile<sup>[33]</sup> can be coupled reductively to yield the corresponding dimers or polymers, the aim of the second part of this work is the synthesis of the cyano- and chloro-substituted bis(pyridinio)benzenes **17**<sup>2+</sup> and **18**<sup>2+</sup> and the chloro-substituted triarylborane **19** as monomeric precursors for electron-deficient conjugated polymers. These compounds (and were appropriate their corresponding polymers) are characterised by cyclic voltammetry and UV/Vis spectroscopy. Additionally, compound **26** is synthesised as a model compound for testing the conditions required for reductive electropolymerisation.<sup>[23]</sup>



## 3.2 Electron Deficient Conjugated Borane Polymers

### 3.2.1 Synthesis of the Monomer

2-Bromo-5-chloro-1,3-dimethylbenzene (**25**) was synthesised by a Sandmeyer-like substitutive deamination of the corresponding aniline with  $\text{CuBr}_2$  according to a literature procedure (Scheme 3.1).<sup>[34]</sup>



**Scheme 3.1:** Synthesis of the chloro-substituted TAB **19**.



TAB **19** was then obtained by lithiation of **25** with *t*BuLi and subsequent reaction of the aryllithium species with  $\text{BF}_3 \cdot \text{Et}_2\text{O}$  at  $-78\text{ }^\circ\text{C}$ . It was found that the aryllithium species of **25** must be directly treated with  $\text{BF}_3 \cdot \text{Et}_2\text{O}$  at  $-78\text{ }^\circ\text{C}$ , as temporary warming up to  $0\text{ }^\circ\text{C}$  leads to significantly reduced yields of **19** ( $< 5\%$ ).

### 3.2.2 Cyclic Voltammetry

Cyclic voltammetry was measured for **19** in a variety of solvents and solvent mixtures with  $\text{TBAPF}_6$  (in  $\text{CH}_2\text{Cl}_2$ , MeCN) or TBAP (in THF, toluene/MeCN 5:1) as the supporting electrolyte. TAB **19** is reduced chemically reversibly at  $E_{1/2} = -2210\text{ mV}$  (vs.  $\text{Fc}/\text{Fc}^+$ ) in THF at scan rates  $\nu > 250\text{ mV/s}$ . At lower scan rates ( $\nu < 250\text{ mV/s}$ ) the electrochemical reduction turns out to be chemically irreversible (see inset diagram). In other solvents and solvent mixtures the reduction of TAB **19** is chemically irreversible even at higher scan rates ( $\nu > 5000\text{ mV/s}$ ). However, no indication for the formation of polymers was observed in any solvent/electrolyte system.

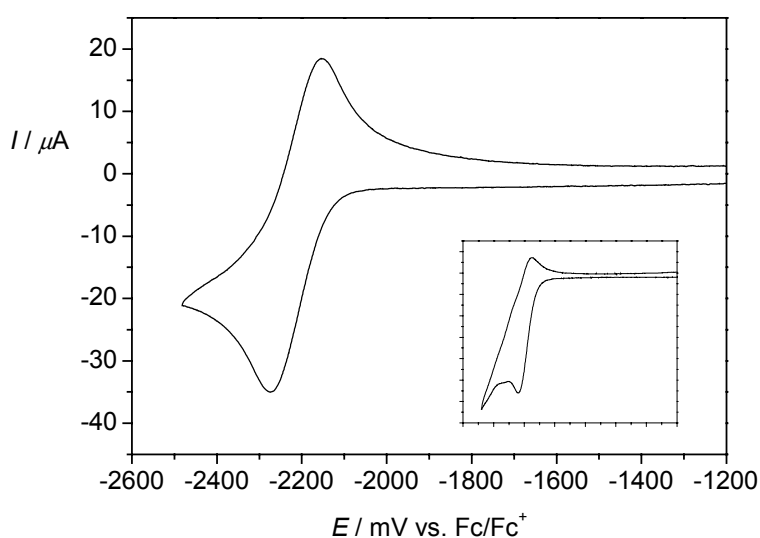


**Figure 3.1:** Cyclic voltammogram of **19** in 0.3 M THF/TBAP,  $\nu = 500\text{ mV/s}$ . Inset diagram: CV in the same solvent at  $\nu = 50\text{ mV/s}$ .

It is noteworthy that TAB **19** is reduced at the same potential as the carbazole-substituted TAB **4** ( $E_{1/2} = -2215$  mV). This is in good agreement with the comparable electronegativities of nitrogen and chlorine (3.04 and 3.16, respectively)<sup>[35]</sup> and again substantiates the hypothesis that the electron affinity of the boron atom is mainly determined by inductive rather than by mesomeric effects (see Section 2.3.2). However, a poor  $\pi$ - $\pi$ -interaction of the boron atom with the adjacent phenyl rings will most likely lead to a localisation of the unpaired electron on the boron atom in the TAB **19** radical anion. On the other hand, a significant delocalisation of the unpaired electron into the phenyl rings (especially in the *para*-positions) is a prerequisite for the radical-radical coupling of two TAB molecules and hence for the reductive electropolymerisation of **19**. This might be the reason that TAB **19** could not be electropolymerised successfully.

### 3.2.3 Absorption and Emission Spectroscopy

The UV/Vis absorption spectrum of TAB **19** in  $\text{CH}_2\text{Cl}_2$  is mainly characterised by a transition at  $30200\text{ cm}^{-1}$  (Figure 3.2), which can be attributed to a photo-induced charge transfer from the aryl rings to the central boron atom.<sup>[36-38]</sup> This absorption band is shifted to higher energies compared to the donor-substituted TABs **4-6** which is due to the electron withdrawing chloro-substituents in **19**. However, it should be noted that the absorption maximum of **19** is nearly identical with that of trimesitylborane<sup>[37]</sup>, indicating that the electronic effects of chloro- and methyl substituents on the CT transition energy are almost equal. The emission maximum of **19** in  $\text{CH}_2\text{Cl}_2$  is located at  $26700\text{ cm}^{-1}$  with a relatively small Stokes-shift of  $3500\text{ cm}^{-1}$  compared to the TABs **4-6** ( $5000$ – $5700\text{ cm}^{-1}$ ). This suggests that the polarity of the excited state of **19** is lower than that of the donor-substituted analogues **4-6**.

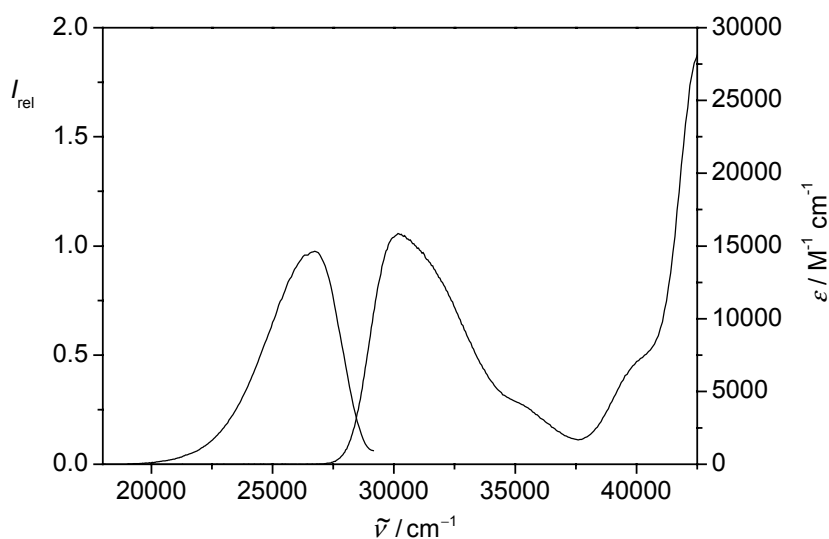


**Figure 3.2:** UV/Vis absorption and fluorescence spectra of **19** in  $\text{CH}_2\text{Cl}_2$ .

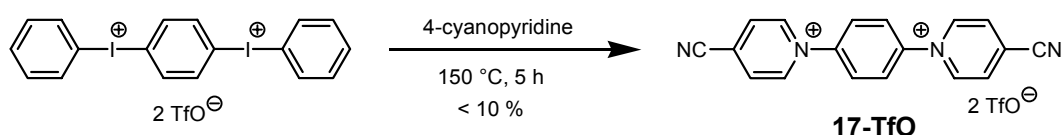
### 3.2.4 Conclusions

It has been demonstrated that the electrochemical reduction of the chloro-substituted TAB **19** is chemically irreversible without formation of polymers on the electrode. This is thought to arise from the propeller-shaped arrangement of the sterically demanding dimethylphenyl-substituents leading to a strong localisation of the unpaired electron on the boron atom. This is consistent with the rather weak B–N  $\pi$ – $\pi$ -interaction in the analogous TABs **4–6**. It has also been shown that chlorine- and methyl-substituents in *para*-position to the boron atom have the same the electronic effects on the spectral position of the CT transition maximum in these compounds.

### 3.3 Electron Deficient Poly(*para*-phenylene)-Analogues Based on 4,4'-Bipyridinium (Viologen)

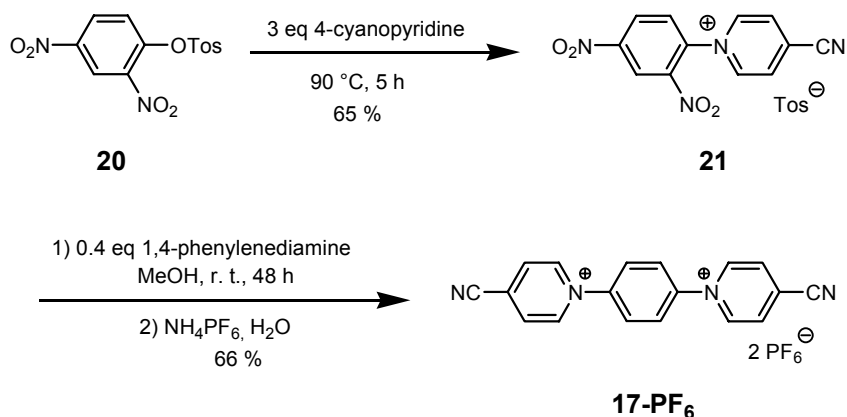
#### 3.3.1 Synthesis of the Monomers

The cyano-substituted bispyridinio compound **17**<sup>2+</sup> has been synthesised in my Diploma thesis according to Scheme 3.2.<sup>[39]</sup> However, this reaction gave unsatisfactorily low yields (< 10 %) besides the problem of a difficult variation of the spacer unit.



**Scheme 3.2:** Synthetic route A to 1,4-bis-(4-cyanopyridinio)benzene ditriflate (**17-TfO**).

Thus, a new synthetic strategy was developed which is outlined in Scheme 3.3. 2,4-Dinitrophenyl-4-toluenesulfonate (**20**) was synthesised according to a procedure described by Ullmann and Nadai.<sup>[40]</sup> Reaction of **20** with 4-cyanopyridine gave the 4-cyanopyridinium-tosylate **21** in 65 % yield.

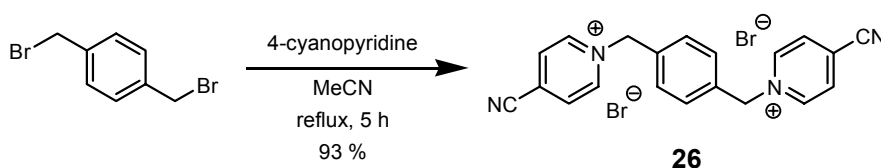


**Scheme 3.3:** Synthetic route B to 1,4-bis-(4-cyanopyridinio)benzene dihexafluorophosphate (**17-PF<sub>6</sub>**).

The bispyridinio-tosylate **17-Tos** can then be obtained by reaction of 1,4-phenylenediamine with two equivalents of **21**. Finally, the tosylate salt, which is soluble in H<sub>2</sub>O was converted into the hexafluorophosphate salt **17-PF<sub>6</sub>** (soluble in MeCN) by

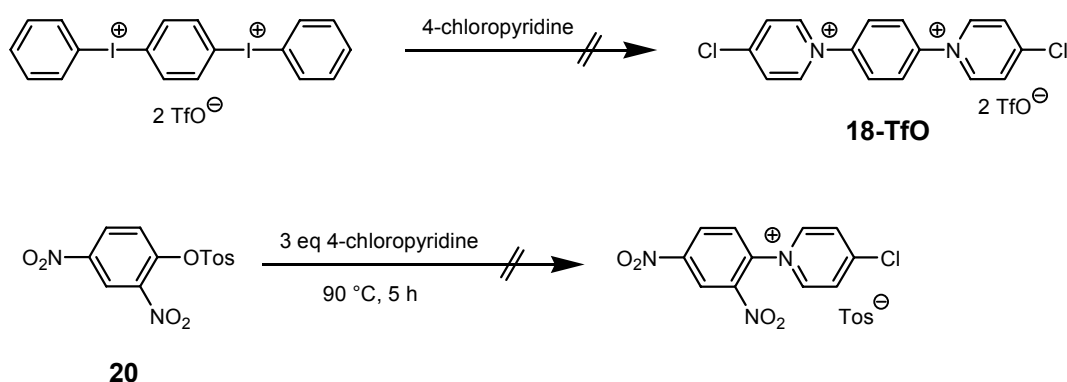
precipitation with  $\text{NH}_4\text{PF}_6$  in water. The corresponding bromide salt **17-Br** was obtained by treatment of **17-PF<sub>6</sub>** with tetrabutylammonium bromide in acetonitrile. This improved synthetic route gives acceptable yields and the spacer unit can easily be varied by changing the diamino reactant in the last step.

The model compound **26** was synthesised by reaction of 4-cyanopyridine with  $\alpha,\alpha'$ -dibromo-*p*-xylene according to a procedure described previously (Scheme 3.4).<sup>[23]</sup>

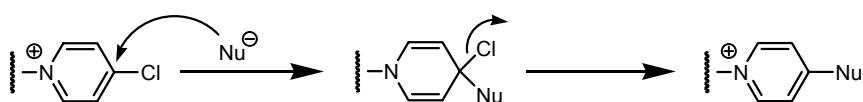


**Scheme 3.4:** Synthesis of the model compound **26**.<sup>[23]</sup>

Attempts to synthesise the chloro-substituted bispyridinio compound **18<sup>2+</sup>** by the same strategy as its cyano-substituted analogue failed (Scheme 3.5). This can be explained by the highly electrophilic nature of the 4-chloropyridinio entity which facilitates the attack of nucleophiles (e. g. 4-chloropyridine) and hence substitution of the chlorine atom (Scheme 3.6). Moreover, it has been reported that 4-chloropyridine tends to spontaneous oligomerisation due to its high reactivity.<sup>[41]</sup>

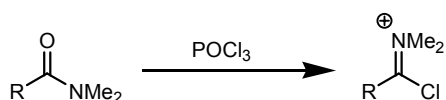


**Scheme 3.5:** Failed attempts of the synthesis of **18<sup>2+</sup>**.



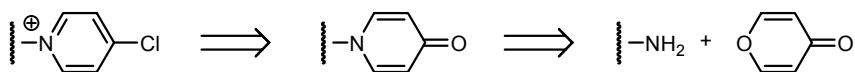
**Scheme 3.6:** Nucleophilic aromatic substitution of the chlorine atom in the 4-chloropyridinio unit.

It is thus necessary to introduce the chlorine atom in the last step of a reaction sequence. According to its structure and reactivity the 4-chloropyridinio unit can also be regarded as a vinylogue chloroiminium ion. This class of compounds can be synthesised from the corresponding amide by treatment with a chlorinating agent like  $\text{POCl}_3$  (e. g. Vilsmeier reaction<sup>[42]</sup>) according to Scheme 3.7.



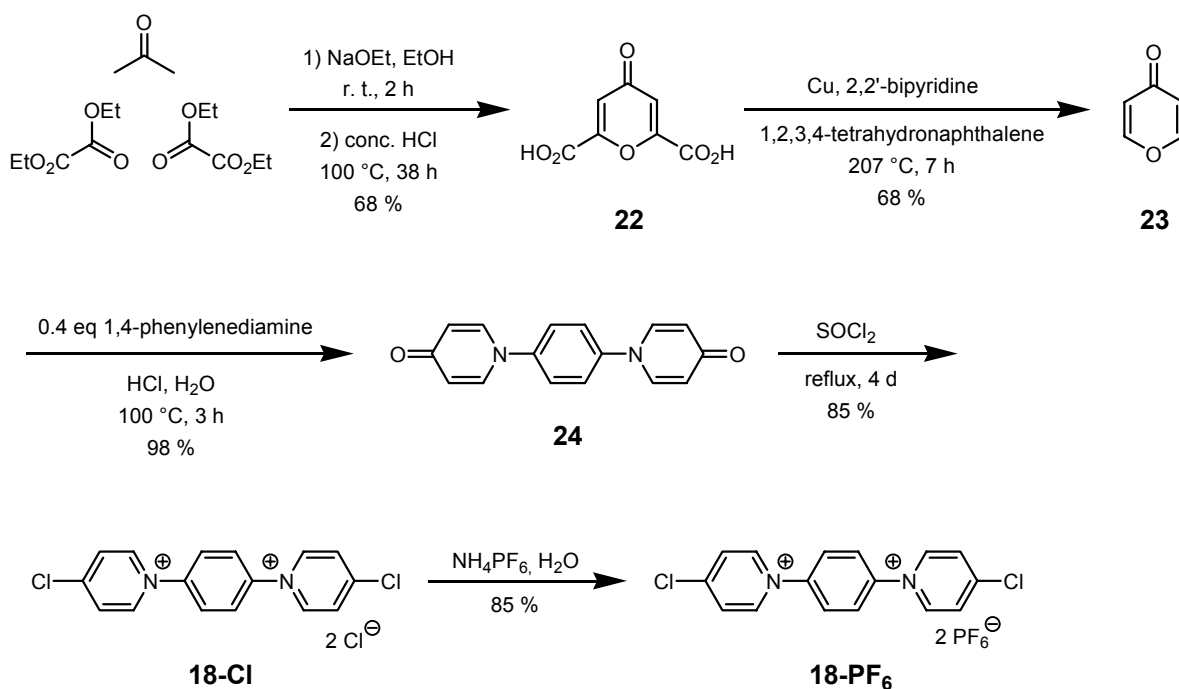
**Scheme 3.7:** Conversion of an amide into a chloroiminium ion.

Hence, it should be possible to synthesise  $\mathbf{18}^{2+}$  on the basis of the retrosynthetic analysis depicted in Scheme 3.8.



**Scheme 3.8:** Retrosynthetic analysis for the synthesis of 4-chloropyridinio compounds.

The chloro-substituted bispyridinio compound  $\mathbf{18}^{2+}$  was obtained according to Scheme 3.9 following a procedure for the synthesis of *N*-substituted 4-chloropyridinium salts reported earlier by Hünig and Köbrich.<sup>[43]</sup>



**Scheme 3.9:** Synthesis of 1,4-bis-(4-chloropyridinio)benzene dihexafluorophosphate (**18-PF<sub>6</sub>**).

$\gamma$ -Pyrone (**23**) was synthesised by copper-catalysed decarboxylation of chelidonic acid (**22**) in boiling tetralin.<sup>[44]</sup> Chelidonic acid can be obtained in large quantities by condensation of acetone with two equivalents of diethyl oxalate.<sup>[45]</sup> Reaction of 1,4-phenylenediamine with two equivalents of **23** gave the 1,4-bispyridone **24** in excellent yield (98 %). Finally, the chloride salt of **18**<sup>2+</sup> was obtained by reaction of **24** with SOCl<sub>2</sub> (as solvent) and was converted into the hexafluorophosphate salt **18-PF<sub>6</sub>** by precipitation with NH<sub>4</sub>PF<sub>6</sub>. This synthetic route also has the advantage of allowing easy variation of the spacer unit by reaction of **23** with different aromatic (or aliphatic) diamines.

### 3.3.2 Cyclic Voltammetry

In order to reproduce the conditions for the reductive electropolymerisation of 4-cyanopyridinium salts reported by Saika et al.,<sup>[23]</sup> cyclic voltammetry was measured for the model compound **26** in 0.1 M aqueous phosphate buffer at pH 7.4. However, no polymerisation was observed upon potentiodynamic redox cycling neither with a platinum electrode nor with an ITO electrode. A cyclic voltammogram of the irreversible reduction of **26** is depicted in Figure 3.3.

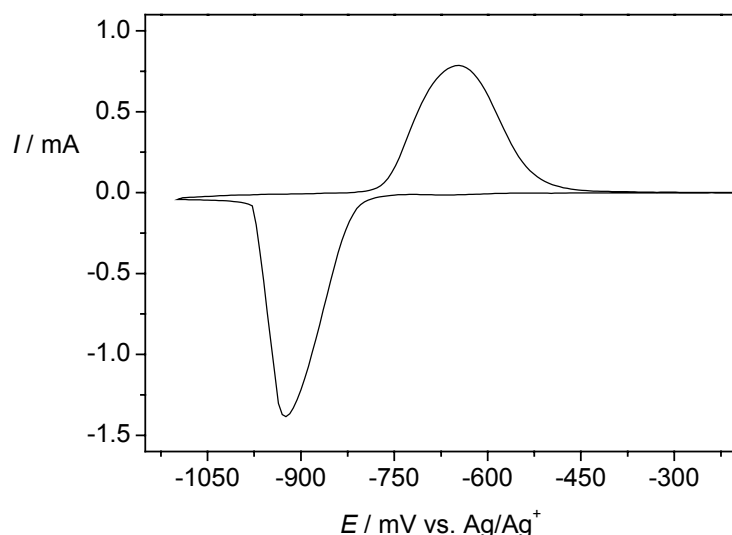
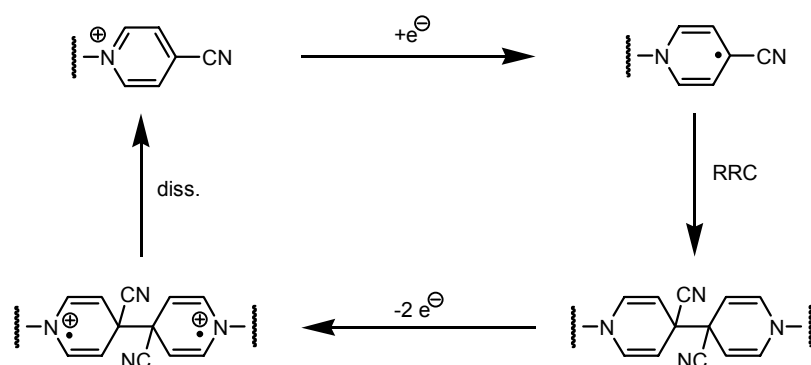


**Figure 3.3:** Cyclic voltammogram of **26** in 0.1 M phosphate buffer at  $v = 100$  mV/s. Working electrode: ITO ( $\sim 1.5$  cm<sup>2</sup>).

Obviously, the reduction of **26** at  $E_{\text{red}} = -920$  mV (vs. Ag/Ag<sup>+</sup>) leads to a chemical reaction (e. g. radical–radical coupling, RRC) of the radical cation or neutral form without splitting off the cyano groups. Upon back oxidation at  $E_{\text{ox}} = -650$  mV the newly formed bond is broken and the monomer **26** is recovered (Scheme 3.10). Nevertheless, it was possible to electropolymerise **26** under potentiostatic conditions by applying a voltage of -1.0 V for 15 minutes (0.1 M phosphate buffer, ITO working electrode). The so obtained polymer exhibits a similar electrochemical behaviour in monomer-free solution (Figure 3.4) as the corresponding polymer synthesised earlier by potentiodynamic electropolymerisation.<sup>[23]</sup>





**Scheme 3.10:** Proposed mechanism for the reductive radical-radical coupling (RRC) of 4-cyanopyridinium compounds and the subsequent oxidative dissociation of the 4,4'-tetrahydrobipyridine.

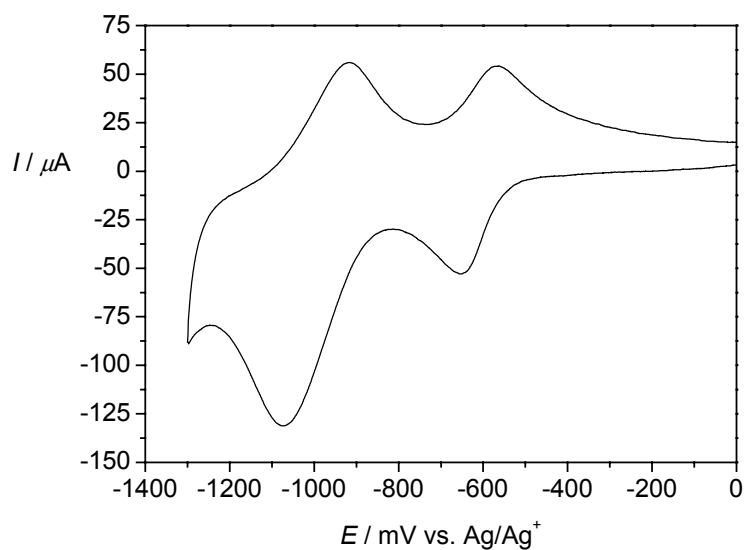


**Figure 3.4:** Cyclic voltammogram of *poly-26* in monomer free aqueous solution (0.1 M phosphate buffer),  $\nu = 100 \text{ mV/s}$ . Working electrode: ITO ( $\sim 1.5 \text{ cm}^2$ ).

It has been demonstrated recently in my Diploma thesis that the potentiodynamic reduction of **17-PF<sub>6</sub>** in 0.1 M MeCN/TBAPF<sub>6</sub> is completely reversible at low scan rates with reduction potentials of  $E_{1/2}^1 = -770$  mV and  $E_{1/2}^2 = -920$  mV (Figure 3.5).<sup>[39]</sup>

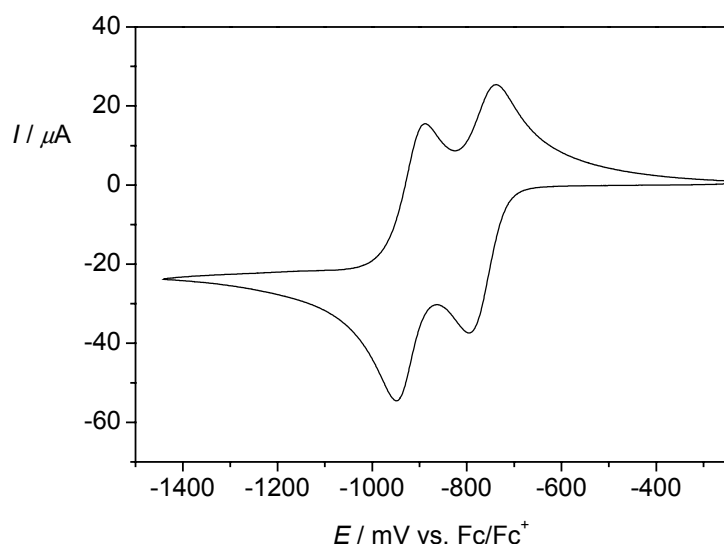


**Figure 3.5:** Cyclic voltammogram of **17-PF<sub>6</sub>** in 0.1 M MeCN/TBAPF<sub>6</sub>,  $v = 20$  mV/s. Working electrode: platinum disc ( $\varnothing$  3 mm).

In 0.1 M aqueous phosphate buffer (pH 7.4) the corresponding bromide salt (**17-Br**) is reduced chemically irreversibly at  $E_{\text{red}} = -650$  mV vs. Ag/Ag<sup>+</sup> (Figure 3.6). Obviously, the radical cation **17<sup>•+</sup>** and the neutral species **17** are effectively stabilised by the surrounding solvent molecules in MeCN but not in aqueous solution. No indication for polymerisation could be observed upon continuous potentiodynamic reduction of **17-Br** (neither with a platinum electrode nor with an ITO electrode). The CV further suggests that—similar to **26**—reduction of **17-Br** leads to radical–radical coupling of the corresponding monomers without splitting off the cyano groups and subsequent oxidative dissociation of the formed oligomers or polymers (Scheme 3.10). Moreover, no electropolymerisation was achieved in a potentiostatic experiment with an ITO working electrode. Obviously, the quality of the cyanide ion as a leaving group is not sufficient for this type of electrochemical polymerisation reaction.

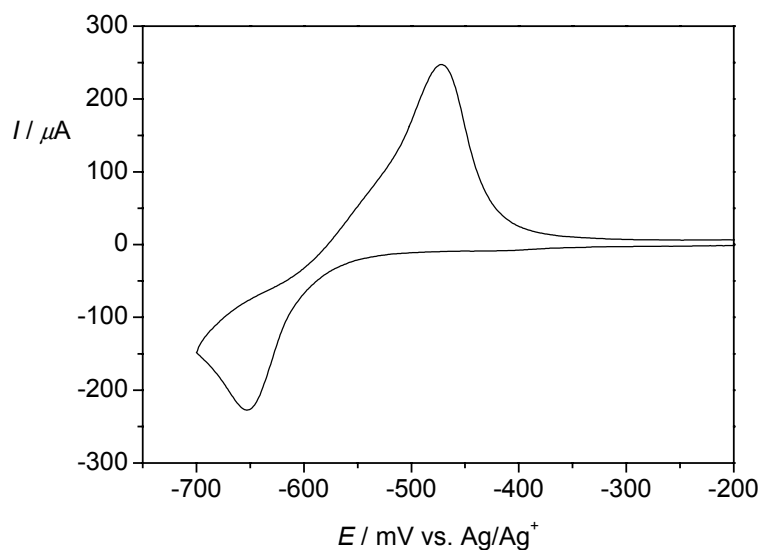


**Figure 3.6:** Cyclic voltammogram of **17-Br** in 0.1 M aqueous phosphate buffer (pH 7.4) at  $\nu = 100$  mV/s. Working electrode: platinum disc ( $\varnothing$  3 mm).

The chloro-substituted bispyridinio monomer **18-PF<sub>6</sub>** is reduced chemically irreversible at  $E_{\text{red}}^1 = -1140$  mV and  $E_{\text{red}}^2 = -1240$  mV in 0.2 M MeCN/TBAPF<sub>6</sub> using a platinum-disc working electrode. The products of the chemical follow up reaction exhibit oxidation signals at -670 mV and -410 mV (Figure 3.7).

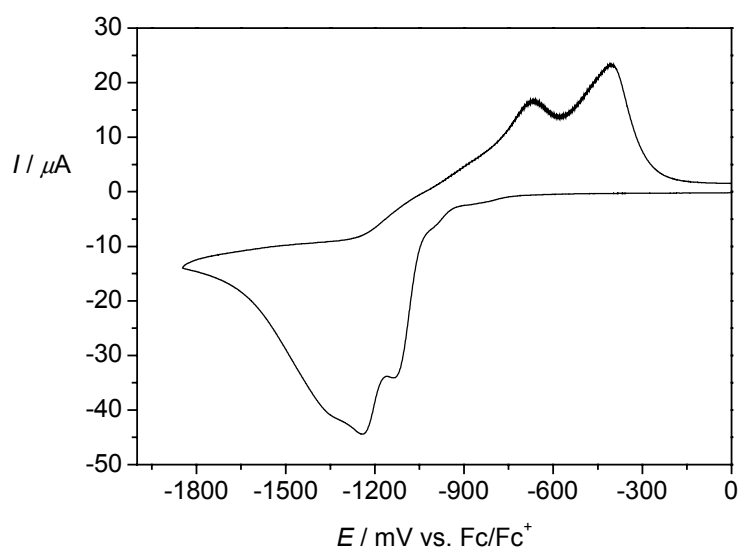


**Figure 3.7:** Cyclic voltammogram of **18-PF<sub>6</sub>** in 0.2 M MeCN/TBAPF<sub>6</sub>,  $\nu = 100$  mV/s. Working electrode: platinum disc ( $\varnothing$  3 mm).

Moreover, the peak current increases with each cycle upon consecutive potentiodynamic reduction indicating the formation of oligomers or polymers adsorbed on the electrode surface (Figure 3.8). It should be noted that the reduction potential of the monomer is shifted to higher values with each additional reduction cycle.

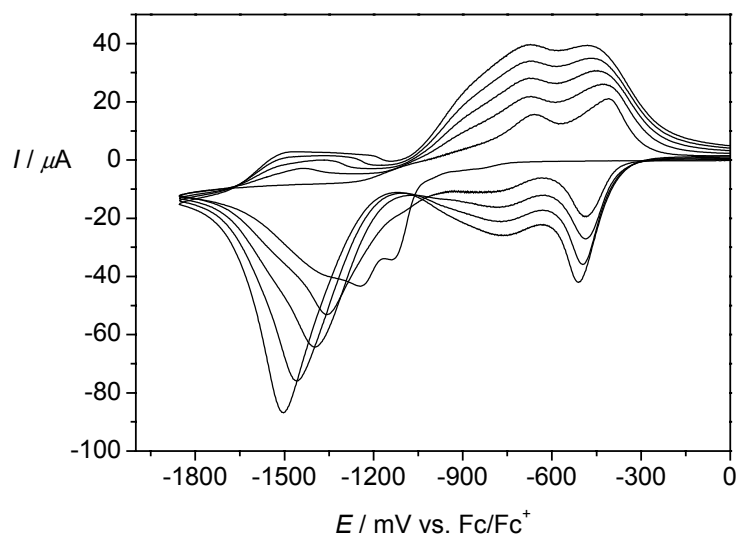


**Figure 3.8:** Multi-sweep cyclic voltammogram of **18-PF<sub>6</sub>** in 0.2 M MeCN/TBAPF<sub>6</sub>,  $\nu = 100$  mV/s. Working electrode: platinum disc ( $\varnothing$  3 mm).

Cyclic voltammetry was measured for *poly-18* in monomer-free 0.2 M MeCN/TBAPF<sub>6</sub> solution. The CV of *poly-18* is characterised by at least two relatively broad reversible reduction signals between -100 to -800 mV and an additional irreversible reduction at -1200 mV (vs. Ag/Ag<sup>+</sup>). The sharp anodic peak at -690 mV is associated with the irreversible reduction process and is not observed when only the first reduction wave is scanned.

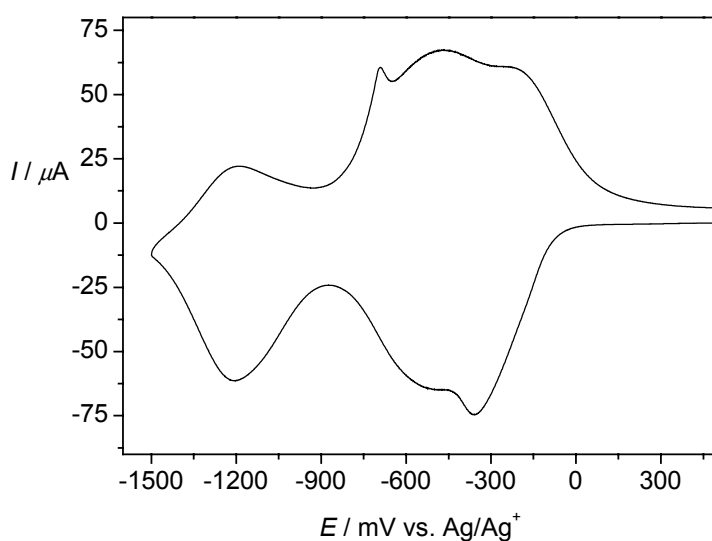


**Figure 3.9:** Cyclic voltammogram of *poly-18* in 0.2 M MeCN/TBAPF<sub>6</sub>,  $v = 250$  mV/s. Working electrode: platinum disc ( $\varnothing$  3 mm).

However, it was not possible to electropolymerise **18-PF<sub>6</sub>** onto a  $\varnothing$  6 mm platinum disc electrode, which was used for the spectroelectrochemical experiments of the oxadiazole and borane polymers (Section 2). After initiation of the potentiodynamic polymerisation (expressed by an increase of the peak current with each cycle in the CV) a sudden drop of the current to almost zero indicated the formation of an insulating material on the electrode surface after 3–5 redox cycles. It is noteworthy that a similar behaviour was observed in ca. 20–30 % of the polymerisations performed with a  $\varnothing$  3 mm platinum disc electrode. Nevertheless, it is not yet clear why **18-PF<sub>6</sub>** can be electropolymerised potentiodynamically onto a  $\varnothing$  3 mm platinum disc electrode (in 70–80 % of the experiments) but not onto a similar electrode with a diameter of 6 mm. It might be concluded that the quality of the chloride ion as a leaving group is still not sufficient to obtain reproducible results.

### 3.3.3 Absorption and Emission Spectroscopy

UV/Vis absorption and fluorescence spectra of the bispyridiniobenzene hexafluorophosphates **17-PF<sub>6</sub>** and **18-PF<sub>6</sub>** were recorded in acetonitrile and are depicted in Figure 3.10. Both compounds exhibit absorption bands at 35200 and 37300 cm<sup>-1</sup>, respectively. The fluorescence maxima of **17-PF<sub>6</sub>** and **18-PF<sub>6</sub>** at 22900 and 26100 cm<sup>-1</sup>, respectively, are extremely bathochromically shifted with respect to the absorption maxima which suggests a highly polar excited state.

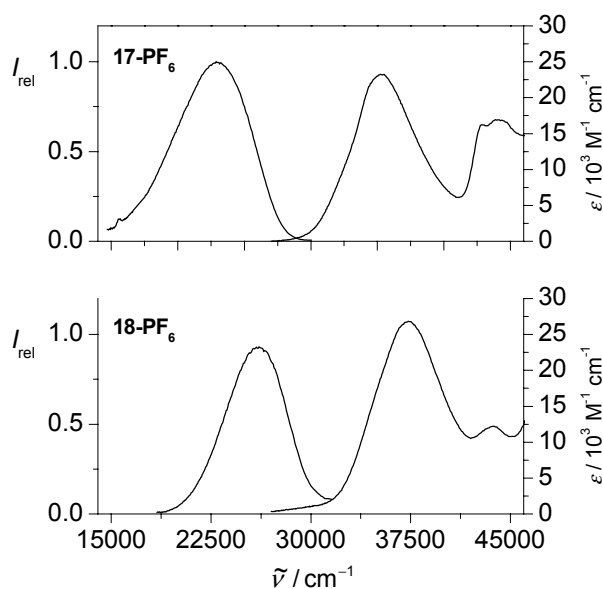


**Figure 3.10:** UV/Vis absorption and fluorescence spectra of **17-PF<sub>6</sub>** and **18-PF<sub>6</sub>** in MeCN.

### 3.3.4 Conductivity Measurements

The two-point method of Zotti et al.<sup>[46]</sup> was used to determine the conductivity of *poly-18* (see Section 2.5). Compound **18-PF<sub>6</sub>** was electropolymerised onto the TBE20 by potentiodynamic polymerisation as well as in galvanostatic and potentiostatic modes. With all methods the polymer growth was found to be insufficient in order to bridge the platinum contacts of the TBE. In the potentiodynamic experiment the reduction potential of **18-PF<sub>6</sub>** was shifted to more negative

values with each redox cycle (Figure 3.8) and after 10–15 cycles the peak current stopped increasing. During the galvanostatic polymerisation a continuous increase of the potential was observed, whereas the current decreased to almost zero in the potentiostatic mode. This may indicate that *poly-18* has only a low conductivity in its reduced state thereby inhibiting the reduction of monomers during polymer growth. It has been reported that the conductivity of a PPV-analogous viologen polymer ( $\sigma \approx 10^{-3}$  S/cm in the cationic oxidised form) decreased dramatically upon reduction of the polymer with  $\text{Na}_2\text{S}_2\text{O}_4$ .<sup>[24]</sup> In contrast, the solid state conductivity of neutral, i.e. reduced *N,N'*-diphenylviologen was found to be three orders of magnitude higher than that of the corresponding radical cation.<sup>[47]</sup>

### 3.3.5 Conclusions

Although the electrochemical dimerisation and polymerisation of 4-cyanopyridinio compounds has been described earlier<sup>[22, 23, 32]</sup> a similar reaction was not attained for the 1,4-bis-(4-cyanopyridinio)benzene dication (**17<sup>2+</sup>**). In acetonitrile solution stable radical cation and neutral species are formed upon electrochemical reduction, whereas in aqueous solution the reduced monomers are reactive enough to undergo a chemical reaction which is most likely the formation of  $\sigma$ -polymers on the electrode. However, the quality of  $\text{CN}^-$  as a leaving group is not sufficient to obtain the fully  $\pi$ -conjugated polymer.

The reaction sequence used for the synthesis of the chloro-substituted analogue 1,4-bis-(4-chloropyridinio)benzene dihexafluorophosphate (**18-PF<sub>6</sub>**) has the advantage of facile variation of both the spacer unit and the leaving group. This allows the synthesis of a broad variety of analogous compounds.

In contrast to **17<sup>2+</sup>** the chloro-substituted bispyridiniobenzene **18-PF<sub>6</sub>** can be polymerised by electrochemical reduction to yield an electroactive polymer film on the electrode surface. This discrepancy can be explained by the fact that  $\text{Cl}^-$  is a better leaving group than  $\text{CN}^-$ . *Poly-18*, which is the first electron-deficient isoelectronic analogue of poly(*para*-phenylene), can be reversibly switched between the cationic and a reduced form. However, it is not yet clear if this reduced form corresponds

either to the neutral or the radical cationic polymer. The “second” reduction process was found to be irreversible and leads to slow degradation of *poly-18*. The potential required for the reduction of *poly-18* is low compared to common electron transport materials (e.g. PBD)<sup>[1, 2]</sup> suggesting a high electron affinity. In OLEDs using p-type emitter materials an ETM with too high electron affinity leads to effective dissociation of the exciton states and consequently to a significant loss of electroluminescence.<sup>[1]</sup> Therefore, the use of *poly-18* as an ETM in OLEDs has to be questioned. On the other hand efficient exciton diffusion is a prerequisite for photovoltaic cells and hence *poly-18* might be used as an acceptor polymer in such a device.

The linear optical properties of the monomers **17-PF<sub>6</sub>** and **18-PF<sub>6</sub>** are characterised by a large Stokes-shift between the absorption and emission maxima. This might be due to a high excited-state dipole moment leading to a significant stabilisation of the excited state in polar solvents with respect to the ground state. Taking into account the symmetric molecular structure of **17-PF<sub>6</sub>** and **18-PF<sub>6</sub>** a high excited-state dipole moment must be due to an unsymmetrical distribution of the two positive charges in the excited state.

In conclusion it was demonstrated that an electron-deficient poly(*para*-phenylene)-analogue can be synthesised by reductive electropolymerisation of the corresponding monomeric precursor. This polymer might be an interesting ETM for use in (opto)electronic thin-film devices such as photovoltaic cells or polymer field effect transistors.

### 3.4 Literature

- [1] A. P. Kulkarni, C. J. Tonzola, A. Babel, S. A. Jenekhe, *Chem. Mater.* **2004**, *16*, 4556-4573.
- [2] G. Hughes, M. R. Bryce, *J. Mater. Chem.* **2005**, *15*, 94-107.
- [3] A. Kraft, A. C. Grimsdale, A. B. Holmes, *Angew. Chem.* **1998**, *110*, 416-443.
- [4] K. M. Coakley, M. D. McGehee, *Chem. Mater.* **2004**, *16*, 4533-4542.
- [5] T. Noda, Y. Shirota, *J. Am. Chem. Soc.* **1998**, *120*, 9714-9715.
- [6] M. Kinoshita, H. Kita, Y. Shirota, *Adv. Funct. Mater.* **2002**, *12*, 780-786.



- [7] C. D. Entwistle, T. B. Marder, *Angew. Chem. Int. Ed.* **2002**, *41*, 2927-2931.
- [8] C. D. Entwistle, T. B. Marder, *Chem. Mater.* **2004**, *16*, 4574-4585.
- [9] M. Miyata, N. Matsumi, Y. Chujo, *Macromolecules* **2001**, *34*, 7331-7335.
- [10] N. Matsumi, T. Umeyama, Y. Chujo, *Macromolecules* **2000**, *33*, 3956-3957.
- [11] R. J. P. Corriu, T. Deforth, W. E. Douglas, G. Guerrero, W. S. Siebert, *Chem. Commun.* **1998**, 963-964.
- [12] N. Matsumi, M. Miyata, Y. Chujo, *Macromolecules* **1999**, *32*, 4467-4469.
- [13] N. Matsumi, K. Naka, Y. Chujo, *J. Am. Chem. Soc.* **1998**, *120*, 10776-10777.
- [14] W. Sliwa, B. Bachowska, N. Zelichowicz, *Heterocycles* **1991**, *32*, 2241-2273.
- [15] L. A. Summers, *The Bipyridinium Herbicides*, Academic Press, New York, **1980**.
- [16] P. S. Braterman, J. I. Song, *J. Org. Chem.* **1991**, *56*, 4678-4682.
- [17] T. Saika, T. Iyoda, T. Shimidzu, *Chem. Lett.* **1990**, 1955-1958.
- [18] O. Ishitani, S. Yanagida, S. Takamuku, C. Pac, *Bull. Chem. Soc. Jpn.* **1987**, *60*, 1801.
- [19] V. Balzani, A. Credi, F. M. Raymo, J. F. Stoddart, *Angew. Chem. Int. Ed.* **2000**, *39*, 3349-3391.
- [20] R. K. Forcé, R. J. McMahon, J. Yu, M. S. Wrighton, *Spectrochim. Acta A* **1989**, *45A*, 23.
- [21] J. D. Batteas, A. Harriman, Y. Kanda, N. Mataga, A. K. Nowak, *J. Am. Chem. Soc.* **1990**, *112*, 126.
- [22] K. Kamata, T. Kawai, T. Iyoda, *Langmuir* **2001**, *17*, 155-163.
- [23] T. Saika, T. Iyoda, T. Shimidzu, *Bull. Chem. Soc. Jpn.* **1993**, *66*, 2054-2060.
- [24] A. Merz, S. Reitmeier, *Angew. Chem.* **1989**, *101*, 827-828.
- [25] R. H. Terrill, J. E. Hutchison, R. W. Murray, *J. Phys. Chem. B* **1997**, *101*, 1535-1542.
- [26] A. Factor, G. E. Heinsohn, *J. Polym. Sci., Part B: Polym. Lett.* **1971**, *9*, 289-295.
- [27] I. Druta, E. Avram, V. Cozan, *Eur. Polym. J.* **2000**, *36*, 221-224.
- [28] M. Valasek, J. Pecka, J. Jindrich, G. Calleja, P. R. Craig, J. Michl, *J. Org. Chem.* **2005**, *70*, 405-412.

- [29] P. K. Bhowmik, R. A. Burchett, H. S. Han, J. J. Cebe, *Macromolecules* **2001**, *34*, 7579-7581.
- [30] P. K. Bhowmik, H. Han, J. J. Cebe, I. K. Nedeltchev, S. W. Kang, S. Kumar, *Macromolecules* **2004**, *37*, 2688-2694.
- [31] F. Y. Lin, S. Z. D. Cheng, F. W. Harris, *Polymer* **2002**, *43*, 3421-3430.
- [32] I. Shain, E. M. Kosower, W. M. Schwarz, *J. Am. Chem. Soc.* **1961**, *83*, 3164.
- [33] S. Tanaka, T. Iso, *J. Chem. Soc. Chem. Commun.* **1994**, 1071-1072.
- [34] M. P. Doyle, B. Siegfried, J. F. Dellaria, Jr., *J. Org. Chem.* **1977**, *42*, 2426-2431.
- [35] L. Pauling, *J. Am. Chem. Soc.* **1932**, *54*, 3570-3582.
- [36] B. Ramsey, M. A. Elbayoumi, M. Kasha, *J. Chem. Phys.* **1961**, *35*, 1502-1503.
- [37] B. G. Ramsey, *J. Phys. Chem.* **1966**, *70*, 611-618.
- [38] J. C. Doty, B. Babb, M. E. Glogowski, J. L. Williams, P. J. Grisdale, *J. Organomet. Chem.* **1972**, *38*, 229-236.
- [39] R. Stahl, *Diploma Thesis*, Würzburg, **2001**.
- [40] F. Ullmann, G. Nadai, *Chem. Ber.* **1908**, *41*, 1870-1878.
- [41] J. P. Wibaut, F. W. Brockman, *Rec. trav. chim.* **1959**, *78*, 593-603.
- [42] A. Vilsmeier, A. Haack, *Ber. Dtsch. Chem. Ges.* **1927**, *60*, 119-122.
- [43] S. Hünig, G. Köbrich, *Ann. Chem.* **1958**, *617*, 181-202.
- [44] C. De Souza, Y. Hajikarimian, P. W. Sheldrake, *Synth. Commun.* **1992**, *22*, 755-759.
- [45] E. R. Riegel, F. Zwiilmeyer, *Org. Syn. Coll. Vol. II* **1944**, 126-128.
- [46] G. Schiavon, S. Sitran, G. Zotti, *Synth. Met.* **1989**, *32*, 209-217.
- [47] W. W. Porter III, T. P. Vaid, *J. Org. Chem.* **2005**, *70*, 5028-5035.

## 4 Summary

In this work the electrochemical and spectroelectrochemical properties of a series of  $\pi$ -conjugated organic polymers were studied. The polymers were deposited on platinum electrodes or ITO-coated glass substrates by potentiodynamic electropolymerisation of the corresponding monomeric precursor molecules. The electrochemical and photophysical properties of the triarylborane monomers were studied in detail in order to estimate possible influences on the behaviour of the corresponding polymer.

The first part of this work aimed at the synthesis and investigation of conjugated donor–acceptor polymers which combine the prerequisites of an OLED within one material: the transport of positive and negative charges and the formation of emissive excited states.

With the carbazole-substituted oxadiazoles **1–3** it was shown that on the one hand the carbazole functionality is suitable for enabling the electrochemical polymerisation of the monomers and on the other hand it facilitates reversible p-doping of the resultant polymers. Although n-doping of *poly-1–poly-3* is possible due to the electron-deficient oxadiazole rings, it causes the continuous degradation of these electron-acceptor units. Interestingly, this process does not influence the capability of p-doping of the polymers.

With respect to its electrochemical and spectroelectrochemical properties the behaviour of the borane polymer *poly-4* is absolutely identical with that of the oxadiazole polymers. Moreover, the optical excitation of *poly-4* in the solid state leads to the emission of blue-green light which suggests that this polymer might also possess electroluminescent properties. AFM-measurements of *poly-4* films on ITO-coated glass substrates revealed, that the film thickness can be controlled to a certain extent by the number of polymerisation redox cycles.

It was shown from the electrochemical and photophysical properties of the triarylboranes **4–6** that the  $\pi$ – $\pi$ -interaction between boron and nitrogen atoms is comparably weak in these molecules. This leads to an unexpected ground-state polarisation with a partially positive boron atom and a partially negative nitrogen

atom. Moreover, it was found that TAB **4** possesses a lower symmetry than  $D_3$  in solution and that excitation energy can be transferred amongst the three subchromophores of **4**.

By titration experiments it was also demonstrated that TAB **4** can reversibly bind fluoride ions and that the binding event significantly influences the optical absorption characteristics of the chromophore.

It can be assumed, that the above mentioned properties, which have a profound influence on the photophysical behaviour of these triarylborane chromophores, also determine the behaviour of the corresponding polymer in a solid state environment.

The aim of the second part of this work was the investigation of purely n-conducting materials based on electron-deficient borane and viologen polymers. The corresponding precursor molecules should be polymerised on platinum electrodes by reductive electropolymerisation.

However, a reductive polymerisation was not possible for the borane monomer **19** which is thought to be due to a strong localisation of the unpaired electron on the central boron atom of the radical anion. An electropolymerisation of the cyano-substituted bispyridinio-compound **17**<sup>2+</sup> failed because of the poor quality of CN<sup>-</sup> as a leaving group. Thus, a synthesis of the analogous isomer **18**<sup>2+</sup> was developed, in which the cyano-substituents were exchanged by the better leaving group Cl<sup>-</sup>. The viologen polymer *poly-18*, which can be regarded as an electron-deficient iso-electronic analogue of poly(*para*-phenylene), was successfully deposited on a platinum electrode by reductive electropolymerisation of **18**<sup>2+</sup>. *Poly-18* can be reversibly n-doped at comparably low potentials; however, at higher potentials the polymer is overcharged and destroyed irreversibly. As the synthetic strategy for **18**<sup>2+</sup> allows the variation of both spacer unit and leaving group in the last two steps of the reaction sequence, a series of analogous compounds can be easily synthesised using this route.

## 5 Experimental Section

### 5.1 Analytical Methods

#### NMR spectroscopy

- Bruker AC 250 FT-Spectrometer ( $^1\text{H}$ : 250.13 MHz,  $^{13}\text{C}$ : 62.91 MHz)
- Bruker Avance 400 FT-Spectrometer ( $^1\text{H}$ : 400.1 MHz,  $^{13}\text{C}$ : 100.6 MHz)
- Bruker Avance DMX 600 FT-Spectrometer ( $^1\text{H}$ : 600.13 MHz,  $^{13}\text{C}$ : 150.92 MHz)

All  $^1\text{H}$ - and  $^{13}\text{C}$ -NMR spectra were recorded at room temperature unless otherwise indicated. The signal of the respective solvent was used as the internal reference and the chemical shifts are given in ppm ( $\delta$ -scale) versus TMS. Multiplicities were denoted as *s* (singlet), *bs* (broad singlet), *d* (doublet), *t* (triplet), *m* (multiplet) and *sh* (shoulder). Coupling constants are given in Hz.

NMR-Spectroscopy data are quoted as follows: chemical shift (multiplicity, coupling constants, number of protons, assignment).

#### Mass spectrometry

- Finnigan MAT 90
- Bruker Daltonik microTOF focus

Mass spectra were recorded at the Institute of Organic Chemistry, University of Würzburg. For ESI-spectra 10  $\mu\text{M}$  solutions of the sample in acetonitrile or methanol were prepared. Mass spectrometry data are quoted as follows: *m/z* (relative intensity, assignment). For high resolution mass spectra only the *m/z* values of the  $\text{M}^+$ -ion are given.

#### Elemental analysis

- Leco CHNS-932

The elemental analyses were performed at the Institute of Inorganic Chemistry, University of Würzburg.

### Melting points

All melting points were measured with a Tottoli melting-point apparatus from Büchi and are not corrected.

### Differential Scanning Calorimetry (DSC)

- TA Instruments DSC Q1000

DSC measurements for the triarylboranes **4**, **5** and **6** were performed at the Institute of Organic Chemistry (AK Würthner), University of Würzburg.

### UV/Vis/NIR spectroscopy

- Jasco V-570 UV/Vis/NIR spectrophotometer

All spectra were recorded in 1 cm quartz cells (Hellma) in solvents of spectroscopic grade unless otherwise indicated.

Mode of quotation:  $\tilde{\nu}_{\text{abs}}$  in  $\text{cm}^{-1}$  ( $\epsilon$  in  $\text{M}^{-1} \text{cm}^{-1}$ )

### UV/Vis Titration of TAB 4

A 1.0 mM solution of tetrabutylammonium fluoride in anhydrous THF was added stepwise (20  $\mu\text{l}$  aliquots) to 2 ml of a THF solution of triarylborane **4** (46.8  $\mu\text{M}$ ) in a UV quartz cell. UV/Vis spectra were recorded after attainment of equilibrium ( $\sim 5$  min) and the binding constant  $K_{\text{b}}$  was determined using the global-analysis software SPECFIT/32<sup>TM</sup>.<sup>[1]</sup>

### Fluorescence spectroscopy

- Photon Technology International QuantaMaster<sup>TM</sup> Model QM-2000-4 including a cooled photomultiplier (type R928P) and a 75 W xenon short arc lamp (type UXL-75XE, Ushio).
- Photon Technology International TimeMaster<sup>TM</sup> Model TM-2/2003 fluorescence lifetime spectrometer including a nanosecond flash-lamp (filled with  $\text{H}_2/\text{N}_2 = 1:1$ ).

Mode of quotation:  $\tilde{\nu}_{\text{fl}}$  in  $\text{cm}^{-1}$ .

All spectra were recorded in 1 cm quartz cells (Hellma) in solvents of spectroscopic grade unless otherwise indicated. The solute concentration was about  $10^{-6}$  M and traces of oxygen were removed by bubbling a stream of argon through the solutions for about 5 minutes prior to each scan. The fluorescence quantum yields were determined from the absorption and fluorescence spectra according to Equation 5-1, where  $I_f$ ,  $OD$  and  $n$  denote the intensity of the fluorescence, the optical density of the solution at the excitation wavelength ( $< 0.1$ ) and the refractive index of the solvent, respectively.

$$\Phi_f = \Phi_{f,\text{ref}} \frac{\int I_f(\tilde{\nu}) \frac{OD_{\text{ref}}}{OD} \frac{n^2}{n_{\text{ref}}^2}}{\int I_f(\tilde{\nu})_{\text{ref}} \frac{OD_{\text{ref}}}{OD} \frac{n^2}{n_{\text{ref}}^2}} \quad (\text{eq. 5-1})$$

A solution of Rhodamin 101 in ethanol was used as the reference (index *ref*) as this compound possesses a constant quantum yield of 1.0 over a wide temperature range.<sup>[2]</sup>

For time-dependent fluorescence decay measurements the instrument response of the nanosecond flash-lamp was determined using coffee creamer or colloidal silica (Ludox<sup>®</sup>) in de-ionised water as a scatterer. The fluorescence decay curves were fitted with a single exponential decay function in order to obtain the corresponding fluorescence lifetimes.

### Solid-State Fluorescence Spectroscopy of Polymer Films

Solid-state fluorescence spectra of polymer films were measured on ITO-coated glass substrates (Merck) which were mounted in the fluorescence spectrometer at an angle of  $30^\circ$  with respect to the direction of the excitation beam. Thereby, the direct reflection of the excitation beam into the detector channel was avoided. A cut-on filter with suitable transmission characteristics was inserted into the emission channel of the spectrometer in order to minimise the amount of detected scattered excitation light. The polymers were deposited onto the ITO sheets from standard solutions (see cyclic voltammetry) by potentiodynamic electropolymerisation.

### **Polarised Steady-State Fluorescence Spectroscopy.**

Fluorescence-anisotropy measurements were carried out in a sucrose-octaacetate (SOA) matrix at room temperature. Two Glan-Thompson polarisers from Photon Technology International were used in an L-format setup. SOA was purchased from Acros Organics and recrystallised twice from ethanol. Sample preparation was done according to a procedure reported in literature.<sup>[3]</sup> The corresponding compound and SOA were dissolved in dichloromethane (Merck, Uvasol). The solution was filtered through a glass frit in order to remove any traces of lints and dust and purged with dry and oxygen free argon for 10 minutes. The dichloromethane was partially removed in vacuo until a viscous oil resulted which was filled into a 1 cm fluorescence quartz cuvette. The cuvette was then kept in an oven at 100 °C for about one hour and at 150 °C for 30 minutes to remove the remaining dichloromethane. The concentrations of the fluorescent dyes in the SOA glass matrix were circa 3  $\mu\text{M}$ . In the case of TAB 5 the excitation anisotropy was measured at an emission wavenumber of 25000  $\text{cm}^{-1}$  and for determination of the emission anisotropy the solution was excited at 28500  $\text{cm}^{-1}$ . For TAB 4 the corresponding emission and excitation wavenumbers were 23000  $\text{cm}^{-1}$  and 27000  $\text{cm}^{-1}$ , respectively.

### **Cyclic voltammetry**

- Electrochemical Workstation BAS CV-50 W including software version 2.0
- Princeton Applied Research potentiostat/galvanostat model 283 (PAR 283) including software Power Suite

Cyclic voltammetry experiments were carried out under an argon atmosphere (argon dried with Sicapent<sup>®</sup> from Merck, traces of oxygen removed with copper oxide catalyst R3-11 from BASF) in dry and oxygen-free solvents with 0.2–0.3 M supporting electrolyte (TBAPF<sub>6</sub> or TBAP). The concentration of the analyte ranged from 0.2–2 mM depending on its solubility and the test solutions were saturated with argon prior to the experiments. A conventional three electrode setup consisting of a platinum-disc working electrode ( $\varnothing$  3 mm), a Ag/AgCl pseudo-reference electrode and a platinum-wire counter electrode was used. The redox potentials were referenced against the ferrocene/ferrocenium redox couple as an internal standard.



For measurements under thin-layer conditions the working electrode was placed onto a mobile glass hemisphere.<sup>[4]</sup> Cyclic voltammetry of the polymers was performed in monomer-free electrolyte solutions (ca. 0.2 M). After potentiodynamic electropolymerisation the electrochemical cell was rinsed three times with the pure solvent and finally the electrolyte solution was added.

### Spectroelectrochemistry

- Jasco V-570 UV/Vis/NIR spectrophotometer
- EG & G potentiostat/galvanostat model 363
- Electrochemical Workstation BAS CV-50 W including software version 2.0

Spectroelectrochemical experiments were performed in a specially designed sample compartment consisting of a cylindrical quartz cell, a platinum disc electrode ( $\varnothing$  6 mm), a gold-covered metal (V2A) plate as the counter electrode and a Ag/AgCl pseudo-reference electrode. Deposition of the polymers was accomplished by potentiodynamic oxidation or reduction of the appropriate monomer according to the experimental protocol used for cyclic voltammetry. All spectra were recorded in reflection mode and the optical path-length was varied by adjusting the vertical position of the working electrode with a micrometer screw. The potential applied to the polymer was varied in steps of 10–100 mV and a UV/Vis/NIR spectrum was recorded ca. one minute after increasing the potential.

### Conductivity measurements

In-situ conductivity measurements were carried out with platinum two-band electrodes (TBE) in an experimental setup described previously.<sup>[5]</sup> The TBEs were constructed as follows: Two platinum foils (3 x 12 x 0.1 mm) were separated by an insulating Mylar<sup>®</sup> spacer (10, 20, 50 and 100  $\mu\text{m}$ , DuPont Teijin Films) and sandwiched between two glass sheets (3 x 7 x 1 mm) (Figure 5.1). All components were attached face-to-face with epoxy (UHU Plus) under pressure. The epoxy glue was used in such a small amount that the space between the platinum foils was not significantly increased. Lead contacts were attached at the end of the platinum foils with silver epoxy and the whole assembly was placed into a glass tube ( $\varnothing_{\text{ext}} = 7$  mm,  $\varnothing_{\text{int}} = 5$  mm). Both ends of the tube were sealed with epoxy and finally the electrode

was polished with diamond paste<sup>[b]</sup>. According to their Mylar<sup>®</sup> spacer the electrodes are called TBE10, TBE20, TBE50 and TBE100. From microscope photographs of the TBE20, TBE50 and TBE100 (Figure 5.2) the actual distance between the platinum foils was determined to be  $30 \mu\text{m}$  ( $\pm 10 \mu\text{m}$ ),  $50 \mu\text{m}$  ( $\pm 5 \mu\text{m}$ ) and  $80 \mu\text{m}$  ( $\pm 2 \mu\text{m}$ ), respectively.

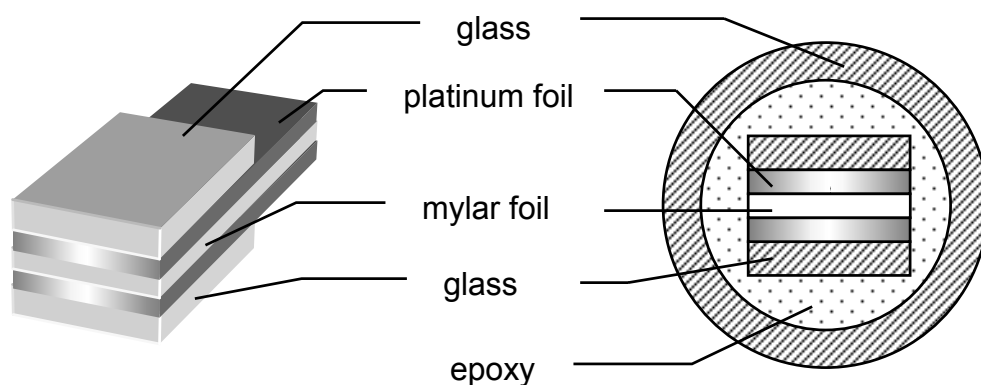


**Figure 5.1:** Schematic representation of a platinum two-band electrode.

A microscope photograph of the TBE50 and TBE100 is shown in Figure 5.2.

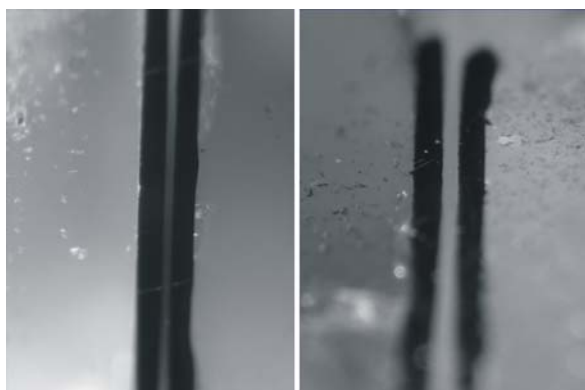


**Figure 5.2:** Microscope photograph of the TBE 50 (left) and the TBE100 (right).

The deposition of the polymers onto the TBEs was accomplished in a standard CV setup with the two contacts of the TBE connected together as one working electrode. In order to obtain homogeneous films<sup>[6]</sup> the electropolymerisation was done in a galvanostatic mode (PAR 283) with current densities of  $0.1\text{--}1 \text{ mA/cm}^2$ . From time to

[b] The TBEs can not be used in solvents like  $\text{CH}_2\text{Cl}_2$  or THF which dissolve the epoxy glue.

time the deposition was interrupted and the resistance between the two TBE contacts was measured with a digital multimeter. When no significant change in the resistance was observed, the deposition process was stopped. This is necessary in order to measure the conductivity under semi-infinite volume conditions where the drain current (see below) is not limited by the polymer thickness.

The experimental setup used for the conductivity measurements is illustrated in Figure 5.3. The conductivity measurements were carried out under monomer-free conditions (solvent/electrolyte) in a standard CV cell. The gate potential ( $E_g$ ) was controlled with an EG & G model 363 potentiostat while the drain current ( $I_d$ ) was measured with a BAS CV-50 W electrochemical workstation (single potential time-based mode). A low drain potential of  $E_d = 10$  mV was applied in order to minimise deviations from equilibrium. The deposited polymer was conditioned by potentiodynamic redox cycling (2–3 cycles) before the conductivity measurements<sup>[c]</sup>. Then, the polymer film was brought to the desired gate potential and after 5–10 minutes equilibration time the corresponding drain current was measured<sup>[d]</sup>. The specific conductivity ( $[\sigma] = \Omega^{-1} \text{ cm}^{-1}$ ) can then be calculated according to Equation 5-2,

$$\sigma = \frac{I_d}{E_d} \cdot d \quad (\text{eq. 5-2})$$

where  $E_d$ ,  $I_d$  and  $d$  denote the drain potential, drain current and the distance between the two platinum foils (electrode spacing), respectively.

It should be noted that the total measurable resistance ( $R_t$ ) consists of the polymer resistance ( $R_p$ ) and the contact resistance ( $R_c$ ) at the polymer/electrode interface.  $R_c$  can be determined by measuring  $R_t$  for different electrode spacings ( $d$ ) and plotting  $R_t$  versus  $d$ . Assuming a linear relationship, an extrapolation of  $R_t$  to  $d = 0$  (and consequently  $R_p = 0$ ) yields the contact resistance  $R_c$ .<sup>[5]</sup>

[c] The overall polymer resistance was found to be lower when redox cycling was stopped in the charged state in most cases.

[d] It was found that the current range of the gate potentiostat should be set as low as possible in order to improve the signal-to-noise ratio (minimised ground loop current).

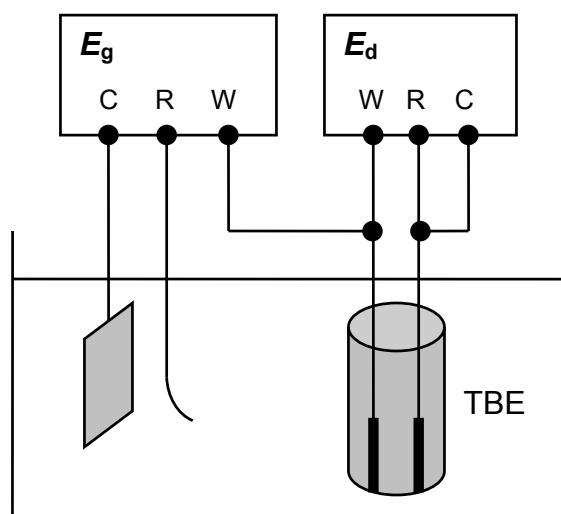


**Figure 5.3:** Experimental setup used for the in-situ conductivity measurements with the platinum two-band electrodes (TBE). W, R and C denote the working, reference and counter electrode contacts of the potentiostats used to control the gate ( $E_g$ ) and drain ( $E_d$ ) potential.

### Atomic Force Microscopy (AFM)

AFM measurements were accomplished with a commercial AFM MultiMode (Nanoscope IV, Veeco, Santa Barbara, CA) operated in TappingMode™. The AFM was equipped with a 12  $\mu\text{m}$  scanner. Olympus silicon cantilevers with a resonance frequency of  $\sim 300$  kHz were used.

The samples were prepared by potentiodynamic electropolymerisation of the appropriate monomer from 0.3 mM methylene chloride solutions on indium tin oxide (ITO) coated glass sheets (0.9 x 0.9 mm, Merck). The electrolyte concentration was 0.2 M TBAPF<sub>6</sub> for **1** and 0.2 M TBAP for **4**. After polymerisation each film was rinsed with methylene chloride to remove traces of the monomer. The thickness of the polymer-film was controlled by varying the number of consecutive redox cycles during polymerisation.

### Electrooptical Absorption Measurements (EOAM).

The EOA technique measures the influence of the square of the electric field on the molar decadic absorption coefficient. The relative change induced by the field is a function of the wavenumber and the angle between the polarisation vector of the incident light and the applied field. Typically the EOA spectrum is recorded for two polarisations ( $0^\circ$  and  $90^\circ$ ), and multilinear regression analysis in terms of the optical

absorption spectrum, its first and second derivative yields a set of regression coefficients, from which the ground-state dipole moment and the dipole difference between ground state and the excited state may be calculated.<sup>[7]</sup> EOAM spectra were recorded in 1,4-dioxane at 298 K. The solvent was dried by distillation from Na under an argon atmosphere prior to use. Details of the EOAM apparatus are given elsewhere.<sup>[8]</sup> Supplementary optical absorption spectra were performed with a Perkin-Elmer Lambda 900 spectrometer.

### **Synthesis**

All reactions were carried out in standard glassware unless otherwise indicated. The reagents were of standard quality (Fluka, Aldrich, Merck, Acros, Avocado) and used without further purification. Reactions under inert-gas conditions (nitrogen, dried with Sicapent<sup>®</sup> from Merck, traces of oxygen removed with copper oxide catalyst R3-11 from BASF) were carried out in flame-dried Schlenk vessels, the solvents were purified and dried by standard procedures and kept under inert-gas atmosphere.

### **Chromatography**

- silica gel for flash chromatography (32–63  $\mu\text{m}$ , MP Biomedicals)

## 5.2 Syntheses

### 5.2.1 General Experimental Procedures

#### 5.2.1.1 Copper-catalysed amination of aryl halides with CuI<sup>[9]</sup> (EP1)

Carbazole, CuI (2–5 mol%), *trans*-1,2-cyclohexanediamine (10 mol%), potassium phosphate and the aryl halide are suspended in absolute dioxane under a nitrogen atmosphere and stirred for 24–72 h at 110 °C. The reaction mixture is suspended in CH<sub>2</sub>Cl<sub>2</sub> and washed with water. The aqueous phase is extracted with CH<sub>2</sub>Cl<sub>2</sub> and the combined organic extracts are dried over MgSO<sub>4</sub>. The crude product is purified by column chromatography unless otherwise indicated.

#### 5.2.1.2 Halogenation of arylamines with copper(II) halides<sup>[10]</sup> (EP2)

At room temperature a solution of the arylamine in dry acetonitrile is added dropwise to a stirred suspension of *tert*-butyl nitrite and the copper(II) halide in dry acetonitrile. The reaction mixture is stirred at room temperature for 48 h and then poured onto 20% hydrochloric acid. The aqueous phase is extracted several times with diethylether and the combined organic extracts are washed with 20% HCl and dried over MgSO<sub>4</sub>. The crude product is purified by column chromatography.

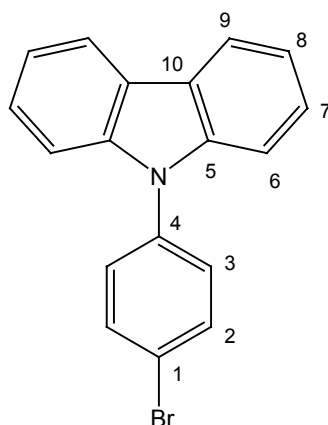
#### 5.2.1.3 Palladium-catalysed cross-coupling of aryl bromides with 2,5-Bis-(4-iodophenyl)-1,3,4-oxadiazole (EP3)

The aryl bromide was converted into the corresponding Grignard reagent by standard procedures. If necessary, 1,2-dibromoethane was added to start the Grignard-reaction. Under a nitrogen atmosphere 2,5-bis-(4-iodophenyl)-1,3,4-oxadiazole and Pd(PPh<sub>3</sub>)<sub>2</sub>Cl<sub>2</sub> were suspended in absolute THF. The Grignard solution in THF was added dropwise and the reaction mixture was stirred at room temperature for 3–4 days. The reaction mixture was suspended in CH<sub>2</sub>Cl<sub>2</sub> and washed with water. The

aqueous phase was extracted several times with  $\text{CH}_2\text{Cl}_2$  and the combined organic extracts were dried over  $\text{MgSO}_4$ . The solvent was removed in vacuo. The crude product was stirred in boiling acetone for three hours, filtered and dried in vacuo.

### 5.2.2 Synthesis of the Carbazole-Substituted Precursors

9-(4-Bromophenyl)-9*H*-carbazole (**8**)



CA: [57102-42-8]

Synthesis according to *EP1*

1-Bromo-4-iodobenzene:	13.1 g	46.3 mmol
Carbazole:	5.19 g	31.0 mmol
Copper(I) iodide:	250 mg	1.31 mmol
<i>trans</i> -1,2-Cyclohexanediamine:	0.38 ml	3.16 mmol
Potassium phosphate:	13.8 g	65.0 mmol
Dioxane (abs.):	45 ml	

The crude product was purified by flash chromatography with dichloromethane/ petrol ether (1:5).

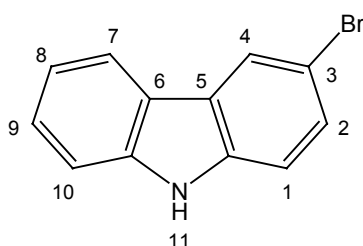
**Formula:** C<sub>18</sub>H<sub>12</sub>BrN (322.20)

**Yield:** 7.73 g (24.0 mmol, 77%) off-white solid

**Melting point:** 146 °C (dichloromethane/petrol ether), lit.<sup>[11]</sup>: 146-147 °C (MeCN)

**<sup>1</sup>H-NMR (400 MHz, acetone-d<sub>6</sub>):**  $\delta$  = 8.22 (m, 2H, H9), 7.87 (AA', 2H, H2), 7.61 (BB', 2H, H3), 7.46 - 7.41 (4H, H6, H7 or H8), 7.30 (m, 2H, H8 or H7)

### 3-Bromo-9H-carbazole (**9**)



CA: [1592-95-6]

Synthesis according to lit.<sup>[12]</sup>

Carbazole:	4.18 g	25.0 mmol
Pyridinium hydrobromide perbromide:	9.50 g	29.7 mmol
Toluene:	90 ml	
Ethanol:	90 ml	

To a stirred suspension of carbazole in 150 ml toluene/ethanol was added dropwise at room temperature a solution of pyridinium hydrobromide perbromide in 30 ml toluene/ethanol. The reaction mixture was stirred at room temperature for 4.5 h and diluted with 150 ml of H<sub>2</sub>O and 100 ml of CH<sub>2</sub>Cl<sub>2</sub>. The organic phase was removed and the aqueous phase was extracted twice with 50 ml of CH<sub>2</sub>Cl<sub>2</sub>. The combined organic extracts were dried over MgSO<sub>4</sub> and the solvent was removed in vacuo. The crude product was recrystallised twice from chloroform.



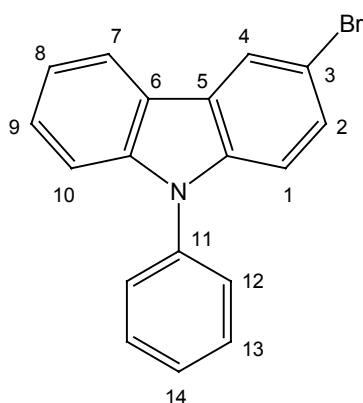
**Formula:** C<sub>12</sub>H<sub>8</sub>BrN (246.10)

**Yield:** 3.65 g (14.8 mmol, 59 %) colourless plates

**Melting point:** 199-201 °C (chloroform), lit.<sup>[13]</sup>: 197-200 °C (petrol ether/acetone)

**<sup>1</sup>H-NMR (400 MHz, acetone-d<sub>6</sub>):**  $\delta$  = 10.46 (br s, 1H, H11), 8.29 (m, 1H, H4), 8.16 (m, 1H, H7), 7.54-7.47 (3H, H1,H2 ,H10), 7.43 (m, 1H, H9), 7.21 (m, 1H, H8)

### 3-Bromo-9-phenyl-9H-carbazole (**10**)



CA: [1153-85-1]

Synthesis according to *EP1*

3-Bromo-9H-carbazole:	1.00 g	4.06 mmol
Iodobenzene:	6.24 g	30.6 mmol
Copper(I) iodide:	38.9 mg	0.204 mmol
<i>trans</i> -1,2-Cyclohexanediamine:	49 $\mu$ l	0.408 mmol
Potassium phosphate:	1.82 g	8.57 mmol
Dioxane (abs.):	10 ml	

The crude product was purified by flash chromatography with dichloromethane/petrol ether (1:9) and subsequent recrystallisation from THF/methanol (5:95).

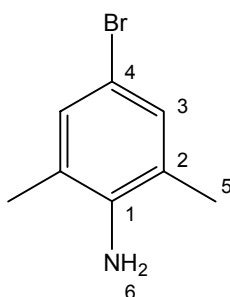
**Formula:** C<sub>18</sub>H<sub>12</sub>BrN (322.20)

**Yield:** 1.18 g (3.66 mmol, 90 %) colourless solid

**Melting point:** 75-77 °C (THF/methanol), lit.<sup>[14]</sup>: 79-80 °C (ethanol/ethyl acetate)

**<sup>1</sup>H-NMR (400 MHz, acetone-d<sub>6</sub>):**  $\delta$  = 8.40 (m, 1H, H4), 8.27 (m, 1H, H7), 7.71 (m, 2H, H13), 7.63 (m, 2H, H12), 7.59-7.53 (2H, H14, H2), 7.48 (m, 1H, H9), 7.39 (m, 1H, H10), 7.35 (2H, H8, H1)

4-Bromo-2,6-dimethylaniline (**11**)



CA: [24596-19-8]

Synthesis according to lit.<sup>[15]</sup>

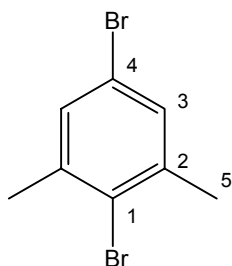
2,6-Dimethylaniline:	30.3 g	250 mmol
Bromine:	12.9 ml	250 mmol
Acetic acid:	75 ml	

**Formula:** C<sub>8</sub>H<sub>10</sub>BrN (200.08)

**Yield:** 45.4 g (227 mmol, 91 %) grey solid

**Melting point:** 49-50 °C (H<sub>2</sub>O), lit.<sup>[16]</sup>: 50 °C (dist.)

**<sup>1</sup>H-NMR (400 MHz, CDCl<sub>3</sub>):**  $\delta$  = 7.06 (m, 2H, H3), 3.52 (br s, 2H, H6), 2.15 (m, 6H, H5)

2,5-Dibromo-1,3-dimethylbenzene (**12**)

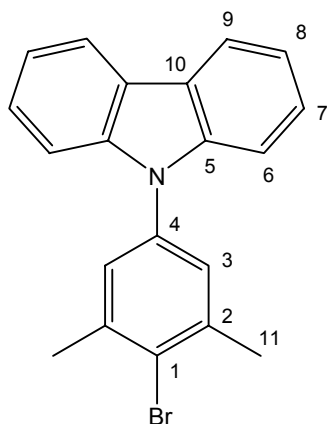
CA: [100189-84-2]

Synthesis according to *EP2*

4-Bromo-2,6-dimethylaniline:	15.0 g	75.0 mmol
Copper(II)-bromide:	20.1 g	90.0 mmol
<i>tert</i> -Butyl nitrite:	13.4 ml	113.5 mmol
Acetonitrile (abs.):	350 ml	
Hydrochloric acid (20%):	600 ml	

The crude product was purified by flash chromatography with 100% petrolether.

**Formula:** C<sub>8</sub>H<sub>8</sub>Br<sub>2</sub> (263.96)**Yield:** 15.1 g (57.2 mmol, 76%) colourless liquid**Melting point:** –**<sup>1</sup>H-NMR (400 MHz, CDCl<sub>3</sub>):** δ = 7.21 (m, 2H, H3), 2.38 (m, 6H, H5)**<sup>13</sup>C-NMR (63 MHz, CDCl<sub>3</sub>):** δ = 140.3, 131.0, 126.4, 120.4, 23.8

9-(4-Bromo-3,5-dimethylphenyl)-9*H*-carbazole (**13**)

CA: -

Synthesis according to *EP1*

2,5-Dibromo-1,3-dimethylbenzene:	8.70 g	33.0 mmol
Carbazole:	8.27 g	49.5 mmol
Copper(I) iodide:	0.314 g	1.65 mmol
<i>trans</i> -1,2-Cyclohexanediamine:	0.40 ml	3.33 mmol
Potassium phosphate:	22.1 g	104 mmol
Dioxane (abs.)	35 ml	

The crude product was purified by flash chromatography with dichloromethane/ petrol ether (1:10).

**Formula:** C<sub>20</sub>H<sub>16</sub>BrN (350.25)

**Yield:** 10.0 g (28.6 mmol, 87%) colourless solid

**Melting point:** 125-127 °C (dichloromethane/petrol ether)

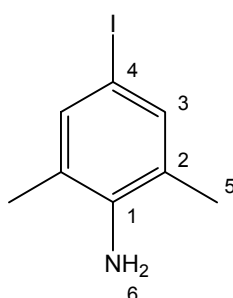
**<sup>1</sup>H-NMR (400 MHz, acetone-d<sub>6</sub>):** δ = 8.20 (m, 2H, H9), 7.43-7.41 (6H, H3, H6, H7 or H8), 7.28 (m, 2H, H8 or H7), 2.54 (m, 6H, H11)

**<sup>13</sup>C-NMR (100 MHz, acetone-d<sub>6</sub>):** δ = 141.6, 141.1, 137.2, 127.5, 127.0, 126.6, 124.3, 121.1, 121.0, 110.7, 24.0

**EI-MS (high resolution, PI):** calc. for  $C_{20}H_{16}BrN$ :  $m/z = 349.04606$ , exp.:  $m/z = 349.04615$ ,  $\Delta = 0.26$  ppm

### 5.2.3 Synthesis of the Diphenylamino Precursor

4-Iodo-2,6-dimethylaniline (**14**)



CA: [4102-53-8]

Synthesis according to lit.<sup>[17]</sup>

2,6-Dimethylaniline:	30.3 g	250 mmol
Potassium iodide:	27.9 g	168 mmol
Potassium iodate:	17.8 g	83.2 mmol
Hydrochloric acid (2.56 M):	100 ml	256 mmol
Methanol:	125 ml	
Water:	750 ml	

For purification the crude product was treated three times with 250 ml of boiling *n*-hexane. The combined organic extracts were kept at -30 °C for 16 h and the resulting suspension was filtered. The solid residue was dried in vacuo.

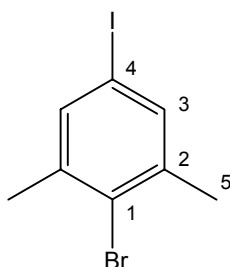
**Formula:** C<sub>8</sub>H<sub>10</sub>I  
(247.08)

**Yield:** 11.3 g (45.7 mmol, 18 %) orange solid

**Melting point:** 50-52 °C (*n*-hexane), lit.<sup>[18]</sup>: 51 °C (methanol)

**<sup>1</sup>H-NMR (400 MHz, acetone-d<sub>6</sub>):** δ = 7.17 (m, 2H, H3), 4.37 (br s, 2H, H6), 2.12 (m, 6H, H5)

2-Bromo-5-iodo-1,3-dimethylbenzene (**15**)



CA: [689260-53-5]

Synthesis according to *EP2*

4-Iodo-2,6-dimethylaniline:	4.94 g	20.0 mmol
Copper(II) bromide:	5.36 g	24.0 mmol
<i>tert</i> -Butyl nitrite:	3.56 ml	30.0 mmol
Acetonitrile (abs.):	80 ml	
Hydrochloric acid (20%):	800 ml	

In contrast to *EP2* the reaction mixture was stirred at 65 °C for 1.5 h. After flash chromatography (100% petrol ether) of the crude product 2.76 g of a reddish liquid were obtained which contained ca. 50 mol% of 2,5-dibromo-1,3-dimethylbenzene. The yield of 2-bromo-5-iodo-1,3-dimethylbenzene was estimated by <sup>1</sup>H-NMR. This mixture was directly used for the synthesis of (4-bromo-3,5-dimethylphenyl)-diphenylamine.

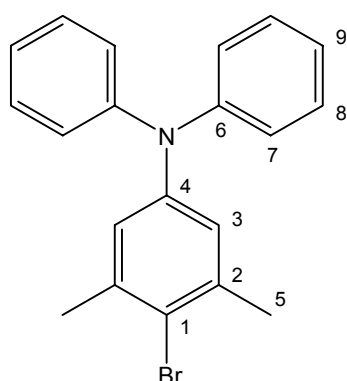
**Formula:** C<sub>8</sub>H<sub>8</sub>BrI (310.96)

**Yield:** 1.50 g (4.83 mmol, 24 %) reddish liquid

**Melting point:** -

**<sup>1</sup>H-NMR (400 MHz, CDCl<sub>3</sub>):**  $\delta$  = 7.40 (m, 2H, H3), 2.36 (m, 6H, H5)

(4-Bromo-3,5-dimethylphenyl)-diphenylamine (**16**)



CA: -

Synthesis according to lit.<sup>[19]</sup>

2-Bromo-5-iodo-1,3-dimethylbenzene:	1.24 g	4.00 mmol
Diphenylamine:	0.676 g	4.00 mmol
Potassium <i>tert</i> -butanolate:	0.449 g	4.00 mmol
2,2'-Bipyridine:	25.0 mg	0.160 mmol
Copper(I) iodide:	30.5 mg	0.160 mmol
Toluene (abs.):	3 ml	

All reagents were stirred under nitrogen atmosphere at 120 °C for 16 h. The reaction mixture was suspended in CH<sub>2</sub>Cl<sub>2</sub> and washed with water. The aqueous phase was extracted with CH<sub>2</sub>Cl<sub>2</sub> and the combined organic extracts were dried over MgSO<sub>4</sub>. The solvent was removed in vacuo and the crude product was purified by flash chromatography with dichloromethane/petrol ether (1:9).

**Formula:** C<sub>20</sub>H<sub>18</sub>BrN

**Yield:** 0.701 g (2.00 mmol, 50.0 %) colourless solid

**Melting point:** 168-170 °C (dichloromethane/petrol ether)

**<sup>1</sup>H-NMR (400 MHz, acetone-d<sub>6</sub>):**  $\delta$  = 7.29 (m, 4H, H8), 7.07-7.02 (6H, H7, H9), 6.83 (m, 2H, H3), 2.29 (m, 6H, H5)

**<sup>13</sup>C-NMR (100 MHz, acetone-d<sub>6</sub>):**  $\delta$  = 148.5, 147.7, 139.8, 130.3, 125.2, 125.1, 124.6, 124.0, 23.9

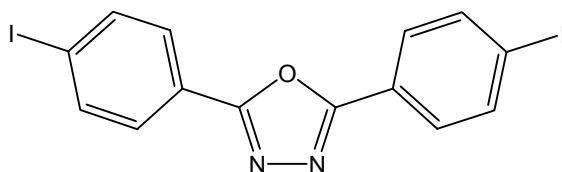
**Elemental analysis:**

calc.:	C 68.19	H 5.15	N 3.98
exp.:	C 67.28	H 5.28	N 3.90

**EI-MS (high resolution, PI):** calc. for C<sub>20</sub>H<sub>18</sub>BrN:  $m/z$  = 351.06171, exp.:  $m/z$  = 351.06158,  $\Delta$  = 0.37 ppm

## 5.2.4 Synthesis of the 2,5-Diaryl-1,3,4-oxadiazoles

2,5-Bis(4-iodophenyl)-1,3,4-oxadiazole (**7**)



CA: [100541-43-3]

Synthesis according to lit.<sup>[20]</sup>

4-Iodobenzoic acid:	1.06 g	4.27 mmol
Hydrazine dihydrochloride:	0.231 g	2.20 mmol
Phosphorus pentoxide:	1.90 g	13.4 mmol
Phosphorus oxychloride:	0.40 ml	4.4 mmol
Phosphoric acid (85 %):	1.14 ml	



The crude product was recrystallised in chloroform.

**Formula:** C<sub>14</sub>H<sub>8</sub>I<sub>2</sub>N<sub>2</sub>O (474.04)

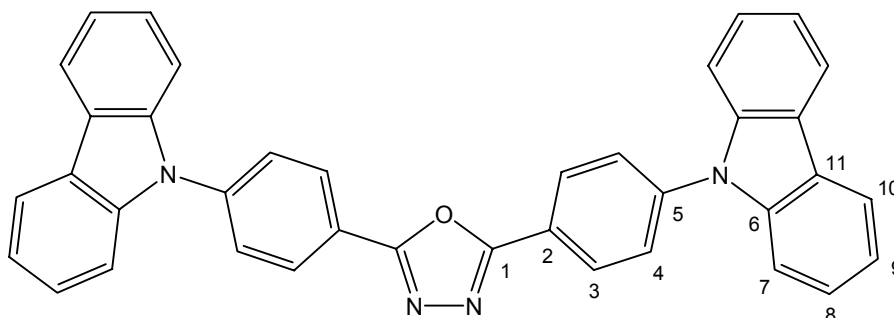
**Yield:** 0.690 g (1.46 mmol, 69 %) colourless needles

**Melting point:** 278 °C (chloroform), lit.<sup>[21]</sup>: 276 °C (toluene)

**<sup>1</sup>H-NMR (250 MHz, CDCl<sub>3</sub>):** δ = 7.92 - 7.83 (AA'BB', 8H, Ar-H)

**Elemental analysis:** calc.: C 35.47, H 1.70, N 5.91; exp.: C 35.42, H 1.72, N 5.89

2,5-Bis(4-(9H-carbazol-9-yl)phenyl)-1,3,4-oxadiazole (**1**)



CA: [733038-87-4]

Synthesis according to *EP1*

2,5-Bis-(4-iodophenyl)-1,3,4-oxadiazole:	0.440 g	0.930 mmol
Carbazole:	0.392 g	2.33 mmol
Copper(I) iodide:	25 mg	0.13 mmol
<i>trans</i> -1,2-Cyclohexanediamine:	15 μl	0.12 mmol
Potassium phosphate:	0.866 g	4.08 mmol
Dioxane (abs.):	3 ml	

The crude product was suspended in 25 ml of acetone and heated to reflux for one hour. After cooling to room temperature the suspension was filtered and the solid residue was dried in vacuo.

**Formula:** C<sub>38</sub>H<sub>24</sub>N<sub>4</sub>O (552.62)

**Yield:** 0.250 g (0.452 mmol, 49%) pale yellow solid

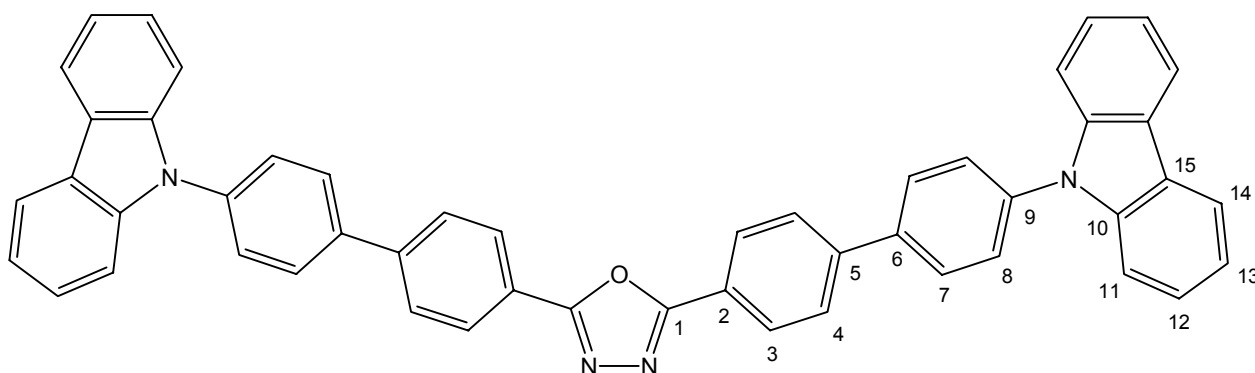
**Melting point:** 273 °C (acetone)

**<sup>1</sup>H-NMR (400 MHz, CDCl<sub>3</sub>):** δ = 8.44 (AA', 4H, H3), 8.18 (m, 4H, H10), 7.83 (BB', 4H, H4), 7.53 (m, 4H, H7), 7.47 (m, 4H, H8), 7.35 (m, 4H, H9)

**<sup>13</sup>C-NMR (150 MHz, CDCl<sub>3</sub>)<sup>[e]</sup>:** δ = 141.3, 140.5, 128.8, 127.5, 126.4, 124.0, 122.6, 120.8, 120.7, 109.9

**EI-MS (high resolution, PI):** calc. for C<sub>38</sub>H<sub>24</sub>N<sub>4</sub>O: *m/z* = 552.19446, exp.: *m/z* = 552.19461, Δ = 0.27 ppm

2,5-Bis(4-(4-(9*H*-carbazol-9-yl)phenyl)phenyl)-1,3,4-oxadiazole (**2**)



CA: -

Synthesis according to *EP3*

2,5-Bis(4-iodophenyl)-1,3,4-oxadiazole:	3.36 g	7.09 mmol
9-(4-Bromophenyl)-9 <i>H</i> -carbazole:	6.85 g	21.3 mmol
Magnesium:	0.568 g	23.4 mmol
Pd(PPh <sub>3</sub> ) <sub>2</sub> Cl <sub>2</sub> :	0.497 g	0.709 mmol
THF (abs.):	100 ml	

[e] Two overlapping signals could not be resolved.

**Formula:** C<sub>50</sub>H<sub>32</sub>N<sub>4</sub>O (704.82)

**Yield:** 3.30 g (4.68 mmol, 66%) colourless solid

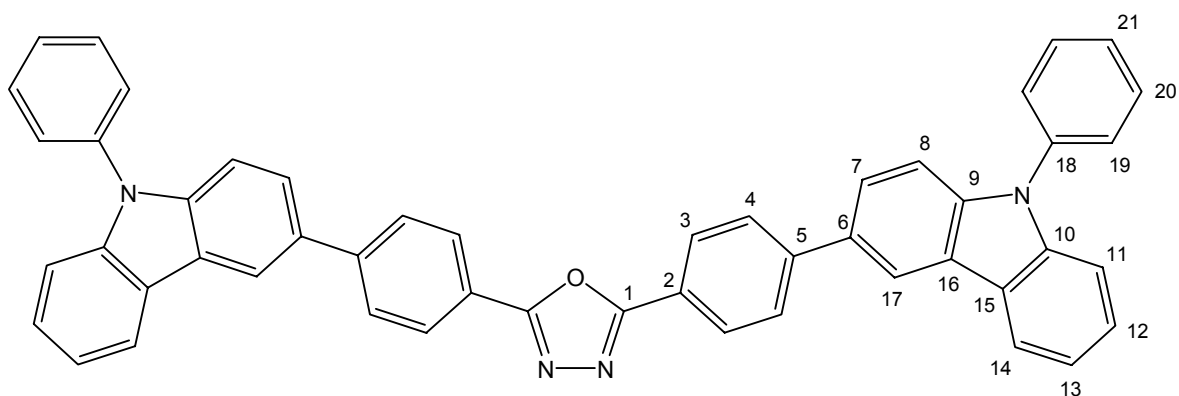
**Melting point:** 288 °C (acetone) decomp.

**<sup>1</sup>H-NMR (600 MHz, CD<sub>2</sub>Cl<sub>2</sub>):** δ = 8.33 (AA', 4H, H3), 8.18 (m, 4H, H14), 7.98 - 7.94 (AA'BB', 8H, H4, H7), 7.74 (BB', 4H, H8), 7.52 (m, 4H, H11), 7.46 (m, 4H, H12), 7.32 (m, 4H, H13)

**<sup>13</sup>C-NMR (150 MHz, CD<sub>2</sub>Cl<sub>2</sub>):** δ = 164.9, 143.9, 141.2, 139.2, 138.2, 129.0, 128.2, 127.9, 127.8, 126.4, 123.9, 123.6, 120.7, 120.5, 110.2

**EI-MS (high resolution, PI):** calc. for C<sub>50</sub>H<sub>32</sub>N<sub>4</sub>O: *m/z* = 704.25706, exp.: *m/z* = 704.25584, Δ = 1.7 ppm

2,5-Bis(4-(9-phenyl-9*H*-carbazol-3-yl)phenyl)-1,3,4-oxadiazol (3)



CA: -

Synthesis according to EP3

2,5-Bis-(4-iodophenyl)-1,3,4-oxadiazole:	0.379 g	0.800 mmol
3-Bromo-9-phenyl-9 <i>H</i> -carbazole:	0.773 g	2.40 mmol
Magnesium:	0.128 g	5.27 mmol
Pd(PPh <sub>3</sub> ) <sub>2</sub> Cl <sub>2</sub> :	56.2 mg	80.0 μmol
1,2-Dibromoethane:	4.7 mg	0.025 mmol
THF (abs.):	8 ml	

**Formula:** C<sub>50</sub>H<sub>32</sub>N<sub>4</sub>O (704.82)

**Yield:** 170 mg (0.241 mmol, 30 %) off-white solid

**Melting point:** 160-163 °C (acetone)

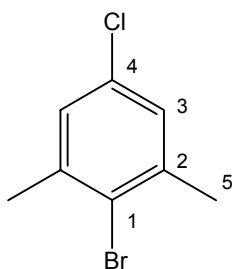
**<sup>1</sup>H-NMR (600 MHz, CD<sub>2</sub>Cl<sub>2</sub>):** δ = 8.50 (m, 2H, H17), 8.29 (AA', 4H, H3), 8.25 (m, 2H, H14), 7.97 (BB', 4H, H4), 7.79 (m, 2H, H7), 7.67 (m, 4H, H20), 7.63 (m, 4H, H19), 7.54-7.52 (4H, H8, H21), 7.47-7.46 (4H, H11, H12), 7.35 (m, 2H, H13)

**<sup>13</sup>C-NMR (150 MHz, CD<sub>2</sub>Cl<sub>2</sub>):** δ = 165.0, 145.4, 141.9, 141.3, 137.8, 132.2, 130.4, 128.1, 128.0, 127.7, 127.4, 126.8, 125.7, 124.4, 123.7, 122.5, 120.7, 120.6, 119.2, 110.7, 110.4

**EI-MS (high resolution, PI):** calc. for C<sub>50</sub>H<sub>32</sub>N<sub>4</sub>O: *m/z* = 704.25706, exp.: *m/z* = 704.25687, Δ = 0.27 ppm

## 5.2.5 Synthesis of the Triarylboranes

2-Bromo-5-chloro-1,3-dimethylbenzene (**25**)



CA: [103724-99-8]

Synthesis according to *EP2*

4-Chloro-2,6-dimethylaniline:	3.13 g	20.1 mmol
Copper(II) bromide:	5.63 g	25.2 mmol
<i>tert</i> -Butyl nitrite:	3.56 ml	29.7 mmol
Acetonitrile (abs.):	100 ml	

Hydrochloric acid (20%): 300 ml

The crude product was purified by flash chromatography with 100% petrol ether.

**Formula:** C<sub>8</sub>H<sub>8</sub>BrCl (219.51)

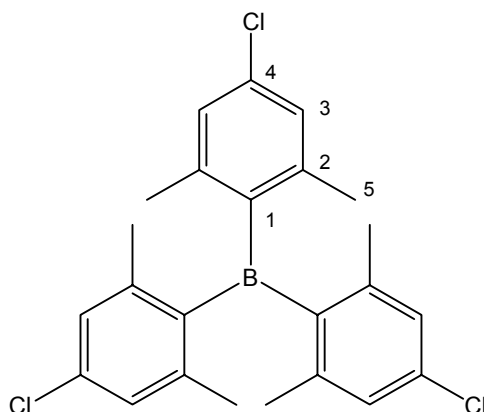
**Yield:** 3.36 g (15.3 mmol, 76%) colourless liquid

**Melting point:** –

**<sup>1</sup>H-NMR (400 MHz, CDCl<sub>3</sub>):** δ = 7.07 (m, 2H, H3), 2.39 (m, 6H, H5)

**<sup>13</sup>C-NMR (100 MHz, CDCl<sub>3</sub>):** δ = 140.0, 132.4, 128.1, 125.6, 23.9

Tris(4-chloro-2,6-dimethylphenyl)borane (**19**)



CA: -

2-Bromo-5-chloro-1,3-dimethylbenzene:	0.766 g	3.49 mmol
<i>tert</i> -Butyllithium (1.5 M in <i>n</i> -pentane):	4.66 ml	6.99 mmol
Borontrifluoride diethyl etherate:	0.146 ml	1.16 mmol
Diethylether (abs.):	20 ml	

Under a nitrogen atmosphere *tert*-butyllithium (1.5 M in *n*-pentane) was added dropwise to a stirred solution of 2-bromo-5-chloro-1,3-dimethylbenzene in diethylether at -78 °C. The reaction mixture was stirred for one hour at -78 °C and

then borontrifluoride diethyl etherate was added. The solution was stirred for another 15 min at  $-78\text{ }^{\circ}\text{C}$  and then for 18 h at room temperature. About 5 g of silica gel were added, the solvent was removed in vacuo and the crude product was purified by flash chromatography with 100% petrol ether.

**Formula:**  $\text{C}_{24}\text{H}_{24}\text{BCl}_3$  (429.62)

**Yield:** 0.370 g (0.861 mmol, 74%) colourless solid

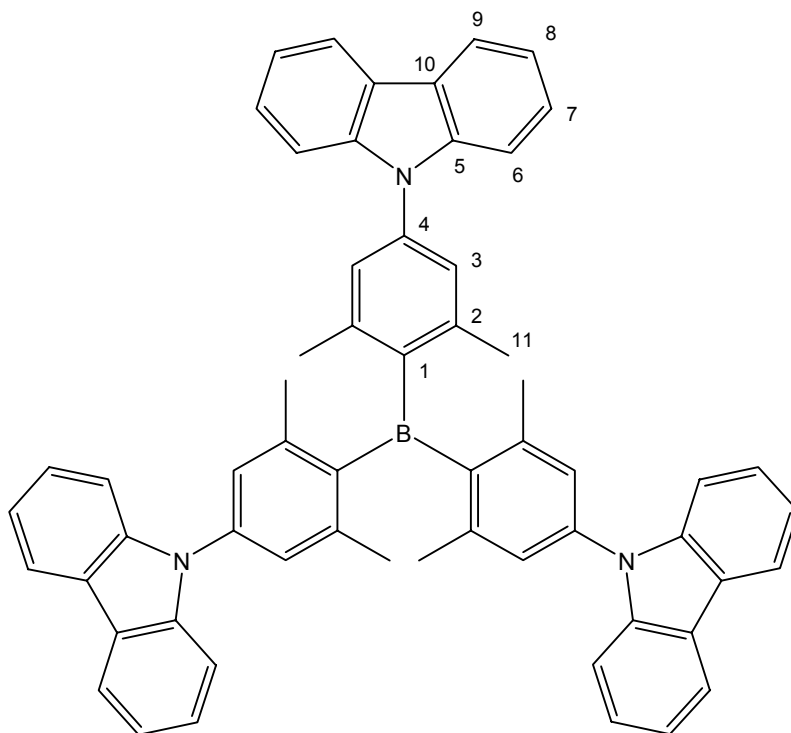
**Melting point:**  $234\text{ }^{\circ}\text{C}$  (petrol ether)

**$^1\text{H-NMR}$  (400 MHz,  $\text{CDCl}_3$ ):**  $\delta = 6.95$  (m, 6H, H3),  $1.98$  (m, 18H, H5)

**$^{13}\text{C-NMR}$  (400 MHz,  $\text{CDCl}_3$ )<sup>[f]</sup>:**  $\delta = 142.5, 135.8, 128.1, 22.9$

**EI-MS (high resolution, PI):** calc. for  $\text{C}_{24}\text{H}_{24}^{11}\text{BCl}_3$ :  $m/z = 428.10311$ , exp.:  $m/z = 428.10349$ ,  $\Delta = 0.89$  ppm

Tris(4-(9*H*-carbazol-9-yl)-2,6-dimethylphenyl)borane (**4**)



[f] The signal of C1 is extremely broadened due to the boron quadrupole moment.

CA: [643758-16-1]

9-(4-Bromo-3,5-dimethylphenyl)-9 <i>H</i> -carbazole:	2.56 g	7.31 mmol
<i>tert</i> -Butyllithium (1.5 M in <i>n</i> -pentane):	9.75 ml	14.6 mmol
Borontrifluoride diethyl etherate:	0.306 ml	2.44 mmol
Diethylether (abs.):	60 ml	

Under a nitrogen atmosphere 9-(4-bromo-3,5-dimethylphenyl)-9*H*-carbazole was dissolved in 60 ml of absolute diethylether and cooled to -78 °C. A solution of <sup>t</sup>BuLi (1.5 M in *n*-pentane) was slowly added and the yellow reaction mixture was stirred at -78 °C for 20 min. The acetone/dry ice bath was removed for 20 min and the solution was allowed to warm up. The reaction mixture was cooled again to -78 °C and borontrifluoride diethyl etherate was added. After stirring at -78 °C for 1 h the solution was stirred at room temperature for 18 h. The reaction mixture was suspended in 300 ml CH<sub>2</sub>Cl<sub>2</sub> and extracted three times with 100 ml of H<sub>2</sub>O. The aqueous phases were washed three times with 100 ml CH<sub>2</sub>Cl<sub>2</sub> and the combined organic extracts were dried over MgSO<sub>4</sub>. The solvent was removed in vacuo and the crude product was purified by flash chromatography with dichloromethane/petrol ether (1:3 → 1:1).

**Formula:** C<sub>60</sub>H<sub>48</sub>BN<sub>3</sub> (821.85)

**Yield:** 1.74 g (2.12 mmol, 87%) pale yellow solid

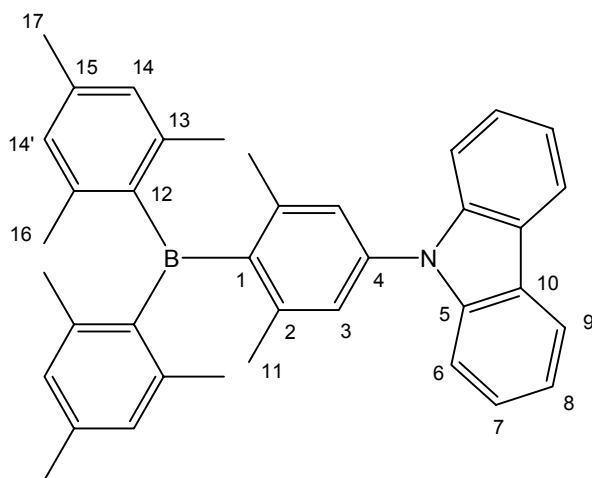
**Melting point:** 345 °C decomp.<sup>[g]</sup> (dichloromethane/petrol ether)

**<sup>1</sup>H-NMR (400 MHz, CD<sub>2</sub>Cl<sub>2</sub>):** δ = 8.17 (m, 6H, H9), 7.55 (m, 6H, H6), 7.46 (m, 6H, H7), 7.33-7.29 (12H, H3, H8), 2.35 (m, 18H, H11)

**<sup>13</sup>C-NMR (100 MHz, CDCl<sub>3</sub>):** δ = 145.8, 142.9, 140.8, 139.2, 126.3, 126.1, 123.7, 120.5, 120.1, 110.2, 23.4

**EI-MS (high resolution, PI):** calc. for C<sub>60</sub>H<sub>48</sub><sup>10</sup>BN<sub>3</sub>: *m/z* = 820.39721, exp.: *m/z* = 820.39805, Δ = 1.02 ppm

[g] Determined by DSC under argon atmosphere.

9-(4-(Dimesitylboryl)-3,5-dimethylphenyl)-9*H*-carbazole (**5**)

CA: -

9-(4-Bromo-3,5-dimethylphenyl)-9 <i>H</i> -carbazole:	0.337 g	0.962 mmol
<i>tert</i> -Butyllithium (1.5 M in <i>n</i> -pentane):	1.28 ml	1.92 mmol
Dimesitylboron fluoride:	0.261g	0.972 mmol
Diethylether (abs.):	15 ml	

Under a nitrogen atmosphere 9-(4-bromo-3,5-dimethylphenyl)-9*H*-carbazole was dissolved in 10 ml of absolute diethylether and cooled to -78 °C. A solution of <sup>t</sup>BuLi (1.5 M in *n*-pentane) was slowly added and the yellow reaction mixture was stirred at -78 °C for 20 min. The acetone/dry ice bath was removed and the solution was allowed to warm up. After 20 min the reaction mixture was added via a canula to a solution of dimesitylboron fluoride in 5 ml diethylether which was cooled to -78 °C. The resulting suspension was stirred at -78 °C for five minutes and then at room temperature for two hours. The reaction mixture was suspended in CH<sub>2</sub>Cl<sub>2</sub> and filtered through silica gel. The solvent was removed in vacuo and the crude product was purified by flash chromatography with dichloromethane/petrol ether (1:5).



**Formula:** C<sub>38</sub>H<sub>38</sub>BN (519.53)

**Yield:** 0.270 g (0.520 mmol, 53%) colourless solid

**Melting point:** 293 °C (dichloromethane/petrol ether)

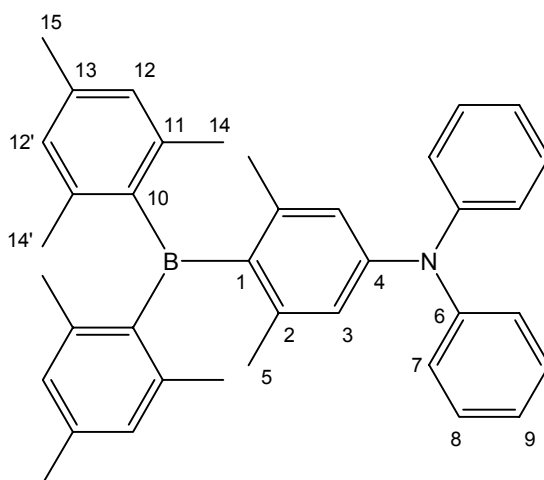
**Glass transition temperature (T<sub>g</sub>):** 90 °C

**<sup>1</sup>H-NMR (400 MHz, CD<sub>2</sub>Cl<sub>2</sub>):** δ = 8.14 (m, 2H, H9), 7.46 (m, 2H, H6), 7.41 (m, 2H, H7), 7.27 (m, 2H, H8), 7.14 (m, 2H, H3), 6.83 (m, 2H, H14 or H14'), 6.81 (m, 2H, H14' or H14), 2.30 (m, 6H, CH<sub>3</sub>), 2.11 (m, 12H, CH<sub>3</sub>), 2.04 (m, 6H, CH<sub>3</sub>)

**<sup>13</sup>C-NMR (100 MHz, CD<sub>2</sub>Cl<sub>2</sub>):** δ = 142.8, 141.2, 141.1, 141.0, 140.1, 138.5, 129.13, 129.08, 126.2, 126.0, 123.7, 120.5, 120.1, 110.4, 23.05, 23.01, 21.3

**EI-MS (high resolution, PI):** calc. for C<sub>38</sub>H<sub>38</sub><sup>10</sup>BN: *m/z* = 518.31281, exp.: *m/z* = 518.31184, Δ = 1.87 ppm

*N*-(4-(Dimesitylboryl)-3,5-dimethylphenyl)-diphenylamine (**6**)



CA: -

(4-Bromo-3,5-dimethylphenyl)-diphenylamine:	0.528 g	1.50 mmol
Dimesitylboron fluoride:	0.483 g	1.80 mmol
<i>tert</i> -Butyllithium (1.5 M in <i>n</i> -pentane):	2.20 ml	3.30 mmol
THF (abs.):	25 ml	

Under a nitrogen atmosphere *tert*-butyllithium (1.5 M in *n*-pentane) was added dropwise to a stirred solution of (4-bromo-3,5-dimethylphenyl)-diphenylamine in 15 ml THF at -78 °C. The reaction mixture was stirred for one hour at -78 °C and then a solution of dimesitylboron fluoride in 10 ml THF (cooled to -78 °C) was added. After stirring for 16 h at room temperature the reaction mixture was quenched with 50 ml H<sub>2</sub>O and extracted three times with 50 ml CH<sub>2</sub>Cl<sub>2</sub>. The combined organic extracts were dried over MgSO<sub>4</sub> and the solvent was removed in vacuo. The crude product was purified by flash chromatography with dichloromethane/petrol ether (1:9 → 100 % CH<sub>2</sub>Cl<sub>2</sub>)

**Formula:** C<sub>38</sub>H<sub>40</sub>BN (521.54)

**Yield:** 0.495 g (0.949 mmol, 63 %) yellow solid

**Melting point:** 230 °C (dichloromethane/petrol ether)

**Glass transition temperature (T<sub>g</sub>):** 75 °C

**<sup>1</sup>H-NMR (400 MHz, acetone-d<sub>6</sub>):** δ = 7.30 (m, 4H, H8), 7.10-7.04 (6H, H7, H9), 6.80 (m, 2H, H12 or H12'), 6.77 (m, 2H, H12' or H12), 6.61 (m, 2H, H3), 2.25 (m, 6H, CH<sub>3</sub>), 2.09 (m, 6H, CH<sub>3</sub>), 1.98 (m, 6H, CH<sub>3</sub>), 1.90 (m, 6H, CH<sub>3</sub>)

**<sup>13</sup>C-NMR (100 MHz, acetone-d<sub>6</sub>)<sup>[h]</sup>:** δ = 149.9, 148.4, 143.1, 141.1, 140.0, 130.3, 129.5, 125.7, 124.2, 122.5, 23.4, 23.2, 23.0, 21.3

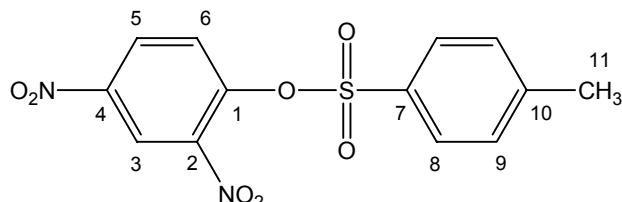
**EI-MS (high resolution, PI):** calc. for C<sub>38</sub>H<sub>40</sub><sup>10</sup>BN: *m/z* = 520.32846, exp.: *m/z* = 520.32848, Δ = 0.04 ppm

---

[h] The signals of C1 and C10 are extremely broadened due to the boron quadrupole moment.

### 5.2.6 Synthesis of the *para*-Substituted 1,4-Bis(pyridinio)benzenes

#### 2,4-Dinitrophenyl-4-toluenesulfonate (**20**)



CA: [742-25-6]

Synthesis according to lit.<sup>[22]</sup>

2,4-Dinitrophenol:	9.20 g	50.0 mmol
<i>p</i> -Toluenesulfonylchloride:	10.0 g	52.4 mmol
Na <sub>2</sub> CO <sub>3</sub> :	6.0 g	56.6 mmol
H <sub>2</sub> O:	20 ml	

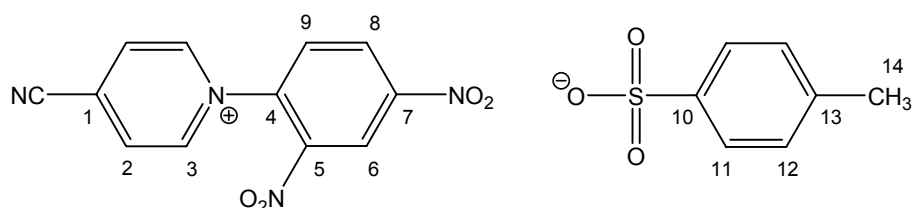
**Formula:** C<sub>13</sub>H<sub>10</sub>N<sub>2</sub>O<sub>7</sub>S (338.29)

**Yield:** 10.2 g (30.2 mmol, 60%) yellow solid

**Melting point:** 119 °C (H<sub>2</sub>O), lit.<sup>[22]</sup>: 121 °C (EtOH/AcOH)

**<sup>1</sup>H-NMR (250 MHz, CDCl<sub>3</sub>):** δ = 8.76 (m, 1H, H3), 8.49 (dd, <sup>3</sup>J<sub>HH</sub> = 9.2, <sup>4</sup>J<sub>HH</sub> = 2.8, 1H, H5), 7.80 (AA', 2H, H8), 7.72 (m, 1H, H6), 7.39 (BB', 2H, H9), 2.49 (s, 3H, H11)

#### 4-Cyano-1-(2,4-dinitrophenyl)pyridinium-toluene-4-sulfonate (**21**)



CA: [53365-02-9]

Synthesis according to lit.<sup>[23]</sup>

2,4-Dinitrophenyl-4-toluenesulfonate:	1.53 g	4.52 mmol
4-Cyanopyridine:	1.41 g	13.6 mmol

The crude product was stirred for one hour in boiling acetone, filtered and dried in vacuo.

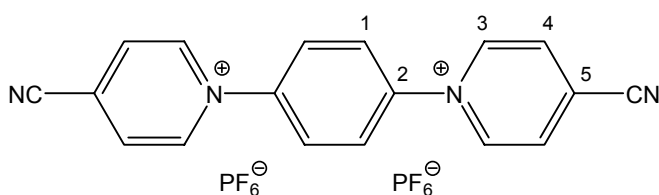
**Formula:** C<sub>19</sub>H<sub>14</sub>N<sub>4</sub>O<sub>7</sub>S (442.40)

**Yield:** 1.30 g (2.94 mmol, 65%) brown solid

**Melting point:** 215 °C (acetone), lit.<sup>[23]</sup>: 215-217 °C (MeOH)

**<sup>1</sup>H-NMR (250 MHz, CD<sub>3</sub>OD):** δ = 9.60 (AA', 2H, H3), 9.24 (m, 1H, H6), 8.88 (dd, <sup>3</sup>J<sub>HH</sub> = 8.7, <sup>4</sup>J<sub>HH</sub> = 2.6, 1H, H8), 8.79 (BB', 2H, H2), 8.29 (m, 1H, H9), 7.62 (AA', 2H, H11), 7.21 (BB', 2H, H12), 2.37 (s, 3H, H14)

1,4-Bis-(4-cyanopyridinio)benzene dihexafluorophosphate (**17-PF<sub>6</sub>**)



CA: -

Synthesis according to lit.<sup>[24]</sup>

4-Cyano-1-(2,4-dinitrophenyl)pyridinium-toluene-4-sulfonate:	0.351 g	0.793 mmol
1,4-Phenylenediamine:	34.3 mg	0.317 mmol
Methanol:	10 ml	

4-Cyano-1-(2,4-dinitrophenyl)pyridinium-toluene-4-sulfonate and 1,4-phenylenediamine were dissolved in 10 ml methanol and stirred at room temperature for 48 h. About 20 ml of Et<sub>2</sub>O were added and the resulting precipitate was filtered, dried and dissolved in 10 ml H<sub>2</sub>O. To this solution 1.7 g NH<sub>4</sub>PF<sub>6</sub> in 5 ml H<sub>2</sub>O were added and the resulting precipitate was filtered, washed with water and dried in vacuo.

**Formula:** C<sub>18</sub>H<sub>12</sub>F<sub>12</sub>N<sub>4</sub>P<sub>2</sub> (574.24)

**Yield:** 0.120 g (0.209 mmol, 66%) light brown solid

**Melting point:** 320 °C decomp. (H<sub>2</sub>O)

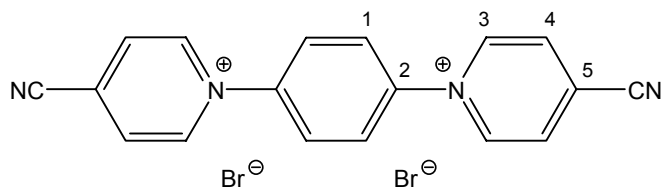
**<sup>1</sup>H-NMR (250 MHz, DMSO-d<sub>6</sub>):** δ = 9.74 (AA', 4H, H3), 8.97 (BB', 4H, H4), 8.29 (s, 4H, H1)

**<sup>13</sup>C-NMR (63 MHz, DMSO-d<sub>6</sub>):** δ = 146.6, 144.2, 131.1, 128.4, 126.9, 114.7

**Elemental analysis:**

calc.:	C 37.65	H 2.11	N 9.76
exp.:	C 36.63	H 2.24	N 9.16

1,4-Bis-(4-cyanopyridinio)benzene dibromide (**17-Br**)



CA: -

1,4-Bis-(4-cyanopyridinio)benzene dihexafluorophosphate:	1.02 g	1.78 mmol
Tetrabutylammonium bromide:	2.87 g	8.90 mmol
Acetonitrile:	40 ml	

1,4-Bis-(4-cyanopyridinio)benzene dihexafluorophosphate was dissolved in 30 ml acetonitrile and a solution of tetrabutylammonium bromide in 10 ml acetonitrile was

added. After stirring for one hour the resulting precipitate was filtered, washed with acetone and dried in vacuo.

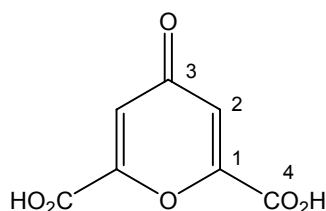
**Formula:** C<sub>18</sub>H<sub>12</sub>Br<sub>2</sub>N<sub>4</sub> (444.12)

**Yield:** 0.500 g (1.13 mmol, 63 %) brown solid

**Melting point:** > 340 °C (acetonitrile)

**<sup>1</sup>H-NMR (400 MHz, DMSO-d<sub>6</sub>):** δ = 9.76 (AA', 4H, H3), 8.98 (BB', 4H, H4), 8.32 (s, 4H, H1)

4-Oxo-4*H*-pyran-2,6-dicarboxylic acid (chelidonic acid) (**22**)



CA: [99-32-1]

Synthesis according to lit.<sup>[25]</sup>

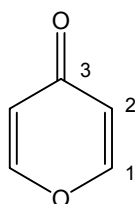
Acetone (abs.):	73.4 ml	1.00 mol
Diethyl oxalate:	287 ml	2.12 mol
Sodium:	47.0 g	2.04 mol
Ethanol (abs.):	600 ml	

**Formula:** C<sub>7</sub>H<sub>4</sub>O<sub>6</sub> (184.10)

**Yield:** 125 g (0.679 mol, 68%) brown solid

**Melting point:** 269 °C (H<sub>2</sub>O) decomp., lit.<sup>[25]</sup>: 257 °C (H<sub>2</sub>O) decomp.

**<sup>1</sup>H-NMR (400 MHz, DMSO-d<sub>6</sub>):** δ = 6.94 (s, 2H, H2)

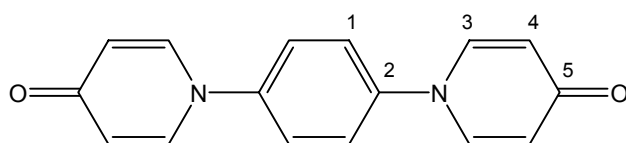
4*H*-Pyran-4-one (**23**)

CA: [108-97-4]

Synthesis according to lit.<sup>[26]</sup>

4-Oxo-4 <i>H</i> -pyran-2,6-dicarboxylic acid:	35.0 g	190 mmol
Copper (powder):	4.0 g	63 mmol
2,2'-Bipyridine:	1.48 g	9.48 mmol
1,2,3,4-Tetrahydronaphthalene:	360 ml	

In contrast to literature<sup>[26]</sup> the reaction mixture was heated under reflux for seven hours instead of three.

**Formula:** C<sub>5</sub>H<sub>4</sub>O<sub>2</sub> (96.08)**Yield:** 12.5 g (130 mmol, 68%) yellow needles**Melting point:** 31 °C (2-propanol), lit.<sup>[27]</sup>: 32.5 °C (dist.)**<sup>1</sup>H-NMR (400 MHz, acetone-*d*<sub>6</sub>):** δ = 7.98 (AA', 2H, H1), 6.25 (BB', 2H, H2)1,4-Bis(4-pyridon-1-yl)benzene (**24**)

CA: -

Synthesis according to lit.<sup>[28]</sup>

1,4-Phenylenediamine:	5.86 g	54.2 mmol
4 <i>H</i> -Pyran-4-one:	12.5 g	130 mmol
Hydrochloric acid (6 N):	20 ml	

1,4-Phenylenediamine and 4*H*-pyran-4-one were dissolved in 20 ml 6 N hydrochloric acid and heated under reflux for three hours. The solid residue was suspended in water, filtered and washed with 6 N HCl and water. The crude solid was stirred in 25% ammonia for three hours, filtered and washed with water. The filtrate from the first filtration was alkalisied with 25% ammonia and the precipitate was filtered and washed with water. Both solid fractions were combined and dried in vacuo.

**Formula:** C<sub>16</sub>H<sub>12</sub>N<sub>2</sub>O<sub>2</sub> (264.28)

**Yield:** 14.0 g (53.1 mmol, 98%) light brown solid

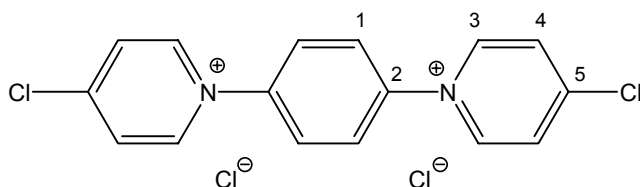
**Melting point:** > 300 °C (H<sub>2</sub>O)

**<sup>1</sup>H-NMR (400 MHz, CD<sub>3</sub>OD):** δ = 8.14 (AA', 4H, H3), 7.78 (s, 4H, H1), 6.60 (BB', 4H, H4)

**<sup>13</sup>C-NMR (100 MHz, CD<sub>3</sub>OD):** δ = 181.4, 144.3, 142.2, 126.0, 119.0

**EI-MS (high resolution, PI):** calc. for C<sub>16</sub>H<sub>12</sub>N<sub>2</sub>O<sub>2</sub>: *m/z* = 264.08933, exp.: *m/z* = 264.08948, Δ = 0.57 ppm

1,4-Bis-(4-chloropyridinio)benzene dichloride (**18-Cl**)



CA: -



Synthesis according to lit.<sup>[29]</sup>

1,4-Bis(4-pyridon-1-yl)benzene:            0.957 g        3.62 mmol  
 Thionyl chloride:                            10 ml

Under a nitrogen atmosphere 1,4-bis(4-pyridon-1-yl)benzene was suspended in 10 ml thionyl chloride and heated under reflux for four days. The solid was filtered under N<sub>2</sub>, washed with Et<sub>2</sub>O (abs.) and dried in vacuo.

**Formula:** C<sub>16</sub>H<sub>12</sub>Cl<sub>4</sub>N<sub>2</sub>                            (374.09)

**Yield:** 1.15 g (3.07 mmol, 85%) light brown solid

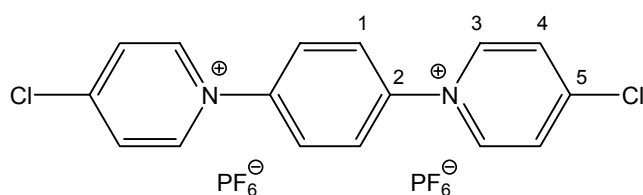
**Melting point:** > 300 °C (Et<sub>2</sub>O)

**<sup>1</sup>H-NMR (400 MHz, D<sub>2</sub>O):** δ = 9.24 (AA', 4H, H3), 8.43 (BB', 4H, H4), 8.17 (s, 4H, H1)

**<sup>13</sup>C-NMR (100 MHz, D<sub>2</sub>O, TSC-d<sub>4</sub><sup>[i]</sup>):** δ = 159.7, 148.2, 146.9, 132.0, 129.6

**ESI-MS (high resolution):** calc. for C<sub>16</sub>H<sub>12</sub>Cl<sub>2</sub>N<sub>2</sub>: *m/z* = 151.01833, exp.: *m/z* = 151.01848, Δ = 1.01 ppm

1,4-Bis-(4-chloropyridinio)benzene dihexafluorophosphate (**18-PF<sub>6</sub>**)



CA: -

1,4-Bis-(4-chloropyridinio)benzene dichloride:            0.100 g        0.267 mmol  
 Ammonium hexafluorophosphate:                            1.00 g        6.13 mmol

[i] 2,2,3,3-Tetradeutero-3-trimethylsilylpropionate, sodium salt

1,4-Bis-(4-chloropyridinio)benzene dichloride was dissolved in 5 ml water and a solution of ammonium hexafluorophosphate in 5 ml water was added. After stirring for one hour the resulting precipitate was filtered, washed with water and dried in vacuo.

**Formula:**  $C_{16}H_{12}Cl_2F_{12}N_2P_2$  (593.11)

**Yield:** 0.135 g (0.228 mmol, 85%) light brown solid

**Melting point:** 295 °C (H<sub>2</sub>O) decomp.

**<sup>1</sup>H-NMR (400 MHz, CD<sub>3</sub>CN):**  $\delta$  = 8.92 (AA', 4H, H3), 8.31 (BB', 4H, H4), 8.02 (s, 4H, H1)

**<sup>13</sup>C-NMR (100 MHz, CD<sub>3</sub>CN):**  $\delta$  = 157.6, 146.6, 145.1, 130.2, 128.0

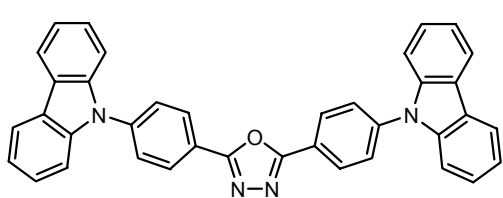
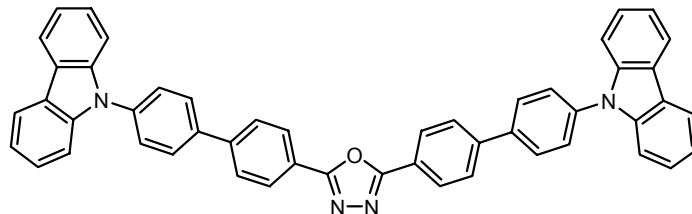
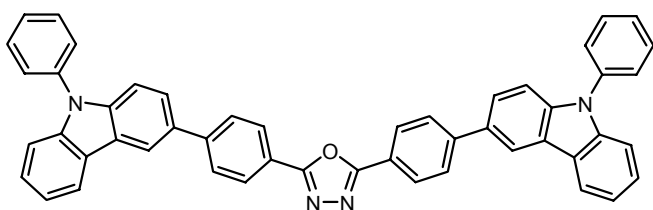
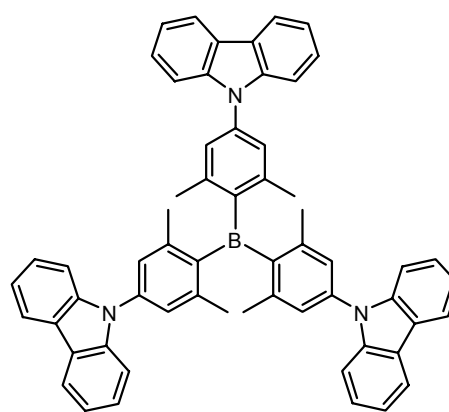
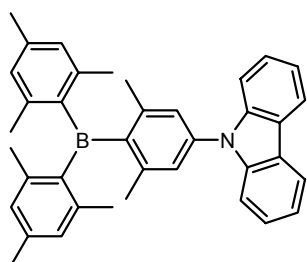
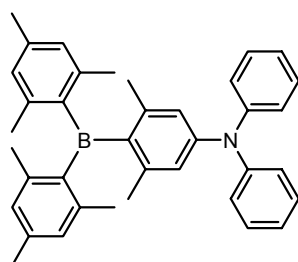
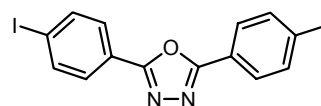
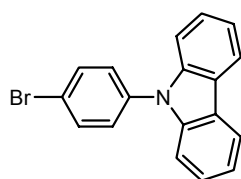
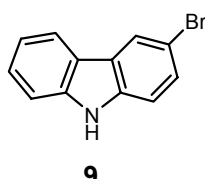
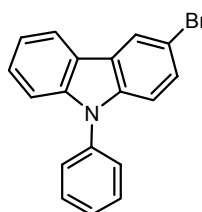
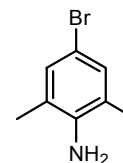
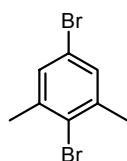
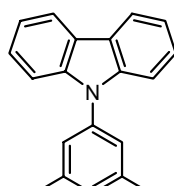
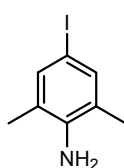
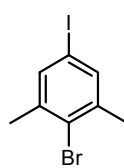
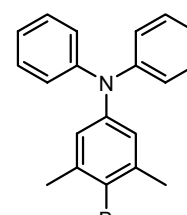
**ESI-MS (high resolution):** calc. for  $C_{16}H_{12}Cl_2N_2$ :  $m/z$  = 151.01833, exp.:  $m/z$  = 151.01871,  $\Delta$  = 2.52 ppm

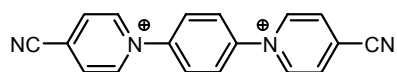
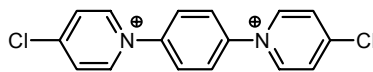
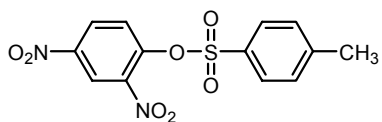
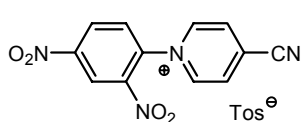
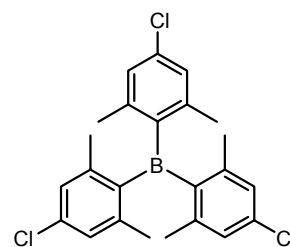
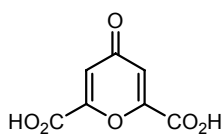
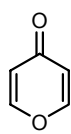
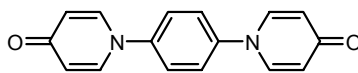
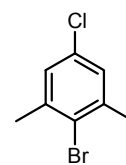
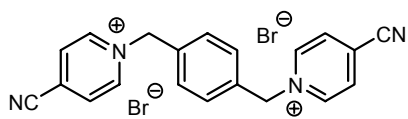
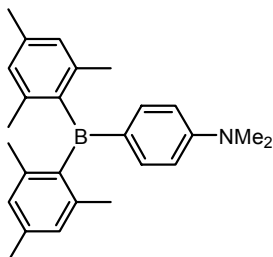
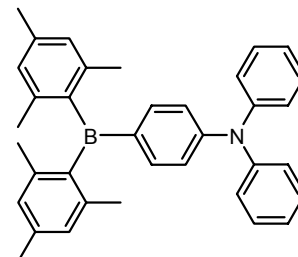
### 5.3 Literature

- [1] R. A. Binstead, B. Jung, A. D. Zuberbühler, SPECFIT/32<sup>TM</sup> V3.0.33, Program for Multivariate Data Analysis, 1993, Spectrum Software Associates, Marlborough (USA).
- [2] T. Karstens, K. Kobs, *J. Phys. Chem.* **1980**, *84*, 1871-1872.
- [3] R. C. Dorfman, Y. Lin, M. D. Fayer, *J. Phys. Chem.* **1989**, *93*, 6388-6396.
- [4] R. Carlier, J. Simonet, *Bull. Soc. Chim. Fr.* **1988**, *5*, 831-833.
- [5] G. Schiavon, S. Sitran, G. Zotti, *Synth. Met.* **1989**, *32*, 209-217.
- [6] K. West, L. Bay, M. M. Nielsen, Y. Velmurugu, S. Skaarup, *J. Phys. Chem. B* **2004**, *108*, 15001.
- [7] R. Wortmann, K. Lukaszuk in *Nonlinear Optical Responses of Molecules, Solides and Liquides: Methods and Applications* (Ed.: M. G. Papadopoulos), Research Signpost, Trivandrum (India), **2003**, pp. 179-193.
- [8] W. Baumann, *Ber. Bunsen-Ges. Phys. Chem.* **1976**, *80*, 231-240.
- [9] A. Klapars, J. C. Antilla, X. Huang, S. L. Buchwald, *J. Am. Chem. Soc.* **2001**, *123*, 7727-7729.

- [10] M. P. Doyle, B. Siegfried, J. F. Dellaria, Jr., *J. Org. Chem.* **1977**, *42*, 2426-2431.
- [11] C. Buchanan, S. H. Tucker, *J. Chem. Soc.* **1958**, 2750-2755.
- [12] M. V. Jovanovic, E. R. Biehl, *J. Org. Chem.* **1984**, *49*, 1905-1908.
- [13] E. Keschmann, E. Zbiral, *Ann. Chem.* **1973**, 1445-1456.
- [14] G. W. Steinhoff, M. C. Henry, *J. Org. Chem.* **1964**, *29*, 2808-2809.
- [15] J. H. de Groot, K. Dillingham, H. Deuring, H. J. Haitjema, F. J. van Beijma, K. Hodd, S. Norrby, *Biomacromolecules* **2001**, *2*, 1271-1278.
- [16] A. G. Giumanini, G. Verardo, M. Poiana, *J. Prakt. Chem.* **1988**, *330*, 161-174.
- [17] S. Adimurthy, G. Ramachandraiah, P. K. Ghosh, A. V. Bedekar, *Tetrahedron Lett.* **2003**, *44*, 5099-5101.
- [18] W. J. Mijs, S. E. Hoekstra, R. M. Ulmann, E. Havinga, *Rec. trav. chim.* **1958**, *77*, 746-752.
- [19] A. A. Kelkar, N. M. Patil, R. V. Chaudhari, *Tetrahedron Lett.* **2002**, *43*, 7143-7146.
- [20] F. Bentiss, M. Lagrenée, *J. Heterocycl. Chem.* **1999**, *36*, 1029-1032.
- [21] F. N. Hayes, B. S. Rogers, D. G. Ott, *J. Am. Chem. Soc.* **1955**, *77*, 1850-1852.
- [22] F. Ullmann, G. Nadai, *Chem. Ber.* **1908**, *41*, 1870-1878.
- [23] A. J. De Gee, W. J. Sep, J. W. Verhoeven, T. J. De Boer, *J. Chem. Soc., Perkin Trans. 1* **1974**, 676-679.
- [24] A. M. Birch, P. A. Bradley, J. C. Gill, F. Kerrigan, P. L. Needham, *J. Med. Chem.* **1999**, *42*, 3342-3355.
- [25] E. R. Riegel, F. Zwiilmeyer, *Org. Syn. Coll. Vol. II* **1944**, 126-128.
- [26] C. De Souza, Y. Hajikarimian, P. W. Sheldrake, *Synth. Commun.* **1992**, *22*, 755-759.
- [27] R. Willstätter, R. Pummerer, *Chem. Ber.* **1904**, *37*, 3745.
- [28] S. Hünig, G. Köbrich, *Ann. Chem.* **1958**, *617*, 181-202.
- [29] D. Vorländer, *Ber. Dtsch. Chem. Ges.* **1925**, *58B*, 1893-1914.

## Table of Formulas

**1****2****3****4****5****6****7****8****9****10****11****12****13****14****15****16**

**17<sup>2+</sup>****18<sup>2+</sup>****20****21****19****22****23****24****25****26****27****28**

## Appendix

### **Zusammenfassung**

Im Rahmen der vorliegenden Arbeit wurden die elektrochemischen und spektroelektrochemischen Eigenschaften einer Reihe von  $\pi$ -konjugierten organischen Polymeren untersucht. Die Polymere wurden durch potentiodynamische Elektropolymerisation der entsprechenden monomeren Vorläufermoleküle auf Platinelektroden bzw. ITO-beschichteten Glassubstraten abgeschieden. Im Falle der Triarylborane wurden die elektrochemischen und photophysikalischen Eigenschaften der Monomere genauer untersucht, um mögliche Einflüsse auf das entsprechende Polymer abschätzen zu können.

Der erste Teil dieser Arbeit zielte auf die Synthese und Untersuchung von konjugierten Donor-Akzeptor-Polymeren ab, die die Grundvoraussetzungen für OLEDs in einem Material vereinen: den Transport von positiven und negativen Ladungen sowie die Bildung von emittierenden angeregten Zuständen.

Anhand der Carbazol-substituierten Oxadiazole **1–3** konnte gezeigt werden, dass die Carbazol-Funktionalität einerseits geeignet ist eine elektrochemische Polymerisierbarkeit der Monomere zu gewährleisten und andererseits eine reversible p-Dotierung der resultierenden Polymere möglich macht. Eine n-Dotierung der Polymere *poly-1–poly-3* ist aufgrund der elektronenarmen Oxadiazol-Ringe zwar möglich, führt aber zum schrittweisen Abbau dieser Akzeptor-Einheiten. Interessanterweise lassen sich die Polymere aber weiterhin p-dotieren.

Hinsichtlich seiner elektrochemischen und spektroelektrochemischen Eigenschaften weist das Boran-Polymer *poly-4* ein zu den Oxadiazol-Polymeren absolut identisches Verhalten auf. Darüber hinaus konnte gezeigt werden, dass die optische Anregung von *poly-4* im Festkörper zur Emission von blau-grünem Licht führt, was die Vermutung nahe legt, dass dieses Polymer auch elektrolumineszierende Eigenschaften besitzen könnte. AFM-Messungen an Filmen von *poly-4* auf ITO-beschichteten Glassubstraten ergaben weiterhin, dass sich die Schichtdicke des

Polymers durch die Anzahl der Polymerisationszyklen in einem gewissen Bereich einstellen lässt.

Anhand der elektrochemischen und photophysikalischen Eigenschaften der Triarylborane **4–6** konnte gezeigt werden, dass die  $\pi$ -Konjugation zwischen den Bor- und Stickstoff-Atomen in diesen Molekülen sehr gering ist. Dies führt zu einer ungewöhnlichen Grundzustandspolarisation mit partiell positivem Bor und partiell negativem Stickstoff. Darüber hinaus wurde festgestellt, dass das Triarylboran **4** in Lösung eine geringere Symmetrie als  $D_3$  aufweist und dass die durch eine optische Anregung aufgenommene Energie entlang der identischen Subchromophore von **4** übertragen werden kann.

Durch Titrationsexperimente konnte außerdem gezeigt werden, dass **4** Fluoridionen reversibel binden kann, wobei sich das optische Absorptionsverhalten des Chromophors deutlich ändert.

Es kann angenommen werden, dass die genannten Eigenschaften, die sich entscheidend auf das photophysikalische Verhalten dieser Triarylboran-Chromophore auswirken, auch die Eigenschaften des entsprechenden Polymers im Festkörper beeinflussen.

Im zweiten Teil dieser Arbeit sollten reine n-Leiter Materialien auf der Basis von elektronenarmen Boran- bzw. Viologen-Polymeren untersucht werden. Die entsprechenden Vorläufermoleküle sollten dabei durch reduktive Elektropolymerisation auf Platinelektroden polymerisiert werden.

Im Falle des Boran-Monomers **19** war eine reduktive Polymerisation nicht möglich, was vermutlich auf eine starke Lokalisierung des ungepaarten Elektrons auf dem zentralen Boratom des Radikalanions zurückzuführen ist. Bei der Cyano-substituierten Bispyridinio-Verbindung **17<sup>2+</sup>** scheiterte eine reduktive Elektropolymerisation an der schlechten Qualität von  $\text{CN}^-$  als Abgangsgruppe. Daher wurde eine Synthese für das analoge Isomer **18<sup>2+</sup>** entwickelt, bei dem die Cyano-Substituenten gegen die bessere Abgangsgruppe  $\text{Cl}^-$  ausgetauscht wurden. Durch reduktive Elektropolymerisation von **18<sup>2+</sup>** konnte das entsprechende Viologen-Polymer, welches als elektronenarmes isoelektronisches Analogon zu Poly(*para*-phenylen) angesehen werden kann, auf einer Platinelektrode abgeschieden werden.

Das Viologen-Polymer *poly-18* kann bereits bei relativ niedrigen Potentialen reversibel n-dotiert werden, bei zu hohen Potentialen wird das Polymer jedoch überladen und irreversibel zerstört. Da es die für **18<sup>2+</sup>** verwendete Synthesestrategie erlaubt, sowohl die Spacereinheit als auch die Abgangsgruppe in den letzten zwei Reaktionsschritten zu variieren, sind auf diesem Weg weitere analoge Verbindungen leicht zugänglich.

### **Publikationen**

**Electrochemistry and Photophysics of Donor-Substituted Triarylboranes: Symmetry Breaking in Ground and Excited State**, R. Stahl, C. Lambert, C. Kaiser, R. Wortmann, R. Jakober, *Chem. Eur. J.* manuscript accepted.

**How Delocalized is *N,N,N',N'*-Tetraphenylphenylenediamine Radical Cation? An Experimental and Theoretical Study on the Electronic and Molecular Structure**, A. Szeghalmi, M. Erdmann, V. Engel, M. Schmitt, S. Amthor, V. Kriegisch, G. Nöll, R. Stahl, C. Lambert, D. Leusser, D. Stalke, M. Zabel, J. Popp, *J. Am. Chem. Soc.* **2004**, 126, 7834-7845.

### **Poster**

**Electrochemistry and Photophysical Properties of Carbazole-Substituted Triarylboranes**, R. Stahl, C. Lambert, M. Goebel, R. Wortmann, *Towards Molecular Electronics*, Ulm, **2004**.

**Modified Electrodes by Electropolymerisation of Organic Precursors**, R. Stahl, C. Lambert, *Fifth International Symposium on Functional  $\pi$ -Electron Systems (F $\pi$ 5)*, Neu-Ulm, **2002**.



## **Lebenslauf**

### **Persönliche Daten**

---

**Rainer Stahl**

Diplom-Chemiker

\* 17.07.1975 in Haßfurt

Familienstand: ledig

### **Hochschulbildung**

---

- 10/1996 – 12/2005 Studium der Chemie (Diplom) und Promotion an der Universität Würzburg
- 1/2002 Abschluss als Diplom-Chemiker (Note 1,3)  
Thema der Diplomarbeit:  
*Elektropolymerisation organischer Precursor zum Aufbau halbleitender Schichten.*
- 10/1998 Vordiplomprüfung (Note 1,8)

### **Promotion**

---

- Seit 1/2002 Promotion am Institut für Organische Chemie der Universität Würzburg bei Prof. Dr. C. Lambert  
Thema:  
*Electroactive Conjugated Polymers as Charge-Transport Materials for Optoelectronic Thin-Film Devices.*

### **Praktische Tätigkeiten**

---

- 4/2005 – 7/2005 Leitung des Tutoriums für Studenten im organisch-chemischen Praktikum I
- 4/2002 – 2/2005 Verantwortlicher Assistent in den organisch-chemischen Praktika I und II
- 5/1999 – 7/1999 Studentische Hilfskraft im Chemiepraktikum für Mediziner, Universität Würzburg

### **Auslandserfahrung**

---

- 3/2000 – 5/2000 Forschungspraktikum bei Dr. Alan Berry an der School of Biochemistry and Molecular Biology der Universität Leeds, England

Thema:  
*ATR-FTIR-Spectroscopic Studies on Artificial Transmembrane Proteins.*

---

### Zivildienst

---

4/1996 – 9/1996      Mobiler sozialer Hilfsdienst beim Bayerischen Roten Kreuz in Haßfurt

9/1995 – 3/1996      Internistische Station des Kreiskrankenhauses Haßfurt

---

### Schulbildung

---

1995                    Allgemeine Hochschulreife (Note 1,6)

1986 – 1995            Regiomontanus-Gymnasium Haßfurt

1982 – 1986            Grundschule in Haßfurt

---

### Ehrenamt

---

Seit 1988              ehrenamtliches Engagement in der Wasserwacht des Bayerischen Roten Kreuzes

### **Danksagung**

An dieser Stelle möchte ich allen Personen danken, die in irgendeiner Weise zum Gelingen dieser Arbeit beigetragen haben. Mein ganz besonderer Dank gilt dabei:

*Herrn Dr. M. Grüne, Frau E. Ruckdeschel und Frau H. Herold*, für die Einweisung in die NMR-Geräte und die Aufnahme der NMR-Spektren.

*Frau Dr. G. Lange, Herrn Dr. M. Büchner und Herrn F. Dadrach*, für die Aufnahme der Massenspektren.

*Dirk Leusser (AK Stalke)*, für die Hilfe bei der Röntgenstrukturanalyse.

*Ruth Jakober (AK Wortmann)* für die Messung der Dipolmomente.

*Marina Lysetska* und *Ana-Maria Krause* (beide AK Würthner), für die AFM-Aufnahmen und die DSC-Messungen.

*Dr. Rainer Wolf*, für die Mikroskopiebilder der Platin-TBEs.

*Herrn Ramold*, für die Anfertigung der CV-Elektroden, Messzellen und die Hilfe beim Bau der Platin-TBEs.

*Herrn Ludwig*, für die Anfertigung der Glasgeräte.

*Herrn Bernd „Brunello“ Brunner*, für seine scheinbar endlose Geduld mit dem **Dümmsten Anzunehmenden User** („*Wie kann ich denn unter Windows 2000...?*“).

*Herrn Braun*, für sein außerordentliches Engagement und seine Hilfsbereitschaft.

Allen Angestellten des Instituts für organische Chemie, vor allem *Herrn Dr. Stadler*, *Frau Kempf*, *Frau Wilhelm*, *Frau Dreher*, *Frau Krug*, *Herrn Fromm*, *Herrn Förtsch*, *Herrn Reich*, *Herrn Müller*, *Herrn Heilmann* und *Herrn Wendinger*.

Besonderer Dank gilt den Mitarbeitern des AK Lambert für das lockere Arbeitsklima und für die lustigen Grillfeten im Sommer:

*Gilbert Nöll*, für die Einweisung in die Geheimnisse der Cyclovoltammetrie und der Spektroelektrochemie.

*Jürgen Schelter*, für viele hilfreiche Tipps beim Messen und bei der Auswertung („*D’ohh*“) sowie fürs Korrekturlesen („*Redo!*“) und fürs Mett-Brötchen holen.

*Volker Kriegisch*, für die gute Zusammenarbeit während des Studiums, der Diplomarbeit und der Promotion, für die Organisation der AK Ausflüge, für die vielen lustigen Abende im AK, auf Tagungen, usw.... und natürlich für den Windschatten beim Radfahren.

*Stephan Amthor*, für die AM1-CISD Rechnungen an den Triarylboranen, die Hilfe bei den Jortner-Fits, die Organisation der Weinproben und für die langjährige gute Freundschaft.

*Marco Holzapfel*, fürs Korrekturlesen und für seine Bemühungen, trotz dreier Diplomanden die öffentliche Ordnung und Sicherheit in Labor 116 aufrecht zu erhalten. Vielen Dank auch für Deine Geduld mit einem unbelehrbaren „Clubberer“.

*Sascha Heckmann*, für die Erkenntnis, dass „Tiere in den Zoo“ gehören, der „Amok die Stickel im Weinberg mit einer Hand reinschlägt“ und „dei Mutter sei G'sicht“ ziemlich krass ist. Vielen Dank auch für den unvergesslichen Abend in der Mai Tai Bar und fürs Curry-King-Essen.

*Dirk Rausch*, für die Synthese der Oxadiazole während seines F-Praktikums und für so manche Flasche Schnaps bei den AK-Feiern.

Der Vergnügensbeauftragten *Barbara Geiß*, für die Organisation aller AK-Feiern und für die Betreuung von Sascha H. aus L. ohne die der Seminarraum wohl schnell verwaorlost wäre.

*Simone Krakert*, Welttorhüterin 2004 und 2005, für ihren Einsatz beim ChemCup und für die Erkenntnis, dass in Friedberg echt die Katz gebläut ist!

Den Leibeigenen *Christian MÜLLER!* fürs Stiefelputzen, *Dörte Nowak* für die Fortführung dieses anspruchsvollen Doktorarbeitsthemas und *Conrad „CK“ Kaiser* für die Synthesen im F-Praktikum. Eines Tages werdet Ihr verstehen, dass ich immer nur Euer Bestes wollte!

*Hongchao Li* (Hongji-Dongji, Holiday-Hong), für den widerlichsten Schnaps den ich jemals getrunken habe und für die vielen erheiternden Kommentare („Really?“, „It's an animal?“, „Heating Mushroom?“, etc...).

*Manuel Pölleth*, für die Arbeiten zu den Viologen im Rahmen seines F-Praktikums und für die *baked-out Schlenk-vessels*. Slowly rotate I through...

*Roswitha Scheblein*, für die Hilfe und die vielen Kleinigkeiten, die einem das Leben leichter machen (Leitsalz, Lösungsmittel, Bratwurstgeheck,...).

Den Azubis *Manuela, Kristina, Veronika, Florian, Tatjana, Vilija, Melanie, André* und *David* für die Synthesen und für ihr Engagement.

Allen meinen Kommilitonen, die mich durch die Höhen und Tiefen dieses Studiums begleitet und diese Zeit mehr als erträglich gemacht haben.

Meinem ehemaligen Chemie-Lehrer *Heribert Gerhard* (Hg), dessen Begeisterung für Chemie mich letztendlich zu diesem Studium ermutigt hat.

Meinen Freunden von der Wasserwacht Haßfurt, vor allem *Christine Heusel* und *Thomas Amthor*, für so manchen lustigen Abend im Baron und dafür, dass sie immer ein offenes Ohr für mich haben.

Meiner *Gabriele*, für ihre unendliche Geduld und ihr Verständnis.

Meinem Bruder *Andreas*, für die Computertipps (Linux, Jagged Alliance 2) und für so manches Fass Wernecker Laurentius.

Der größte Dank gilt jedoch meinen *Eltern* und *Großeltern*, die durch ihre finanzielle und ideelle Unterstützung dieses Studium erst ermöglicht haben.

**Erklärung**

Hiermit erkläre ich an Eides statt, dass ich die Dissertation „Electroactive Conjugated Polymers as Charge-Transport Materials for Optoelectronic Thin-Film Devices“ selbstständig angefertigt und keine anderen als die von mir angegebenen Quellen und Hilfsmittel benutzt habe.

Ich erkläre außerdem, dass diese Dissertation weder in gleicher oder anderer Form bereits in einem anderen Prüfungsverfahren vorgelegen hat.

Ich habe früher außer den mit dem Zulassungsgesuch urkundlich vorgelegten Graden keine weiteren akademischen Grade erworben oder zu erwerben versucht.

Würzburg, den 30.11.2005

---

Unterschrift